

Table of Contents

RÉSUMÉ.....	i
ABSTRACT.....	iv
ACKNOWLEDGMENTS.....	vi
TABLE OF CONTENTS.....	vii
LIST OF FIGURES.....	x
LIST OF TABLES.....	xiv
CHAPTER 1 DEFINING THE PROBLEM	1
1.1 INTRODUCTION	2
1.2 OBJECTIVES.....	6
1.3 THESIS LAYOUT	7
CHAPTER 2 LITERATURE SURVEY	8
2.1 INTRODUCTION	9
2.2 ALUMINUM CAST ALLOYS.....	9
2.3 ALUMINUM-SILICON CAST ALLOYS.....	11
2.3.1 Role of alloying elements in Al-Si alloys	13
2.4 EFFECT OF ALLOYING ELEMENTS ON Al-Si ALLOYS	18
2.4.1 Zirconium (Zr)	18
2.4.2 Nickel (Ni)	19
2.4.3 Manganese (Mn)	20
2.4.4 Scandium (Sc)	21
2.4.5 Strontium (Sr).....	22
2.4.6 Titanium (Ti).....	23
2.5 HEAT TREATMENT OF Al-Si-Cu-Mg ALLOYS	23
2.5.1 Solution Heat Treatment	24
2.5.2 Quenching	26
2.5.3 Age Hardening Treatment.....	27
2.6 MICROSTRUCTURE OF Al-Si-Cu-Mg ALLOYS	29
2.7 MECHANICAL PROPERTIES OF Al-Si ALLOYS	32

2.7.1	Effect of additives on high temperature mechanical properties of Al-Si-Cu-Mg alloys.....	34
2.8	FRACTOGRAPHY	36
2.9	QUALITY CHARTS.....	39
CHAPTER 3 EXPERIMENTAL PROCEDURES.....		42
3.1	INTRODUCTION	43
3.2	CLASSIFICATION OF ALLOYS	44
3.3	MELTING AND CASTING PROCEDURES	44
3.4	HEAT TREATMENT	47
3.5	TENSILE TESTING	50
3.6	CHARACTERIZATION OF MICROSTRUCTURE	51
3.6.1	Thermal Analysis	51
3.6.2	Optical Microscopy.....	53
3.6.3	Scanning Electron Microscopy	56
CHAPTER 4 MICROSTRUCTURE CHARACTERIZATION AND POROSITY FORMATION		58
4.1	INTRODUCTION.....	59
4.2	THERMAL ANALYSIS	59
4.2.1	Alloy R (354 + 0.25%Zr).....	61
4.2.2	Alloy S (354 + 0.25%Zr + 2%Ni).....	63
4.2.3	Alloy T (354 + 0.25%Zr + 4%Ni).....	64
4.2.4	Alloy U (354 + 0.25%Zr + 0.75%Mn).....	66
4.2.5	Alloy V (354 + 0.25%Zr + 0.75%Mn + 2%Ni).....	68
4.2.6	Alloy Z (354 + 0.25%Zr + 0.15%Sc).....	70
4.2.7	Alloy L (398 + 0.25%Zr + 0.15%Sc).....	72
4.3	POROSITY FORMATION DUE TO INCIPIENT MELTING.....	74
CHAPTER 5 ROOM AND HIGH TEMPERATURE TENSILE PROPERTIES		90
5.1	INTRODUCTION.....	91
5.2	ROOM TEMPERATURE TENSILE PROPERTIES (AS-CAST AND SOLUTION HEAT-TREATED CONDITIONS).....	92
5.3	INFLUENCE OF ALLOYING ADDITIONS AND HEAT TREATMENT CONDITIONS.....	97
5.4	TENSILE PROPERTIES OF ALLOYS R, S AND U AT ROOM TEMPERATURE	108
5.4.1	Alloy R (354 + 0.25wt% Zr).....	108

5.4.2	Alloy S (354 + 0.25wt% Zr + 2wt% Ni).....	111
5.4.3	Alloy U (354 + 0.25wt% Zr + 0.75wt% Mn).....	114
5.4.4	Quality charts for Alloys R, S and U - room temperature tensile data.....	116
5.4.5	Effect of Zr and Sc addition to 354 and 398 alloys.....	118
5.4.6	Statistical analysis	122
5.5	TENSILE PROPERTIES OF ALLOYS R, S AND U AT HIGH TEMPERATURE	126
5.5.1	Alloy R (354 + 0.25wt% Zr).....	126
5.5.3	Alloy S (354 + 0.25wt% Zr + 2wt% Ni).....	129
5.5.4	Alloy U (354 + 0.25wt% Zr + 0.75wt% Mn).....	131
5.5.5	Quality charts of Alloys R, S and U - high temperature tensile data	133
5.5.6	Comparison between the high temperature tensile properties of as-cast and T6-treated 354 alloy with different alloying additions and a new alloy	138
5.5.7	Statistical analysis	149
	CHAPTER 6 CONCLUSIONS.....	153
	RECOMMENDATIONS FOR FUTURE WORK.....	159
	REFERENCES.....	161

LIST OF FIGURES

CHAPTER 2

Figure 2.1 The binary equilibrium phase diagram of the Al-Si alloy system.....	12
Figure 2.2 Diagram representing precipitation stages with aging time.	15
Figure 2.3 Schematic of the T6 heat treatment process.	24
Figure 2.4 Schematic phase diagram of a heat-treatable alloy, showing temperature ranges for solutionizing and for aging and showing amount of solute precipitated during aging.	26
Figure 2.5 Comparison of the silicon morphology in: (a) unmodified and (b) Sr-modified (300 ppm Sr), near-eutectic aluminum-silicon alloys.	31
Figure 2.6 α -Fe and β -Fe intermetallic phases precipitated in Al 354 alloys.	32
Figure 2.7 Stress-strain curve.	33
Figure 2.8 Schematic diagram showing brittle vs ductile stress-strain behavior	37
Figure 2.9 Photographs showing (a) ductile vs (b) brittle specimens.....	37
Figure 2.10 SEM images showing (a) a ductile fracture surface exhibiting a dimpled structure, and (b) a brittle fracture surface, showing how fracture occurs through the cracking of particles (arrowed).....	39
Figure 2.11 Example of the quality chart proposed by Drouzy et al. [115] with <i>iso-Q</i> and <i>iso-YS</i> lines generated using Equations 1 and 2.....	41

CHAPTER 3

Figure 3.1 Electrical resistance furnace.....	45
Figure 3.2 Graphite degassing impeller.....	45
Figure 3.3 ASTM B-108 permanent mold used for casting tensile test bars.....	46
Figure 3.4 Dimensions of the tensile test bar (in mm).....	46
Figure 3.5 Lindberg Blue M electric furnace.	48
Figure 3.6 (a) MTS mechanical testing machine for room temperature testing, and (b) Instron Universal mechanical testing machine for high temperature testing....	51
Figure 3.7 Schematic drawing showing the graphite mold used for thermal analysis.	53
Figure 3.8 Thermal analysis set-up.....	53
Figure 3.9 Diagram showing the sectioned area for analysis of tensile samples using optical microscopy.....	54
Figure 3.10 Struers LaboPress-3 and TegraForce-5 machines for mounting and polishing of metallography samples.....	55
Figure 3.11 Clemex Vision PE 4.0 image analyzer-optical microscope system.	56
Figure 3.12 Scanning electron microscope system used in this study.....	57
Figure 3.13 Field emission scanning electron microscope used in this study.	57

CHAPTER 4

Figure 4.1 Temperature-time plot and first derivative obtained from the thermal analysis of Alloy R (354 + 0.25% Zr).....	62
---	----

Figure 4.2 Optical microstructure of R (354 + 0.25% Zr) alloy sample obtained from the thermal analysis casting (cooling rate 0.35°C/s), showing the different phases present in the alloy: 1- Al ₂ Cu; 2- AlMgCuSi; 3- AlZrTi.....	62
Figure 4.3 Temperature-time plot and first derivative from the thermal analysis of Alloy S (354 + 2% Ni + 0.25% Zr).....	63
Figure 4.4 Optical microstructure of Alloy S (354 + 2% Ni + 0.25% Zr) sample obtained from the corresponding thermal analysis casting (cooling rate 0.35°C/s), showing the different phases present in the alloy: 2- AlCuNi; 3- AlNiFe; 3a- AlSiNiZr-Fe; 4- Al ₂ Cu.....	64
Figure 4.5 Temperature-time plot and first derivative from the thermal analysis of Alloy T (354 + 4% Ni + 0.25% Zr).....	65
Figure 4.6 Optical microstructure of Alloy T (354 + 4% Ni + 0.25% Zr) sample obtained from the corresponding thermal analysis casting (cooling rate 0.35°C/s), showing the different phases present in the alloy: 1-AlCuNi; 2- AlNiFe; 3- AlTiZr; 4- β-AlFeSi; 5- Al ₂ Cu.	66
Figure 4.7 Temperature-time plot and first derivative from the thermal analysis of Alloy U (354 + 0.75% Mn + 0.25% Zr).	67
Figure 4.8 Optical microstructure of Alloy U (354 + 0.75% Mn + 0.25% Zr) sample obtained from the thermal analysis casting (cooling rate 0.35°C/s), showing the different phases present in the alloy: 2- Al ₂ Cu; 3- AlSiMnFe.....	68
Figure 4.9 Temperature-time plot and first derivative from the thermal analysis of Alloy V (354 + 0.75% Mn + 2% Ni + 0.25% Zr).....	69
Figure 4.10 Optical microstructure of Alloy V (354 + 0.75% Mn + 2% Ni + 0.25% Zr) sample obtained from the thermal analysis casting (cooling rate 0.35°C/s), showing the different phases present in the alloy: 2- AlNiCu; 3- AlFeNiCu; 4- Al ₂ Cu; 5- Zr-rich phase.....	70
Figure 4.11 Temperature-time plot and first derivative from the thermal analysis of Alloy Z (354 + 0.15% Sc + 0.25% Zr).	71
Figure 4.12 Optical microstructure of Alloy Z (354 + 0.15% Sc + 0.25% Zr) sample, obtained from the thermal analysis casting (cooling rate 0.35°C/s), showing the different phases present in the alloy: 1- (Al,Ti)(Sc,Zr); 2- Al ₂ Cu; 4- β-AlFeSi; 5- (Al,Si)(Sc,Zr,Ti).	71
Figure 4.13 Temperature-time plot and first derivative from the thermal analysis of Alloy L (398 + 0.15% Sc + 0.25% Zr).	73
Figure 4.14 Optical microstructure of Alloy L (398 + 0.15% Sc + 0.25% Zr) sample obtained from the thermal analysis casting (cooling rate 0.35°C/s), showing the different phases present in the alloy: 1- Al ₂ Cu; 2- β-AlFeSi; 3- (Al,Si)(Sc,Zr); 4- π-AlMgFeSi.....	74
Figure 4.15 Optical micrographs of alloy R (354 + 0.25%Zr) showing the microstructures observed in (a) as cast, (b) SHT–1 and (c) SHT–2 tensile test samples (500x). Circled areas in (b) highlight dissolution of Cu-phases.....	79

Figure 4.16 Optical micrographs of Alloy S (354 + 0.25% Zr + 2% Ni) showing the microstructures observed in (a) as cast, (b) SHT-1 and (c) SHT-2 tensile test samples (500x).....	81
Figure 4.17 Optical micrographs of Alloy T (354 + 0.25%Zr + 4%Ni) showing the microstructures observed in (a) as cast, (b) SHT-1 and (c) SHT-2 tensile test samples (500x).....	82
Figure 4.18 Optical micrographs of Alloy U (354 + 0.25%Zr + 0.75%Mn) showing the microstructures observed in (a) as cast, (b) SHT-1 and (c) SHT-2 tensile test samples (500x).....	84
Figure 4.19 Optical micrographs of Alloy V (354 + 0.25%Zr + 0.75%Mn + 2%Ni) showing the microstructures observed in (a) as cast, (b) SHT-1 and (c) SHT-2 tensile test samples (500x).....	85
Figure 4.20 Optical micrographs of Alloy Z (354 + 0.25%Zr + 0.15%Sc) showing the microstructures observed in (a) as cast, (b) SHT-1 and (c) SHT-2 tensile test samples (500x).....	87
Figure 4.21 Optical micrographs of Alloy L (398 + 0.25%Zr + 0.15%Sc) showing the microstructures observed in (a, b) as cast, (c) SHT-1 and (d) SHT-2 tensile test samples at 500X magnification. Circled areas in (c) and (d) highlight dissolution of phases.....	89

CHAPTER 5

Figure 5.1 Mean values for UTS, YS, % El for Alloys R, S, T, U and V in the as-cast and SHT 1 and SHT 2 solution heat-treated conditions.	95
Figure 5.2 Quality chart showing relationship between UTS and percent elongation for the 354 alloys investigated in the as-cast and SHT 1 and SHT 2 solution heat treated conditions.	96
Figure 5.3 Mean values for UTS, YS, % El for Alloys R, S, T, U and V obtained under the given heat treatment conditions (without stabilization).....	100
Figure 5.4 Mean values of UTS, YS, % El for Alloys R, S, T, U and V obtained under the given heat treatment conditions (after 200 hours stabilization at 250°C).....	101
Figure 5.5 Quality index-color contour charts for Alloys R, S, T, U and V obtained from room temperature tensile testing data: (a) without stabilization, and (b) after 200 h stabilization at 250°C.....	105
Figure 5.6 Probable yield strength-color contour charts for Alloys R, S, T, U and V obtained from room temperature tensile testing data: (a) without stabilization, and (b) after 200 h stabilization at 250°C.	107
Figure 5.7 Mean values for UTS, YS, % El for Alloy R at the given heat treatment condition: (a) without, and (b) after 200 h stabilization at 250°C prior to testing.....	110
Figure 5.8 Mean values for UTS, YS, % El for Alloy S at the given heat treatment condition: (a) without, and (b) after 200 h stabilization at 250°C prior to testing.....	113

Figure 5.9 Mean values for UTS, YS, % El for Alloy U at the given heat treatment condition: (a) without, and (b) after 200 h stabilization at 250°C prior to testing.....	115
Figure 5.10 Quality charts showing UTS vs % El plots for Alloys R, S and U subjected to various heat treatment conditions, and tested at room temperature without and with 200 h stabilization at 250°C prior testing.	117
Figure 5.11 Comparison of tensile test data of Alloys R, S, U, Z and Alloy L listed in Table 5.4 (Room temperature tensile testing).	121
Figure 5.12 Comparison of tensile properties of R, S and U alloys relative to those of as-cast base alloy R: (a) UTS, (b) YS, and (c) %El without, and after 200h stabilization at 250°C.....	125
Figure 5.13 Mean values for UTS, YS, % El for alloy R at the given heat treatment conditions for; (a) One and (b) 200 hours stabilization at 250°C.....	128
Figure 5.14 Mean values for UTS, YS, % El for alloy S at the given heat treatment conditions for; (a) One and (b) 200 hours stabilization at 250°C.....	130
Figure 5.15 Mean values for UTS, YS, % El for alloy U at the given heat treatment conditions for; (a) One and (b) 200 hours stabilization at 250°C.....	132
Figure 5.16 Quality charts showing UTS vs % El plots for Alloys R, S and U subjected to various heat treatment conditions (testing at 250°C after 1h stabilization). ...	135
Figure 5.17 Quality charts showing UTS vs % El plots for Alloys R, S and U subjected to various heat treatment conditions (testing at 250°C after 200h stabilization).	136
Figure 5.18 Relevant part of Figure 5.17 rescaled to distinguish the contour lines obtained for Alloys R, S and U.....	137
Figure 5.19 Comparison of tensile test data of Alloys R, S, U, Z and Alloy L listed in Table 5.5 (tested at 250°C after 1 h stabilization).....	141
Figure 5.20 Comparison of tensile test data of Alloys R, S, U, Z and Alloy L listed in Table 5.6 (tested at 250°C after 200 h stabilization).....	142
Figure 5.21 Comparison of the precipitates observed in Alloy U tested at 250 °C, after (a) 1 hr, and (b) 200 hrs stabilization at testing temperature.....	145
Figure 5.22 Quality charts showing UTS vs %El plots for Alloys R, S, U, Z and L in the as-cast and T6-heat treated conditions (testing at 250°C after 1 h stabilization at testing temperature).	147
Figure 5.23 Quality charts showing UTS vs %El plots for Alloys R, S, U, Z and L in the as-cast and T6 heat-treated conditions (testing at 250°C after 200 h stabilization at testing temperature).	148
Figure 5.24 Comparison of high temperature tensile properties of R, S and U alloys relative to those of the as-cast base alloy: (a) UTS, (b) YS, and (c) %El after 1 h and 200 h stabilization at 250°C.....	152

LIST OF TABLES

CHAPTER 2

Table 2.1 Cast aluminum alloy designation.....	11
Table 2.2 Common aluminum heat treatment designations	29

CHAPTER 3

Table 3.1 Chemical composition of the as-received 354 alloy.....	45
Table 3.2 Chemical composition of the alloys used in this study.....	47
Table 3.3 Summary of the heat treatment and testing conditions at room and high temperatures	49

CHAPTER 4

Table 4.1 Suggested main reactions occurring during solidification of 354-type alloys	60
Table 4.2 Porosity measurements for Alloys R, S, T, U, V, Z and L.	76

CHAPTER 5

Table 5.1 Mean values for UTS, YS, %El for alloys R, S, T, U, V, Z and L subjected to different heat treatment conditions and tested at ambient temperature; Q values obtained using Equation 1	94
Table 5.2 Mean values of UTS, YS, %El obtained at room temperature (without stabilization) for Alloys R, S, T, U and V subjected to different heat treatment conditions; Q and Probable YS values were obtained using Eqns 1 and 2.....	98
Table 5.3 Mean values of UTS, YS, %El obtained at room temperature (after 200h/250°C stabilization) for Alloys R, S, T, U and V subjected to different heat treatment conditions; Q and Probable YS values were obtained using Eqns 1 and 2.....	99
Table 5.4 Comparison of tensile properties of Alloys R, S, U, Z and L (tested at room temperature without stabilization).....	120
Table 5.5 Comparison of high temperature tensile properties of Alloys R, S, U, Z and L (tested at 250°C after 1 h stabilization at testing temperature)	139
Table 5.6 Comparison of high temperature tensile properties of Alloys R, S, U, Z and L (tested at 250°C after 200 h stabilization at testing temperature).	140
Table 5.7 High temperature tensile properties of reference alloy R, (tested at 250°C after 1 and 200 h stabilization at testing temperature).....	149

CHAPTER 1

DEFINING THE PROBLEM

CHAPTER 1

DEFINING THE PROBLEM

1.1 INTRODUCTION

Aluminum is one of the most versatile of the common foundry metals, with cast products consuming, as a world average, ~20% of this metal. Apart from the light weight, the special advantages of aluminum alloys for castings are their relatively low melting temperatures, negligible solubility for all gases except hydrogen, and the good surface finish that is usually achieved with the final products. Most alloys also display good fluidity and compositions can be selected with solidification ranges appropriate to particular applications.

The first casting alloy used in America was an Al-8% Cu composition, known as No. 12 alloy. An Al-10% Cu alloy (No. 122) was used for automotive pistons and cylinder heads. In 1909, Alfred Wilm discovered that an Al-4.5%Cu-0.5%Mn alloy would strengthen by aging, after a quench from an elevated temperature. This alloy was called “Duralumin” and formed the basis for the Al-Cu family of alloys used today. The Al-Cu alloys have excellent mechanical properties; but they are difficult to cast primarily because of hot cracking. As the years went by, foundrymen discovered that additions of other elements, especially silicon, improved alloy castability. For this reason, cast Al-Cu alloys have been largely supplanted by cast Al-Cu-Si and Al-Si alloys [1].

During the past few decades, the automotive industry has shown a great interest in aluminum for its applications. Today aluminum is an essential material in car manufacturing and its alloys are actually used in the components of cylinder blocks, pistons and other engine parts. It is believed that 1 kg of aluminum can replace up to 2 kg of steel and cast iron in many areas of application [2]. The more aluminum alloys are used in the production of a vehicle, the less the weight of the vehicle is, and the less fuel it will consume, thereby reducing the amount of harmful emissions into the atmosphere. Actually, as an industry, scientific researches must follow the needs of the designers. So they are required to be at the same point of thinking with the designers, and to appreciate the boundary conditions and constraints of their work. Secondly, the casting industry should have the means and tools to tailor and optimize alloys for specific performance/applications. As pointed out above, developing alloys for specific processes is not the norm, although it should be taken into consideration. Therefore, it is important to optimize the performance attained from specific processes by ensuring that the alloys processed are optimized to take advantage of the merits of the particular process.

Today, we have predictive tools that enable us to work in a much more intelligent and effective way than in years past. The trial and error approach of alloy development is not only ineffective but also economically unsustainable. Cast components undergo post-processing operations, such as heat-treating, etc. In complex alloys, the range of elemental composition may make all the difference during heat-treating. Predictive tools mitigate, if not prevent, the occurrence of incidences such as incipient melting. So it is not only during the alloy and processing stages that these enabling tools are useful, but also during post-processing operations.

For aluminum alloys, the principle alloying elements, in addition to silicon (Si), are magnesium (Mg) and copper (Cu). However, most Al-Si alloys are not suitable for high temperature applications because their tensile and fatigue strengths are not as high as desired in the temperature range 230-350°C, a range often observed under service conditions. Most of the Al-Si cast alloys to date are intended for applications at temperatures no higher than about 230°C; however, some interesting improvements have been achieved by modifying the composition of the base alloy with the addition of Mn and Ni, resulting in an increase in strength and ductility at both room and high temperatures. Thus, there is a need in the automobile industry for developing a low-cost, high strength aluminum alloy, exhibiting high wear resistance and a low coefficient of thermal expansion, with better tensile and fatigue strength at temperatures of 260-370°C.

Iron is traditionally considered as a harmful element in Al-Si alloys since platelets of the coarse and brittle lamellar β -iron Al_5FeSi may be formed as a primary phase, when the iron content is more than 0.5 wt.% [3]. It is found that the α -iron $\text{Al}_{15}(\text{Fe}, \text{Mn})_3\text{Si}_2$ phase can be formed, instead, if both Fe and Mn are added under certain solidification rates [4]. Due to its Chinese script morphology, a certain amount of such α -Fe phase particles indeed improve the tensile strength and retard the extension of micro-cracks during tensile testing [3].

Zirconium has a low solubility in aluminum, and only small additions of Zr are therefore necessary to form dispersoids. In many alloys, however, Al_3Zr is heterogeneously distributed, and in the areas where the number density of dispersoids is low, the alloy will be prone to recrystallization [5]. The addition of transition elements such as Ni and Cu is considered to be an effective way to improve the high temperature strength of cast Al-Si

alloys in as-cast and solution-treated conditions through the formation of stable aluminides. Copper and magnesium as alloying elements are often added to improve alloy strength at room temperature as well as at higher temperatures [6].

Hypoeutectic Al-Si-Cu-Mg alloys exhibit three main solidification reactions during the solidification process, starting with the formation of α -Al dendrites followed by the development of two main eutectic phases; eutectic silicon and secondary β -(Al, Si, Fe) phase. The presence of alloying and impurity elements such as Cu, Mg, Mn, Fe leads to more complex constituents, including intermetallic phases, that may be characterized by metallographic techniques [7].

Heat-treatment is of major importance since it is commonly used to alter the mechanical properties of cast aluminum alloys. Heat treatment improves the strength of aluminum alloys through a process known as precipitation hardening, which occurs during the heating and cooling of an aluminum alloy, and in which precipitates are formed in the aluminum matrix. The improvement in the mechanical properties of Al alloys as a result of heat treatment depends upon the change in solubility of the alloying constituents with temperature [8].

A comprehensive study was carried out to investigate the effect of additions of Zr, Ni, Mn and Sc on the microstructure and tensile properties of Al-Si-Cu-Mg 354 type alloys at ambient and high temperatures. Generally, the mechanical properties and microstructure of aluminum cast alloys are dependent on the composition, the melt treatment conditions, the solidification rate, the casting process and the applied thermal treatment. All these parameters were investigated in this study and the results obtained were analyzed in terms

of their effect on the microstructures and, hence, on the mechanical properties obtained for the 354 alloys.

1.2 OBJECTIVES

The current study was carried out to analyze the effect of Ni, Mn, Zr and Sc additions on the strength of cast aluminum alloy 354 (Al-9%Si-1.8%Cu-0.5%Mg), as well as the effect of only Zr and Sc additions on the strength of cast aluminum alloy 398 (Al-16%Si), at room and high temperatures for different holding times. The latter alloy was examined solely for the purpose of comparing how the properties of the 354 alloys investigated in this study stand with respect to the 398 alloy, an alloy developed by NASA and reported to give superior high temperature properties [9].

The evolution of the microstructural features with the addition of the above alloying elements and their consequent effect on the mechanical properties were investigated. Based on this approach, the principal objectives of this study cover the following.

- I. Examining the main microstructural features observed in the alloys, such as phases, intermetallics, and precipitates, together with their identifying characteristics and evolution during controlled exposure at different temperatures and times.
- II. Determining the room temperature tensile properties of the alloys subjected to different aging conditions (temperature and time).
- III. Obtaining the high temperature tensile property values at different temperatures for selected alloys or conditions based on the room temperature tensile testing results.

- IV. Correlating the results obtained from the room temperature and high temperature tensile tests with the principal microstructural features observed in the corresponding alloy samples, in order to analyze and understand the major parameters involved in the strengthening of alloy 354 at high temperatures.
- V. Determining the effect of Zr and Sc as alloying element additions on the mechanical properties of high-strength cast aluminum alloy 398 (Al-16%Si) and comparing the properties obtained with those of 354 aluminum alloy.

1.3 THESIS LAYOUT

The structure of this thesis is presented in five chapters. Chapter 1 introduces the research study which was carried out and defines its objectives. Chapter 2 presents the literature review about the topic of this thesis. Chapter 3 describes the experimental procedures and testing methods which were employed in the given research. Details of the microstructural examination of the alloys investigated, identification and qualitative and quantitative analyses are provided in Chapter 4. Chapter 5 presents the room and high-temperature mechanical properties of the alloys. The results are discussed and analyzed in terms of the microstructural data presented in Chapter 4. Chapter 6 presents conclusions, followed by recommendations for future work. A list of references is provided at the end.

CHAPTER 2
LITERATURE SURVEY

CHAPTER 2

LITERATURE SURVEY

2.1 INTRODUCTION

It is known that aluminum alloys are developed with allowance for the effect of each alloying element on the phase composition and structure from the standpoint of obtaining the desired result, for example, raising the alloy strength or ductility or its high-temperature performance. The alloying is used for providing the maximum possible number of structural mechanisms that can cause an increase in the requisite properties. The efficiency of alloying additions depends on the modifying and refining actions of the alloying elements. A special feature of the alloying process is the possibility of formation of new phases with a complex composition, which can influence the strength and ductility characteristics.

2.2 ALUMINUM CAST ALLOYS

Aluminum casting alloys find wide use in several applications employed in automotive, aerospace and other transportation industries [10-12]. Aluminum alloys have about one-third of the density and modulus of elasticity of steels, high thermal and electrical conductivity, high corrosion resistance [13], high friction coefficient, excellent formability, low melting point, high magnetic neutrality, and the possibility for a wide range of possible surface treatments [14,15]. The increasing demand for the use of aluminum alloys is related not only to their mechanical performance, economical

efficiency and environmental advantages, but also to the fact that these alloys offer advantageous safety features since the ability of aluminum to absorb the energy of impact in case of an accident is twice that of steel for the same weight.

The continuous and steady growth of aluminum alloy usage in industrial applications is directly related to the need for taking advantage of such specific assets as a high strength-to-weight ratio, and by so doing to enhance mechanical performance and to lessen energy consumption [16-18].

Aluminum alloys are classed into two groups, wrought alloys and cast alloys. Furthermore, depending on whether they contain hardening elements such as magnesium and copper, they are further distinguished as heat-treatable or non-heat treatable alloys. Heat-treatable alloys are those whose strength is improved after subjecting the alloy to heat treatment; whereas non-heat treatable alloys are strengthened through mechanical working or deformation, the strengthening process in the two cases being termed 'precipitation hardening' and 'work hardening', respectively.

The cast alloy designation system is based on a 3 digit-plus decimal designation xxx.x (i.e. 356.0). The first digit (Xxx.x) indicates the principal alloying element which has been added to the aluminum alloy (see Table 2). The second and third digits (xXX.x) are arbitrary numbers given to identify a specific alloy in the series. The number following the decimal point indicates whether the alloy is a casting (.0) or an ingot (.1 or .2). A capital letter prefix indicates a modification to a specific alloy [19].

Table 2.1 Cast aluminum alloy designation [19].

Alloy Series	Principal alloying elements
1xx.x	Commercially pure aluminum >99 % purity (non-heat treatable)
2xx.x	Copper (heat treatable)
3xx.x	Silicon plus Copper and/or Magnesium
4xx.x	Silicon (non-heat treatable)
5xx.x	Magnesium (non-heat treatable)
6xx.x	Unused Series
7xx.x	Zinc (heat treatable)
8xx.x	Tin
9xx.x	Other elements

2.3 ALUMINUM-SILICON CAST ALLOYS

Among the most commonly used cast aluminum alloys are those belonging to the Al-Si system. Due to their mechanical properties, excellent castability and corrosion resistance, these alloys are primarily used in engineering and in the automotive industry. Cast Al-Si alloys are divided into three categories: hypoeutectic alloys, with a Si concentration from 4 to 10 mass%, near-eutectic alloys with a Si concentration of 10-13 mass%, and hypereutectic alloys with a Si concentration of 17-26 mass %.

The eutectic–silicon morphology also has a considerable influence on the mechanical properties of these alloys. Acicular-shaped eutectic silicon particles normally observed in the as-cast alloy can be modified to fibrous or spherical ones by the addition of chemical modifiers such as strontium (Sr), sodium (Na) or antimony (Sb), in order to improve the alloy ductility and strength. Heat treatment, or thermal modification, can also change the eutectic silicon morphology [20, 21].

Binary cast aluminum-silicon alloys used in industrial practice contain silicon in a concentration close to the eutectic (10-13 mass% Si). These alloys have optimum cast properties due to eutectic crystallization at a constant temperature, which improves the castability of the molten metal and thus reduces the formation of shrinkage to approximately 1.15% during the casting process. Silicon has a beneficial influence in that it reduces the melting temperature of the aluminum alloy and improves its fluidity and promotes the formation of strengthening precipitates through the expected reaction of Si and Mg present in solid solution to form Mg_2Si [22]. The higher tensile strength can also be attributed to the presence of spheroidized particles of Si that provide substantial dispersion hardening [23].

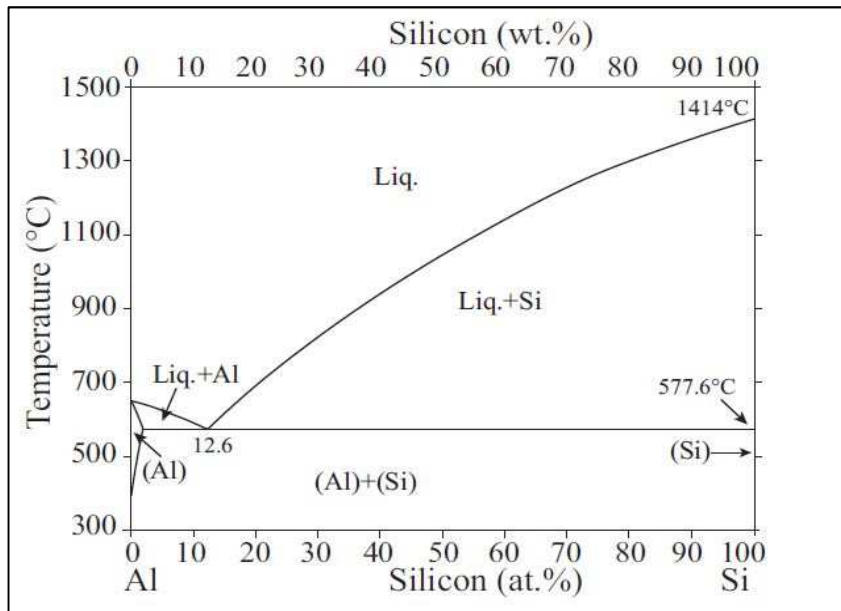


Figure 2.1 The binary equilibrium phase diagram of the Al-Si alloy system.

In spite of these advantages, however, Al-Si alloys are limited to applications which can work up to temperatures of ~250 °C [6] as above this temperature, the alloys lose coherency between the aluminum solid solution matrix and the precipitated particles which will then rapidly coarsen and dissolve again into the solid solution, resulting in an alloy having an undesirable microstructure for high temperature applications [24].

2.3.1 Role of alloying elements in Al-Si alloys

Copper and magnesium are the main alloying elements added to Al-Si cast alloys for use in industrial applications. Addition of these elements increases the alloy strength after aging because of the precipitation of different hardening phases such as θ' (Al_2Cu), S' (Al_2CuMg) and β'' (Mg_2Si) [25]. The Mg content of commercial 354 alloys ranges from 0.4 to 0.7 wt%. The addition of Mg results in the formation of the Q- $\text{Al}_5\text{Mg}_8\text{Si}_6\text{Cu}_2$ phase which grows from the blocky Al_2Cu phase during the last stage of solidification. The coarseness of the Q phase increases with increasing Mg content [26]. In applications where ductility is not the most important factor in material selection, adding Cu to these alloys has the distinct advantage of increased strength at high temperatures. However, the addition of Cu also decreases the solidus eutectic temperatures of the alloy, thereby increasing the solidification range of the alloy, resulting in a tendency to develop porosity and hot cracking [27].

2.3.1.1 Al-Si-Cu alloys

Adding copper to an Al-Si alloy increases its strength and facilitates precipitation hardening but it reduces ductility and corrosion resistance [28]. When the Cu content is above its solubility in Al, the precipitation of the second phase θ' (Al_2Cu) also contributes to the strengthening effect. During solution treatment, copper dissolves rapidly into the

aluminum matrix despite the short duration employed; this element is critical in facilitating age hardening, particularly when Mg and Si are also present [29].

In an Al-Cu alloy, upon appropriate heat treatment, the Cu atoms progressively cluster together to form very small particles which separate out within the matrix grains of the alloy; this process is called precipitation [30]. The strengthening effect of Cu in Al-Si alloys is linked to the precipitation of the secondary eutectic phases of intermetallic Al_2Cu or $\text{Al}_5\text{Cu}_2\text{Mg}_8\text{Si}_6$ that form upon aging during the T6 heat treatment. A solution temperature that exceeds the solidus temperature of incipient melting leads to the occurrence of incipient melting of the Cu-rich phases, which would deteriorate the mechanical properties of these alloys [31, 32].

The alloy is initially in a state far from equilibrium and, given sufficient time at the applied temperature, diffusion of atoms occurs progressively to transform the metallurgical structure towards the equilibrium state. The precipitation process creates precipitate particles that usually provide an appreciable hindrance to plastic deformation by slip. Hence, as precipitation progresses and the size and amount of precipitates increases, the alloy hardens and strengthens with time. The full precipitation occurs only when the alloy is artificially aged at temperatures below the solvus of the Guinier Preston 1 (or GP1) zone.

Many steps in this process may be covered up by aging at temperatures above the Guinier Preston zones, θ' and θ'' , simultaneously with the solvus line of the stable phase θ [33, 34]. The primary hardening at 180 °C is added to GP1 zones. After attaining a critical radius of 5 nm, an incubation time starts, during incubation period the size of the zone and the value of hardness remains unchanged [35, 36].

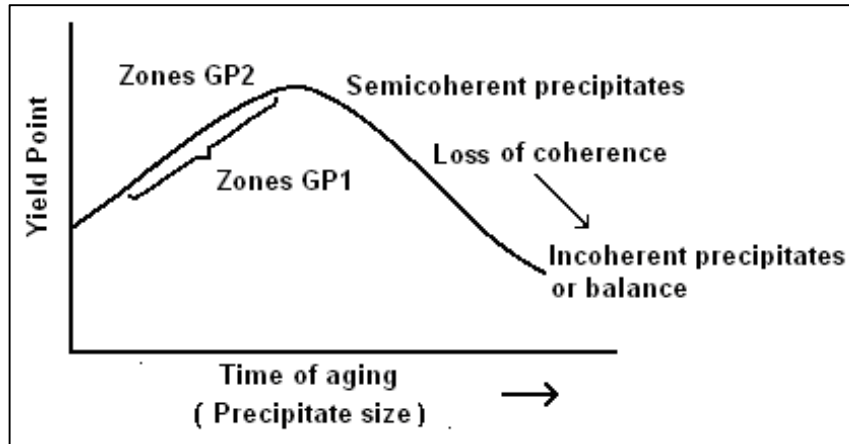


Figure 2.2 Diagram representing precipitation stages with aging time [37].

A content of approximately 1% of copper provides good mechanical properties at high temperature, without significantly affecting the elongation at room temperature [38]. The addition of transition elements such as Cu in addition to Ni is considered to be effective for increasing the room and the high temperature strength of cast Al-Si alloys by forming stable aluminides [39]. As with the as-cast condition, ductility for alloys aged to a T6 temper decreases gradually as the Cu content is raised [22].

2.3.1.2 Al-Si-Mg alloys

Al-Si-Mg alloys are also of great interest in the transportation field due to their high specific strength and good castability. Magnesium provides substantial strengthening and improvement of the work-hardening characteristics of aluminum. It has a relatively high solubility in solid aluminum, and has a major impact on strengthening while decreasing the ductility, as reported by Caceres et al. [40]. In general, corrosion resistance and weldability are also good [41].

When present in combination with Cu and/or Si, Mg is also a very efficient alloying addition for strengthening aluminum alloys. Even small amounts of Mg can have a

profound effect on age hardening [22]. Tavitas-Medrano et al. [42] have reported that additions of 0.4 wt% Mg increase the response of the alloy to artificial aging, thereby increasing the tensile strength and micro-hardness values achievable, however, at the expense of reduced elongation and impact toughness.

Magnesium is added to Al-Si alloys to make them heat treatable whereby, through the formation of Mg_2Si precipitates upon aging, the alloy strength is increased via precipitation hardening. The microstructure of as-cast hypoeutectic aluminum alloys, however, contains coarse primary α -Al dendrites and acicular shaped eutectic silicon particles, which reduce the mechanical properties [43, 44]. With heat treatment, the mechanical properties of Al-Si-Mg alloys can be improved noticeably.

The mechanical properties of heat-treatable cast Al-Si-Mg alloys, such as the A356 alloy, are negatively affected by prolonged exposure at high temperatures [45, 46]. A significant reduction in hardness and tensile strength already occurs at temperatures equal to or higher than 200 °C, thus limiting the application of these alloys in the case of automotive and other engine components.

With the aim of overcoming these limits and ensuring a superior thermal stability, Al-Si-Cu-Mg alloys are currently under extensive study [8, 47-49]. In particular, the alloys being developed are expected to have superior thermal stability in comparison to the widely used A356 and A357 (Al-Si-Mg) casting alloys, thanks to the presence of more stable Cu-based intermetallic precipitates, as observed in Al-Mg-Si-Cu alloys [50]. Al-Si-Mg and Al-Si-Cu alloys are characterized, respectively, by the strengthening phases Mg_2Si and Al_2Cu , whose precipitation sequences were studied in Al-Mg-Si and Al-Cu alloys [51-55]. These sequences respectively occur as:

α (SSS) \rightarrow GP zones $\rightarrow \beta'' \rightarrow \beta'/B' \rightarrow \beta$ in Al-Mg-Si alloys, and

α (SSS) \rightarrow GP zones $\rightarrow \theta'' \rightarrow \theta' \rightarrow \theta$ in Al-Cu alloys,

where β'' , β' , B' and θ'' , θ' are the intermediate coherent/semi-coherent precipitates, while β and θ are the stable incoherent phases.

In quaternary Al-Si-Cu-Mg alloys, the presence of both Cu and Mg induces the formation of further reinforcing compounds, such as the S phase, characterized by the stoichiometry Al_2CuMg , according to the following precipitation sequence [56, 57]:

α (SSS) \rightarrow GPB zones $\rightarrow S'' \rightarrow S' \rightarrow S$

After the decomposition of the supersaturated solid solution (SSS), the formation of Guinier–Preston–Bagaryatsky (GPB) zones occurs, followed by the precipitation of the coherent S'' , semi-coherent S' , and incoherent equilibrium S phase. The quaternary Q phase (AlCuMgSi) was also observed in Al-Cu-Mg-Si alloys, characterized by a complex precipitation sequence, depending on alloy composition [58, 59], which may be expressed by:

α (SSS) \rightarrow QP \rightarrow QC \rightarrow Q' \rightarrow Q

where QP, QC and Q' are the precursors of the stable Q phase. The Cu-containing phases should confer to the quaternary Al-Si-Cu-Mg alloys a superior thermal stability in comparison to the more widely used Al-Si-Mg alloys, leading to a better response of the T6 heat-treated alloys to high temperature exposure (i.e., overaging) [50].

2.4 EFFECT OF ALLOYING ELEMENTS ON Al-Si ALLOYS

Alloying elements are usually added to Al–Si cast alloys in order to improve microstructure features and thus improve mechanical properties. Nickel (Ni) and Zirconium (Zr) are used as alloying additions to increase high temperature strength in aluminum alloys due to the production of the $L1_2$ -type precipitates Al_3Zr or Al_3Ni , which are more able to maintain overaging at higher temperatures than the precipitates existing in cast aluminum alloys such as Al_2Cu and Mg_2Si [60]. Manganese (Mn) is used to neutralize the effect of iron (Fe) and to modify the morphology and type of intermetallic phases formed. Scandium (Sc) in aluminum alloys acts as an effective grain refiner and increases the recrystallization temperature, the corrosion resistance, and weldability.

2.4.1 Zirconium (Zr)

Zirconium is added to aluminum to form fine precipitates of intermetallic particles that inhibit recrystallization [6]. For alloys with zirconium additions, a non-recrystallized structure can be obtained after heat treatment which provides a high level of structural hardening for a wider range of semi-products than in the case of aluminum alloys containing manganese (Mn). These products include virtually all pressed and rolled plates, stampings, forgings, and some cold-deformed semi-products (sheets) obtained from Al-Zn-Mg and Al-Zn-Mg-Cu alloys, which require a lower temperature of heating for hardening (450° - $470^{\circ}C$) than Al-Cu alloys.

Zirconium is usually present in aluminum alloys in an amount ranging from 0.1 to 0.25%. Segregations of the Al_3Zr phase particles formed are finer than those of Mn aluminides (10-100 nm in size) [61]. However, the effect of precipitation hardening due to segregation of the Al_3Zr phase is not high because of the low content of Zr in the alloys similar to the case of the Mn aluminides, although the effect of the finer zirconium aluminide segregates on the process of recrystallization in deformed semi-products and, accordingly, on their grain structure, is considerably stronger [5]. Additionally, it has been shown that Zr increases the resistance to overaging when it is added to binary Al-Sc alloys [62].

2.4.2 Nickel (Ni)

Cast Al-Si alloys usually contain alloying components such as magnesium, copper, nickel, etc. which are widely used in the automotive industry in piston applications [63,64]. These additions form intermetallic phases with complex morphologies and complex compositions. Nickel is added to Al-Cu and Al-Si alloys to improve hardness and strength at elevated temperatures and to reduce the coefficient of thermal expansion, as there is an increasing demand for Al-Si cast alloys with better performance concerning yield and tensile strength at elevated temperatures up to 250 °C [65]. In fact, the addition of alloying elements such as Cu and Ni is an effective and practical way to improve the mechanical properties, especially in relation to the performance of piston alloys which are subjected to high temperature service conditions [66].

The advantages of adding Ni and Zr to Al-Si alloys are that their precipitates (Al_3Ni and Al_3Zr) possess the following important characteristics:

- They are coherent;
- Possess low solubility;
- Directly affect the strength of the material because they act as hard pinning points which inhibit the movement of dislocations in the matrix.

2.4.3 Manganese (Mn)

Manganese is very soluble in aluminum; when the cast is chilled, most of the added manganese is substantially retained in solution. It increases the strength of the alloy either in solid solution or as a finely precipitated intermetallic phase by modifying the morphology of the intermetallic phases which are formed after heat treatment of the given alloy. As reported by Seifeddine et al. [67], it has no adverse effect on corrosion resistance. Manganese combines with Fe in the alloy forming the script-like α -iron phase which is more compact and less detrimental to the mechanical properties [68]. Hwang et al. [69] have reported that as the Mn content is increased up to 0.65 wt% corresponding to an Fe/Mn ratio of 1.2 in the Al-7wt.% Si-3.8 wt.% Cu-0.5 wt.% Fe alloy, the plate-like β - Al_5FeSi iron intermetallic phase is completely converted to the Chinese script α - $\text{Al}(\text{Fe},\text{Mn})\text{Si}$ iron phase, resulting in improved tensile properties. Excess amounts of Mn, however, deteriorate the mechanical properties by increasing the total amount of iron-containing intermetallic phases formed.

2.4.4 Scandium (Sc)

Al-Sc alloys have excellent mechanical properties at ambient and elevated temperatures due to the presence of a high density (as high as 1022 m^{-3}) of elastically-hard $L1_2$ type Al_3Sc precipitates which remain coherent with the α -Al matrix at elevated temperatures [70, 71]. Krug [72], and Seidman and coworkers [73, 74] have reported that the Al_3Sc precipitates coarsen slowly up to $\sim 300^\circ\text{C}$, imparting good creep resistance in coarse-grained cast alloys. The low lattice parameter mismatch of Al and Al_3Sc also contributes to the high creep resistance of Al-Sc alloys. The good interfacial strength between the Al_3Sc precipitates and the aluminium matrix creates a significant lattice strain, which blocks dislocation motion and prevents grain growth [75]. Furthermore, the thermal stability of the Al_3Sc precipitates suppresses recrystallization [76] and leads to a significant strengthening effect. Although Al-Sc alloys appear to be very promising alloys for high temperature applications, their application is limited by the high cost and availability of Sc.

A possible solution to this problem would be to achieve solid solution strengthening using substitute alloying additions that are similar in nature to Sc, to reduce the Sc content without lowering the properties. Kending [77], and Dunand and coworkers [78-82] showed that ternary additions to Al-Sc alloys improve mechanical properties by solid solution strengthening as in the case of Mg, or by substituting for Sc in Al_3Sc precipitates as in the cases of Ti and Zr.

Scandium (Sc) addition to Al alloys results in as-cast grain size refinement, an increase in mechanical properties and improvement of weldability [83]. It acts as an effective grain refiner and increases the recrystallization temperature so that it does not form any second phase intermetallic compounds with other alloying elements such as Fe,

Mg, Mn and Si [84]. While the addition of Sc to Al alloys is more effective in improving resistance to recrystallization than Zr [85] due to the formation of a high density of Al_3Sc particles, the addition of both Sc and Zr produces $\text{Al}_3(\text{Sc,Zr})$ particles which are more stable than the Al_3Sc dispersoids, thus increasing the resistance to recrystallization [86,87]; however, Sc is too expensive to be extensively used in industry [88], so cheaper rare-earth element additions are being studied to replace it.

2.4.5 Strontium (Sr)

As mentioned previously, the eutectic silicon morphology has a considerable influence on the mechanical properties of Al-Si based alloys. The tips of the needle-like eutectic silicon particles in an unmodified Al-Si alloy act as stress raisers which are harmful to the mechanical properties. Acicular-shape eutectic silicon particles normally observed in the as-cast alloy can be modified to fibrous or spherical ones by the addition of chemical modifiers. The most common element used in industry today is strontium (Sr) [89], which is added in the form of Al-Sr master alloy to Al-Si alloy melts in order to change or ‘modify’ the morphology of the eutectic silicon particles from their normally brittle, acicular form to a fibrous form during solidification. Both Sr addition and solidification rate have a strong influence on the microstructure. The change in morphology from acicular to fibrous form results in improving the ductility of the alloy as well as its strength. [90]. According to Merlin and Garagnani [91], one of the disadvantages of modification, however, is that the addition of strontium to the alloy could increase the hydrogen content and, as a result, the presence of gas porosities.

2.4.6 Titanium (Ti)

It is common practice to add Ti to Al-Si foundry alloys because of its potential grain refining effect [92]. Sigworth and Kuhn [93] have reported that the grain refining effect of titanium is enhanced if boron is present in the melt or if the Ti is added in the form of an Al-Ti-B master alloy containing boron and titanium, largely combined as TiB_2 which act as excellent nuclei for the α -Al phase. Titanium diboride has almost no solubility in liquid aluminum; thus, TiB_2 particles produce good refinement at small addition levels. The refinement is also long lasting, when the particles are not allowed to sediment from the melt.

2.5 HEAT TREATMENT OF Al-Si-Cu-Mg ALLOYS

Heat treatment is a controlled process used to modify the microstructure of materials such as alloys to obtain improved properties which benefit the working life of a component, such as increased surface hardness, temperature resistance, ductility and strength. There are various types of heat treatment processes, the main among them being annealing, solution heat treatment, and age hardening. Annealing is basically a stress relieving process in which a material is heated at a temperature above its recrystallization temperature, and then it is maintained at a suitable temperature, followed by cooling. Solution heat treatment is the process of heating the metal well above the upper critical temperature and then quenching it in a medium such as oil or water. After solution treatment and quenching, hardening is achieved either at room temperature (natural ageing) or with a precipitation heat treatment (artificial ageing).

Heat treatment may be applied to Al-Si alloys for the purpose of improving their mechanical properties through a number of microstructural changes which take place as a function of the applied heat treatment parameters, i.e. temperature and time. The most prevalent heat treatment for industrial applications is the T6-treatment [94]. This technique involves three stages: solution heat treatment, quenching, and aging. These are discussed in the following subsections.

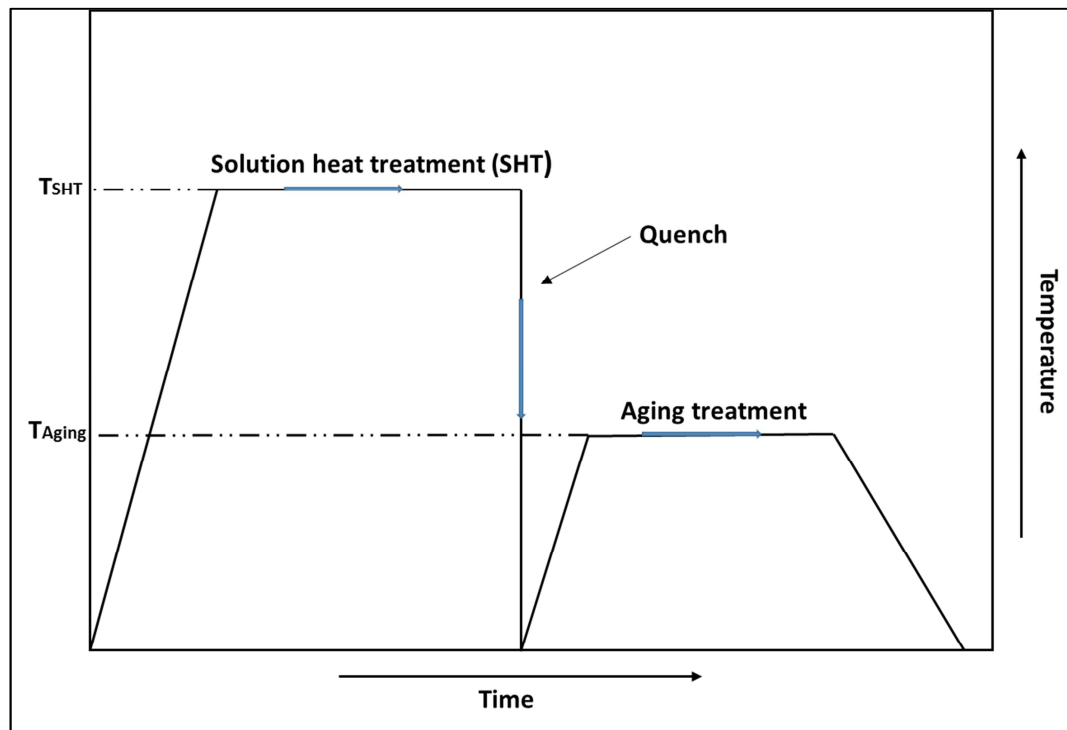


Figure 2.3 Schematic of the T6 heat treatment process.

2.5.1 Solution Heat Treatment

Solution heat treating is a process used to maximize the dissolution of alloying elements particularly strengthening elements such as Mg and Cu in solid solution to take advantage of precipitation hardening during subsequent aging treatment. The process consists of soaking the alloy at a sufficiently high temperature for a time long enough to achieve a nearly homogeneous solid solution. El Sebaie et al. [95] have reported that the

purpose of the solution heat treatment is to dissolve soluble phases formed during and after solidification so the alloying elements are homogenized.

The solution treatment process needs to be optimized because too short a solution treatment time means that not all alloying elements added will be dissolved and made available for precipitation hardening, while too long a solution treatment means using more energy than is necessary.

Solution treatment is carried out at a high temperature close to the solidus temperature of the alloy. Sjölander and Seifeddine [26] have reported that cast Al-Si-Mg alloys are solution treated at 540°C, while alloys containing copper are solution treated at a lower temperature due to the risk of local or incipient melting of Cu-containing phases. The solution temperature of Al-Si-Cu-Mg alloys is thus restricted to 495°C, to avoid such incipient melting of the copper-rich Al₂Cu phase [63]. The solution treatment time must be long enough to homogenize the alloy and to ensure a satisfactory degree of precipitates in solution [96]. In alloys containing high levels of copper, complete dissolution of the Al₂Cu phase is not usually possible. The solution time must then be chosen carefully to allow for the maximum dissolution of this phase, also keeping in mind that solution treatment for long times would be expensive and may not be necessary to obtain the required alloy strength. Moreover, the coarsening of the microstructural constituents and the possible formation of secondary porosity due to long time exposure at such temperatures could also have a harmful effect on the mechanical properties [97].

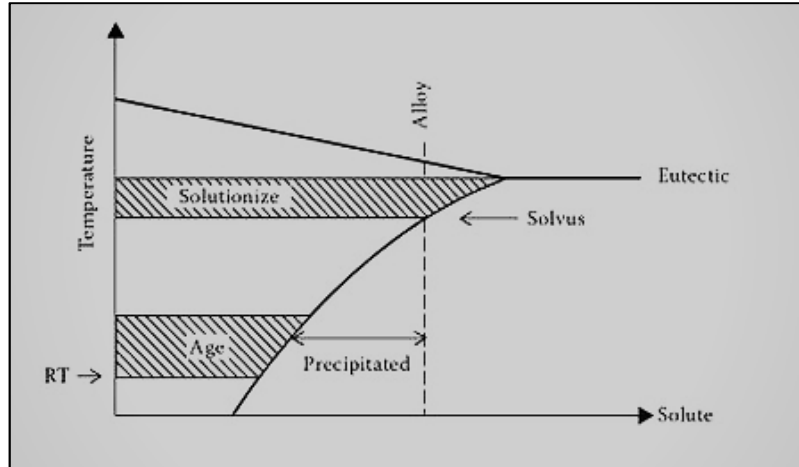


Figure 2.4 Schematic phase diagram of a heat-treatable alloy, showing temperature ranges for solutionizing and for aging and showing amount of solute precipitated during aging [98].

During the solution heat treatment, the eutectic silicon particles undergo changes in size and shape through a process of fragmentation and dissolution; these fragmented segments begin to spheroidize, thus reducing their stress concentration and preventing cracks from propagating in the matrix [47].

2.5.2 Quenching

After an alloy has been heated to a specified temperature, it is “quenched” or cooled rapidly, which “freezes” the alloying elements that were put in solid solution during solution treatment. The objective of quenching is to preserve the solid solution formed at the solution heat-treating temperature, by rapidly cooling to some lower temperature, usually near room temperature. The castings are quenched by rapid cooling to lower temperatures in water, oil, ambient air, or any other suitable quenching medium. In most instances, to avoid those types of precipitation that are detrimental to mechanical properties or to corrosion resistance, the quenching must be carried out rapidly enough without any interruption to produce supersaturated solution at room temperature. Because of a high level of supersaturation and a high diffusion rate for most Al-Si casting alloys at

temperatures between 450 °C and 200 °C, the quench rate is critical as, since the precipitates form rapidly, however, such problems as the formation of residual stresses and distortions of the castings which might accompany a very fast quenching rate need to be avoided [14]. At higher temperatures the supersaturation is too low and at lower temperatures the diffusion rate is too low for precipitation to be critical. The limiting quench rate is $\sim 4^{\circ}\text{C/s}$, above which the yield strength increases slowly with further increase in quench rate [97]. Quenching rate also has a great influence on the microstructure and properties of super high strength aluminum alloy, influencing the ultimate tensile strength and yield strength. With a decrease in the quenching rate, the strength of the samples decreases [99].

2.5.3 Age Hardening Treatment

Age hardening or precipitation hardening is a process that follows solution treatment and quenching where the castings are subjected to a specified temperature for a certain period of time. The age hardening occurs when castings are exposed to a certain temperature that allows the trapped alloying elements to diffuse through the microstructure and form intermetallic precipitates; these precipitates nucleate out of the solid solution and act as reinforcing phases.

Aging, for example, at $100^{\circ}\text{C} - 260^{\circ}\text{C}$ is called artificial aging because the alloy is heated to produce precipitation. Using a lower aging temperature provides properties that are more uniform. When heat-treated alloys are aged at room temperature it is called natural aging. The rate and amount of natural aging varies from one alloy to another. Properties of the alloys depend on the aging temperature and time. Typically, the hardness and strength of the alloy increases initially with time and the precipitate particle size until

it reaches the peak aging point, where maximum strength is obtained. With further aging, the strength and hardness decrease, or softening of the alloy occurs, corresponding to overaging conditions.

Cuniberti et al. [100] investigated the influence of natural aging on precipitation hardening of an Al–Mg–Si alloy by mechanical testing and quantitative transmission electron microscopy. They found that natural aging increases yield stress and reduces ductility, which is attributed to the formation of Mg/Si clusters, as was also confirmed by Mohamed and Samuel [97] in the review on the heat treatment of Al-Si-Cu/Mg casting alloys, in which the precipitation of Mg-rich phases was reported to depend on the Mg-to-Si ratio.

Wang and Jones [101] developed a non-isothermal aging process based on precipitation strengthening, computational thermodynamic and kinetics. The aging temperature varies with time so that the nucleation, growth and coarsening of precipitates can be controlled and optimized. With the non-isothermal aging scheme, the desired yield strength of aluminum alloys can be achieved with minimal time and energy. Table 2.2 lists the most common heat treatment designations that are used to produce desired features of aluminum alloys.

Table 2.2 Common aluminum heat treatment designations [14].

T4: Solution heat treated and naturally aged to a substantially stable condition	It is applied to products that are not cold worked after solution heat treatment, or in which the effect of cold work in flattening or straightening may not be recognized in mechanical property limits.
T5: Cooled from hot working and artificially aged (at elevated temperature)	Artificial aging treatment is carried out at temperatures above ambient, typically in the range of 150-200°C. This type of heat treatment is done at these relatively low temperatures to eliminate growth. They are also used to stabilize the castings dimensionally (improving mechanical properties somewhat) and to improve machinability.
T6: Solution heat treated, quenched and then artificially aged	It is applied to products that are not cold worked after solution heat treatment, or in which the effect of cold work in flattening or straightening may not be recognized in mechanical property limits.
T7: Solution heat treated and stabilized	It is applied to products that are stabilized after solution heat treatment to carry them beyond the point of maximum strength to provide control of some special characteristics.

2.6 MICROSTRUCTURE OF Al-Si-Cu-Mg ALLOYS

In cast aluminium-silicon alloys the primary silicon crystals are precipitated as individual faceted equiaxed crystals. The Si crystal lattice is A4, cubic, of diamond type. Each atom is bonded with four others with covalent bonds, forming a tetrahedron. Eight tetrahedrons form one elementary cell of A4 lattice, face centered, with four additional atoms from the center of each tetrahedron. When observed in polished sections, they appear in a multiplicity of shapes, suggesting the possible existence of a number of different growth mechanisms [102].

In hypoeutectic Al-Si alloys, the primary phase that precipitates is the α -Al dendritic phase, followed by the Al-Si eutectic, whereas in hypereutectic alloys, primary Si is the first phase to precipitate and appears in the form of polygonal particles, followed by the α -Al phase and the Al-Si eutectic. To improve the mechanical properties, the primary Si phase is normally refined using Cu-8% P master alloy, which forms AlP particles in the melt which act as nuclei for the precipitation of the primary Si, bringing about a refinement similar to that obtained with TiB_2 or TiAl_3 used for grain refining of the α -Al grains.

The size and morphology of the eutectic silicon in Al-Si alloys are also important parameters that influence the mechanical properties. The eutectic silicon precipitates as coarse acicular plates which act as internal stress raisers leading to a lowering in the mechanical properties, particularly ductility. Eutectic modification is a common process performed in Al-Si based foundry alloys primarily to improve mechanical properties, particularly tensile elongation, by promoting a structural refinement of the brittle eutectic Si phase by adding certain minor alloying elements such as sodium (Na) or strontium (Sr), upon which the eutectic Si undergoes a morphological transition from its brittle, acicular plate-like form to a fine fibrous form.

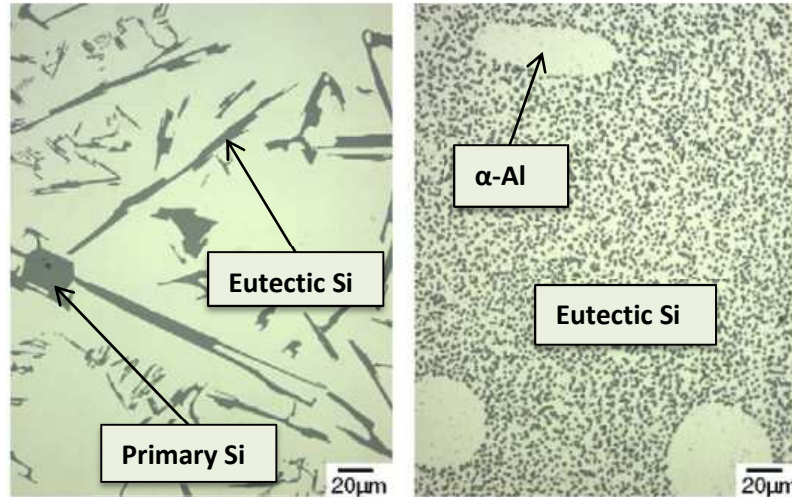


Figure 2.5 Comparison of the silicon morphology in: (a) unmodified and (b) Sr-modified (300 ppm Sr), near-eutectic aluminum-silicon alloys [103].

In Al–Si–Cu–Mg alloys, Cu and Mg are present as Al_2Cu and Mg_2Si respectively or as complex precipitates with the other elements in the alloy. Previous studies [8,68,104] have shown that beside the θ (Al_2Cu) and β (Mg_2Si) phases, there are other phases which exist in these alloys after aging, such as S (CuAl_2Mg) and Q ($\text{Al}_5\text{Cu}_2\text{Mg}_8\text{Si}_6$) phases. For such alloys, the temperature for solution treatment is usually limited to about 500 °C because higher temperatures lead to incipient melting of the copper-rich phases, lowering the mechanical properties of the casting [30].

Asghar and coworkers [105,106] have reported that adding Ni to Al-Si alloys forms nickel aluminides (Al_3Ni) and (Al_9FeNi) in the presence of iron. Copper combines with Ni forming different types of Cu–Ni aluminides such as Al_3CuNi , $\text{Al}_7\text{Cu}_4\text{Ni}$, which are thermally stable and cannot be dissolved during solution treatment [107]. Mohamed et al. [8] concluded that additions of Ni and Zr to 354 alloy result in the formation of high volume fractions of intermetallics such as Al_3NiCu and Al_9FeNi , and $(\text{Al,Si})_3(\text{Zr,Ti})$ respectively.

Manganese (Mn) is always present in aluminum alloys. It is added to control the morphology of the iron precipitates that form during solidification. Iron is traditionally considered as a harmful element in Al–Si alloys since coarse and brittle β -Al₃FeSi crystals may be formed as a primary phase when the Fe content is more than 0.5 wt. % [3]. During the solidification of Al–Si–Cu–Mg alloys, the β -Al₃FeSi phase is formed which is detrimental to the mechanical properties. Mn additions are used to transform the harmful iron intermetallics β phase to the less detrimental chinese script α -Al₁₅(Fe,Mn)₃Si₂ phase.

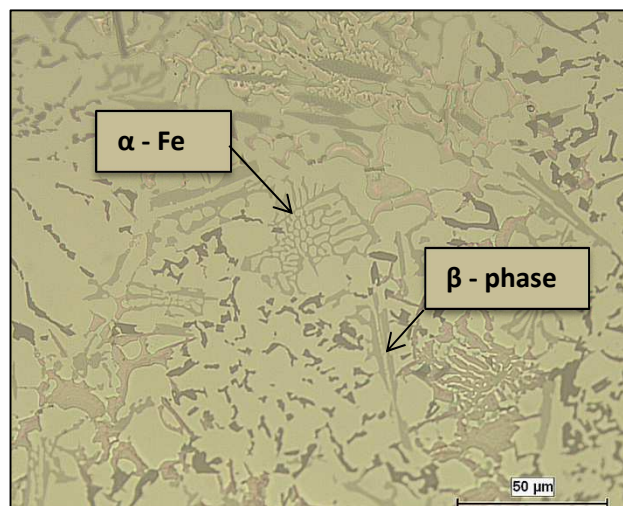


Figure 2.6 α -Fe and β -Fe intermetallic phases precipitated in Al 354 alloys.

2.7 MECHANICAL PROPERTIES OF Al-Si ALLOYS

The engineering tension test is widely used to provide basic design information on the strength of materials and as an acceptance test for the specification of materials. In the tension test, a specimen is subjected to a continually increasing uniaxial tensile force while simultaneous observations are made of the elongation of the specimen.

In tensile testing, a graph is drawn between load versus elongation which is converted after that into a stress-strain curve. A typical engineering stress-strain curve is shown in Figure 2.7. The shape and the magnitude of the stress-strain curve of a material

depends on its composition, solidification rate, heat treatment, strain rate, testing temperature and the state of stress imposed during the testing. The parameters which are used to describe the tensile properties from a stress-strain curve are the ultimate tensile strength (UTS), 0.2% offset yield stress (YS), percent elongation (%El) and reduction of area.

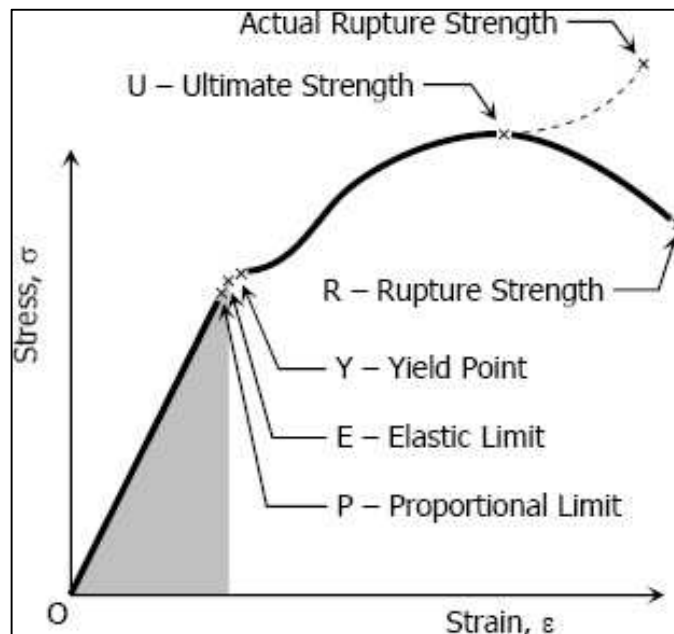


Figure 2.7 Stress-strain curve.

Tensile testing may be carried out at room temperature or at high temperatures. Elevated temperature tensile testing is a reliable process used to evaluate the behavior of materials when subjected to a combination of high heat and tension. High temperature testing is performed routinely in many industries for assessing high performance aluminum casting alloys and other materials that are exposed to high temperatures while in service, such as the engine components in a vehicle.

2.7.1 Effect of additives on high temperature mechanical properties of Al-Si-Cu-Mg alloys

The replacement of aluminum atoms with other alloying elements leads to the deformation or distortion of the lattice, such that the deformation increases at a higher alloying percentage. With the addition of more solute atoms, these distortions inhibit the movement of the dislocations and hence the mechanical properties are improved [108].

Merlin and Garagnani [91] studied the mechanical and microstructural characteristics of A356 alloy castings and observed that the loss of ductility, shock resistance and machinability in such alloys is usually due to the presence of iron.

Ouellet et al. [109] studied the aging behavior of 356 and 319 aluminum alloys. They found that the main parameters that control the mechanical properties are the iron and copper intermetallics, the eutectic silicon particle characteristics, the porosity size and distribution, and the supersaturation level of Mg and Cu in the α -Al matrix after solution heat treatment. The addition of Cu and Mg to Al-Si alloys can improve their room temperature strength by the formation of Mg_2Si and Al_2Cu precipitates [25,109]. The effect of precipitation hardening decreases when these alloys are exposed to temperatures above 150°C because of coarsening of the precipitates. The addition of transition elements such as Ni and Cu is considered to be effective for increasing the room and the high temperature strength of cast Al-Si alloys by forming stable aluminides. Mohamed et al. [8] reported that the ductility of Al-Si-Mg-Cu alloys strongly depends on the size, morphology and distribution of the eutectic silicon particles in the structure, as when the temperature increases, thermally activated cross slip occurs easily in the matrix which facilitates dislocation movement causing deterioration in the ultimate tensile strength as well as the

yield strength. Therefore, achieving a microstructure containing thermally stable and coarsening-resistant particles is preferable for improving the mechanical properties of aluminum casting alloys subjected to high temperature working conditions. Such a microstructure may be obtained provided two conditions are satisfied: first, the energy between the interfaces of the particles and the matrix should be low, and second, the solubility and the diffusion rate of the controlling element are minimal [60] and this shows that Zr is the appropriate element for this task, as it has the lowest diffusion rate in aluminum [110].

Nickel is an important alloying element for improving the high temperature strength of aluminum alloys. Nickel aluminides Al_3Ni and Al_9FeNi increase the elevated temperature strength of aluminum alloys [105]. Moulina et al. [38], observed improvements with the addition of Mn and Ni to their Al–Si–Cu–Mg base alloy, that resulted in an increase in strength and ductility at both room and high temperature. Asghar et al. [106] have reported that the elevated temperature strength of cast Al-Si alloys up to 400°C improved slightly with the addition of 0.6-1.96 wt.% of Ni. In some cases, however, further increasing the nickel level may decrease the overall tensile properties since the aluminides act as stress points, creating instability in the flow strain and leading to a decrease in ductility [102].

2.8 FRACTOGRAPHY

One of the most important and key concepts in understanding the mechanical behavior of materials is fracture. There are only two possible types of fracture, ductile and brittle. In general, the main difference between brittle and ductile fracture can be attributed to the amount of plastic deformation that the material undergoes before fracture occurs. Ductile materials undergo large amounts of plastic deformation while brittle materials show little or no plastic deformation before fracture. Figure 2.8 is a schematic representation of the degree of plastic deformation exhibited by both brittle and ductile materials before fracture.

Crack initiation and crack propagation are essential to fracture. The manner in which the crack propagates through the material gives great insight into the type of fracture that will occur. In ductile materials, the crack moves slowly and is accompanied by a large amount of plastic deformation. The crack will usually not extend unless an increased stress is applied. On the other hand, in dealing with brittle fracture, cracks spread very rapidly with little or no plastic deformation. There are two types of cracking, inter-crystalline cracking and trans-crystalline cracking; the latter depends on the size, shape, and orientation of the particle, and activation of the dislocation source, whereas an inter-crystalline crack can be observed on the fracture surface.

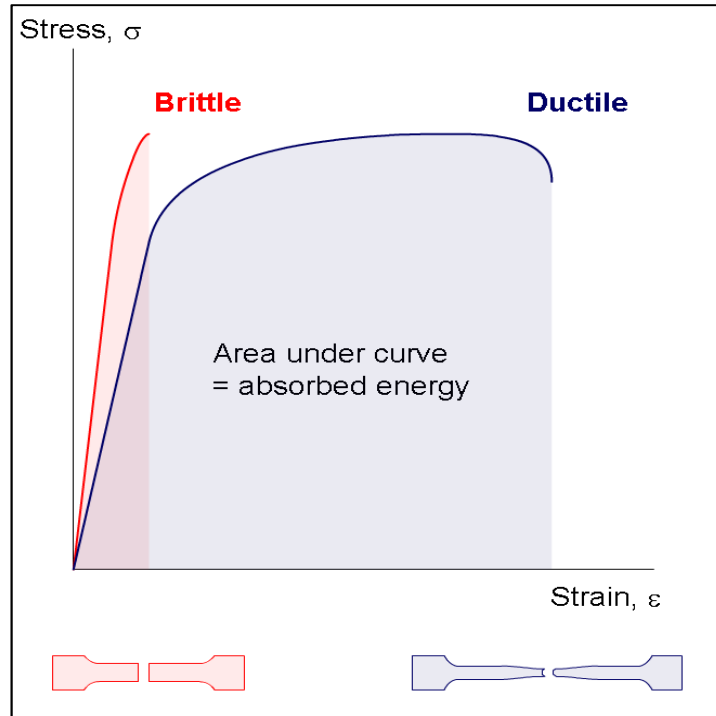


Figure 2.8 Schematic diagram showing brittle vs ductile stress-strain behavior [111].

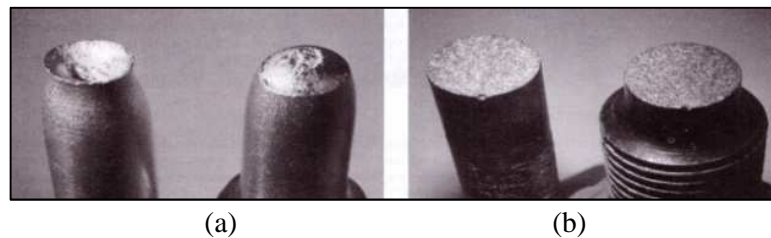


Figure 2.9 Photographs showing (a) ductile vs (b) brittle specimens.

Macroscopically, ductile fracture surfaces have larger necking regions and an overall rougher appearance than a brittle fracture surface. Figure 2.9 shows the macroscopic differences between the ductile and brittle specimens. On the microscopic level, electron images of the fracture surface are obtained using scanning electron microscopy (SEM), as shown in Figure 2.10. A ductile fracture surface is characterized by dimples, the size of which is governed by the number and the distribution of the nucleated micro-voids. Figure 2.10(a) shows an example of the simple dimpled rupture mode of fracture, where particles are observed at the bottom of the dimples. The decohesion of the

particles from the surrounding matrix results in the dimpled appearance of the fracture surface. Figure 2.10(b) shows a brittle fracture surface, where fracture occurs through the cleavage or cracking of brittle particles in the matrix.

The overall appearance of the fracture surface depends not only on the matrix (α -Al phase) but also on the size and shape of the other phases present in the structure. In Al-Si cast alloys, silicon particles have a significant effect on the fracture behavior as they are more brittle than the aluminum matrix. The morphology of these microstructural components (α -Al phase, eutectic silicon and intermetallic phases) will also influence the nature of the fracture surface [112]. For example, there are intermetallic compounds such as those of nickel and zirconium which play an important role in the fracture process [8]. Other microstructural parameters, such as the dendrite arm spacing and the iron intermetallics and other constituents present in the structure would also be expected to influence the fracture characteristics.

Wang [113] reported that in A356 alloys damage is initiated by the cracking of eutectic silicon and Fe-rich intermetallic particles due to the development of internal stresses in the particles during plastic deformation. The main factors that affect particle cracking include particle size, particle aspect ratio, the extent of particle clustering, and the stresses on the particles. Increasing particle size increases the probability of fracture.

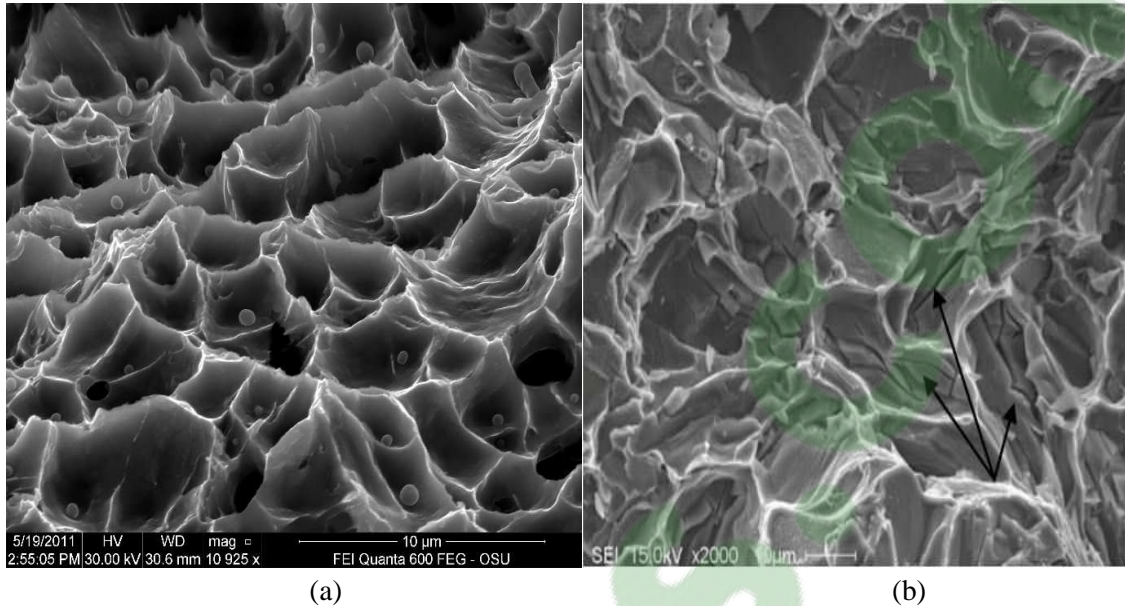


Figure 2.10 SEM images showing (a) a ductile fracture surface exhibiting a dimpled structure, and (b) a brittle fracture surface, showing how fracture occurs through the cracking of particles (arrowed).

Apart from SEM fractography, it is also useful to examine the fracture profile on sections perpendicular to the fracture surface. This can be carried out on a polished section of the fractured sample using an optical microscope, and allows us to determine if any microstructural defects contributed to fracture initiation, as well as determine the nature of the fracture path and whether it is specific to any phase or constituent present in the microstructure [114].

2.9 QUALITY CHARTS

The quality of aluminum casting alloys is considered to be one of the critical factors controlling the selection of an alloy for a specific application. Metallurgical variables which influence the alloy quality include alloy composition, solidification rate, heat treatment, casting defects and other microstructural features such as grain size and intermetallic phases. The quality of an alloy is a reference to its tensile properties (tensile

strength and ductility) and can also provide an indication to the overall performance of the alloy, in terms of possible risk and cost efficiency factors involved in applying different heat treatments to achieve the desired properties.

The quality of aluminum alloy castings may be defined using the quality index Q which provides a correlation to the mechanical properties. Drouzy et al. [115] first proposed the concept of quality index in 1980 in relation to their investigations of the tensile properties of Al-7%Si-Mg alloys containing different levels of Mg, and defined Q in terms of the following equation:

$$Q = R_m + d \cdot \log(A_f) \quad [1]$$

In Eq. [1], R_m stands for the ultimate tensile strength in MPa, A_f stands for the elongation to fracture in pct, and d is an empirical coefficient in MPa chosen such as to make Q practically independent of the aging condition. For the investigated Al-7%Si-Mg or 356 alloys, the coefficient d has been determined to be 150 MPa. The probable yield strength R_p of an Al-Si-Mg alloy may be assessed by the equation:

$$R_p = a \cdot R_m - b \cdot \log(A_f) + c \quad [2]$$

where a , b , and c are alloy-dependent empirically determined coefficients. From the above equations, a quality chart can be generated, as shown in Figure 2.11. In a typical quality chart, which is a diagram of the ultimate tensile strength vs the logarithm of the elongation to fracture, Eqs. [1] and [2] represent sets of parallel lines termed *iso-Q* and *iso-YS* lines, respectively; they fit the experimentally obtained Q and R_p values resulting from variations in chemical composition, solidification conditions, and heat treatment of Al-Si-Mg aluminum alloys with a good approximation. Such charts are therefore very useful in

selecting alloys for specific applications and understanding how the properties may be manipulated to achieve the desired specifications.

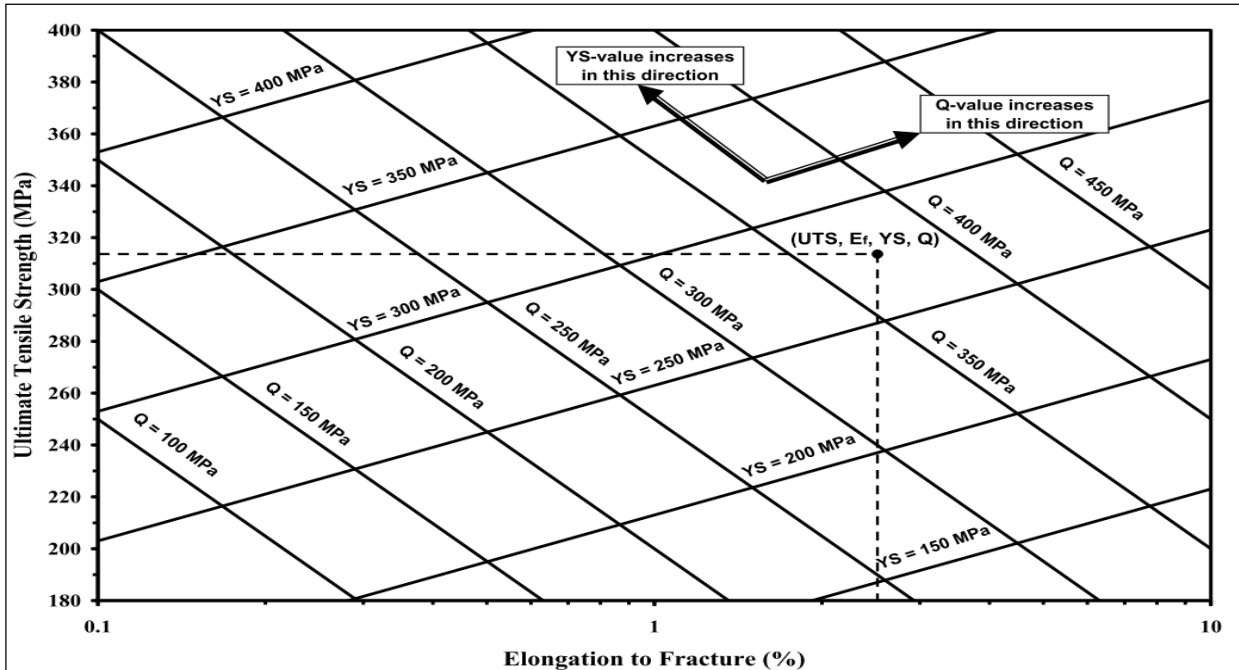


Figure 2.11 Example of the quality chart proposed by Drouzy et al. [115] with *iso-Q* and *iso-YS* lines generated using Equations 1 and 2.

Although the quality index concept was developed for Al-Si-Mg 356 and 357 alloys, it has been applied to other alloy systems including Cu-containing 319 type alloys [116], Mg-base alloys [117], particle-reinforced 359 alloys [118], and an Al-Cu-Mg-Ag alloy [119]. While the application of the quality index to these other alloy systems implies that they would show a similar response to aging as the 356 or 357 alloys, and that the empirical parameters in Eqns. [1] and [2] would be the same, it has been found that in contrast to the linear behavior of 356 alloys, UTS vs %El plots for the Al-Si-Cu-Mg 319 alloys and the Al-Cu-Mg-Ag follow a circular contour when the alloys are aged. This implies that in order to extend the quality index to other alloy systems, the strength-ductility relationship behavior must be determined beforehand [120].

CHAPTER 3

EXPERIMENTAL PROCEDURES

CHAPTER 3

EXPERIMENTAL PROCEDURES

3.1 INTRODUCTION

The present chapter will provide all the details relevant to the 354-Al-9%Si-1.8%Cu-0.5%Mg casting alloy with regard to general melting and casting procedures, heat treatment, the various techniques used for microstructural characterization and phase identification, namely optical microscopy, scanning electron microscopy (SEM) and field-emission scanning electron microscopy (FESEM), as well as the tensile testing method used to determine the mechanical properties. Apart from the analysis of microstructures obtained from tensile test samples, further elaboration of the microstructure involves thermal analysis, which is a method for identifying the main phase reactions related to the solidification of the alloys studied. The alloy codes for the various alloys which were prepared are collectively listed in Table 3.2.

The processes described herein were carried out with the intention of investigating and viewing the effect of additions of nickel, zirconium, manganese and scandium on the mechanical properties of the 354 cast aluminum alloy at different temperatures.

The study was carried out in two parts according to the temperature at which the tensile testing was carried out:

- Ambient Temperature Tensile Testing
 1. No stabilization.

2. 200 hours stabilization at 250°C.
- High Temperature Tensile Testing
 1. One hour stabilization at 250°C.
 2. 200 hours stabilization at 250°C.

3.2 CLASSIFICATION OF ALLOYS

The alloys were classified according to the alloying elements additions made to the base 354 alloy. For comparison purposes with the 354 alloy, a 398 alloy - reported to show good high temperature properties - was also prepared, using the same Zr and Sc additions.

1. Alloy R (354 + 0.25%Zr) - Base Alloy
2. Alloy S (354 + 0.25%Zr + 2%Ni)
3. Alloy T (354 + 0.25%Zr + 4%Ni)
4. Alloy U (354 + 0.25%Zr + 0.75%Mn)
5. Alloy V (354 + 0.25%Zr + 0.75%Mn + 2%Ni)
6. Alloy Z (354 + 0.25%Zr + 0.15%Sc)
7. Alloy L (398 + 0.25%Zr + 0.15%Sc)

3.3 MELTING AND CASTING PROCEDURES

The chemical composition of the 354 base alloy used for this study is listed in Table 3.1. The alloy ingots were cut into smaller pieces, dried and melted in a 120-kg capacity SiC crucible, using an electrical resistance furnace, as shown in Figure 3.1. The melting temperature was maintained at $750 \pm 5^\circ\text{C}$. All the 354 alloy melts prepared were grain refined and modified using Al-5%Ti-1%B and Al-10%Sr master alloys, respectively, to obtain levels of 0.2% Ti and 200 ppm Sr in the melt. Additions of Ni, Zr, Mn and Sc

were in the form of Al-20wt% Ni, Al-20wt% Zr, Al-25wt% Mn and Al-2wt% Sc master alloys, respectively. The melts were degassed for ~15-20 min with a rotary graphite impeller rotating at ~130 rpm, using pure dry argon, as shown in Figure 3.2. Following this, the melt was carefully skimmed to remove oxide layers from the surface.

Table 3.1 Chemical composition of the as-received 354 alloy.

Element (wt. %)					
Si	Fe	Cu	Mn	Mg	Al
9.1	0.12	1.8	0.0085	0.6	87.6



Figure 3.1 Electrical resistance furnace.



Figure 3.2 Graphite degassing impeller.

The melt was poured into an ASTM B-108 permanent mold preheated at 450°C to drive out moisture, in order to prepare the tensile test bars, as shown in Figure 3.3. Each casting provides two test bars, with a gauge length of 70 mm and a cross-sectional diameter of 12.7 mm, as shown in Figure 3.4. Three samplings for chemical analysis were also taken simultaneously at the time of the casting. These were carried out at the beginning, middle and end of the casting process to ascertain the exact chemical

composition of each alloy. The chemical analysis was carried out using a Spectrolab JrCCD Spark Analyzer, and shows the actual chemical compositions of the alloys produced.



Figure 3.3 ASTM B-108 permanent mold used for casting tensile test bars.

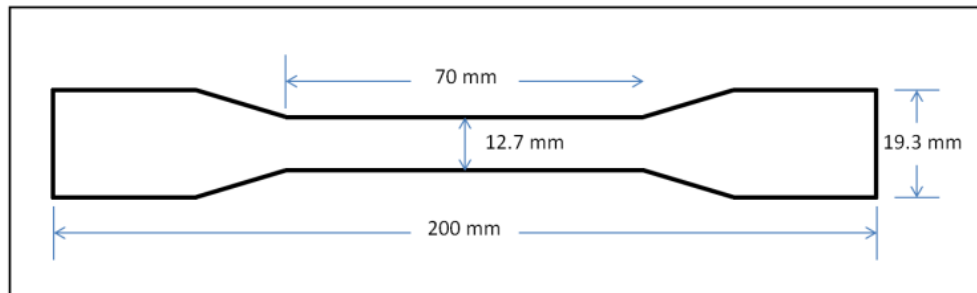


Figure 3.4 Dimensions of the tensile test bar (in mm).

Table 3.2 lists the chemical compositions of the various alloys obtained from the samplings for chemical analysis, taken from the associated melts, and their corresponding codes.

Table 3.2 Chemical composition of the alloys used in this study.

Alloy/ Element	Si	Fe	Cu	Mn	Mg	Ti	Sr	Ni	Zr	Sc	Al
R	8.70	0.20	1.95	0.02	0.73	0.15	0.0143	~	0.25	~	Bal.
S	9.08	0.19	1.88	0.02	0.83	0.16	0.0170	2.0	0.25	~	Bal.
T	8.92	0.18	1.88	0.02	0.78	0.15	0.0175	4.0	0.25	~	Bal.
U	8.85	0.20	1.88	0.75	0.76	0.14	0.0168	~	0.25	~	Bal.
V	8.85	0.20	1.88	0.75	0.76	0.14	0.0168	2.0	0.25	~	Bal.
Z	8.95	0.19	1.87	0.03	0.77	0.14	0.0185	~	0.25	0.15	Bal.
L	16	0.19	1.87	0.03	0.77	0.14	0.0185	~	0.25	0.15	Bal.

3.4 HEAT TREATMENT

Tensile test bars of alloys R, S, T, U, V and Z were heat treated under different conditions, as follows.

- SHT 1: Solution heat treatment at 495°C/5h, following which the test bars were kept in a refrigerator to preserve their properties until the time of testing.
- SHT 2: Multi-step solution heat treatment comprising: 495°C/5h, then 515°C/2h, then 530°C/2h, following which the test bars were kept in a refrigerator to preserve their properties until time of testing.
- T5: Artificial aging treatment only, carried out at 180°C/8h.
- T6: Solution heat treatment at 495°C/5h, followed by quenching in warm water at 60°C, and then artificial aging at 180°C/8h.

- T62: Multi-step solution heat treatment comprising: 495°C/5h, then 515°C/2h, then 530°C/2h, followed by quenching in warm water at 60°C, and then artificial aging at 180°C/8h.
- T7: Solution heat treatment at 495°C/5h, followed by quenching in warm water at 60°C, and then artificial aging at 240°C/4h.

Time was a variable in the precipitation hardening treatment. In all of the heat treatment stages, the soaking time did not begin to be counted until the furnace reached the desired temperature. After aging, the test bars were allowed to cool naturally at room temperature (25°C). A summary of the different conditions used for both the room- and high-temperature tensile testing is presented in Table 3.3. All heat treatments were carried out in a Lindberg Blue M electrical resistance furnace, as shown in Figure 3.5.



Figure 3.5 Lindberg Blue M electric furnace.

Table 3.3 Summary of the heat treatment and testing conditions at room and high temperatures.

Testing Conditions																						
Alloys	Room temperature												High temperature (250°C)									
	Without stabilization							200h@250°C stabilization					1h@250°C stabilization					200 h@250°C stabilization				
R	As Cast	SHT 1	SHT 2	T5	T6	T62	T7	As Cast	T5	T6	T62	T7	As Cast	T5	T6	T62	T7	As Cast	T5	T6	T62	T7
S	As Cast	SHT 1	SHT 2	T5	T6	T62	T7	As Cast	T5	T6	T62	T7	As Cast	T5	T6	T62	T7	As Cast	T5	T6	T62	T7
T	As Cast	SHT 1	SHT 2	T5	T6	T62	T7	As Cast	T5	T6	T62	T7										
U	As Cast	SHT 1	SHT 2	T5	T6	T62	T7	As Cast	T5	T6	T62	T7	As Cast	T5	T6	T62	T7	As Cast	T5	T6	T62	T7
V	As Cast	SHT 1	SHT 2	T5	T6	T62	T7	As Cast	T5	T6	T62	T7										
Z	As Cast	SHT 1	SHT 2	T5	T6	T62	T7						As Cast		T6		T7	As Cast		T6		T7
L	As Cast				T6								As Cast		T6			As Cast		T6		

3.5 TENSILE TESTING

All samples for ambient temperature testing, whether as-cast, solution heat-treated or aged, were tested to the point of fracture using an MTS Servohydraulic mechanical testing machine at a strain rate of $4 \times 10^{-4} \text{ s}^{-1}$, as shown in Figure 3.6(a). An extensometer, or strain gage, was used in the tests to measure the extent of deformation in the samples. Yield strength (YS) at 0.2% offset strain, ultimate tensile strength (UTS), and percent elongation (%El) were obtained from the data acquisition system of the machine. Five samples from each condition covered in this part of the study were tested, for a total of 345 bars covering all alloys.

For testing of the alloys at high temperature, the samples were mounted in the testing chamber which was pre-set to the required temperature, as shown in Figure 3.6(b). After mounting, the sample was maintained at the testing temperature for 30 min before starting the test. As before, five test bars were used for each alloy composition/condition studied for all high temperature tests carried out. The average UTS, YS and %El values obtained from each set of five tests were considered as representing the tensile properties of that alloy/condition. A total of 200 bars were tested for this part of the study.



(a)



(b)

Figure 3.6 (a) MTS mechanical testing machine for room temperature testing, and (b) Instron Universal mechanical testing machine for high temperature testing.

3.6 CHARACTERIZATION OF MICROSTRUCTURE

The aim of characterizing the microstructure of the 354 alloys was to correlate the microstructural features of these alloys with their tensile properties as well as with their quality indices. Several techniques were used in this regard for obtaining a qualitative and quantitative analysis of the microstructural constituents and features, namely, intermetallic phases, hardening precipitates and fracture surface characteristics observed in each case.

3.6.1 Thermal Analysis

In order to obtain the cooling curves and to identify the main reactions and corresponding temperatures occurring during the solidification of 354 alloys, thermal analysis of the alloy melt compositions was carried out. Ingots of the as-received commercial 354 alloy were cut into smaller pieces, cleaned, and then dried to prepare the required alloys. The melting process was carried out in a cylindrical graphite crucible of 2-kg capacity, using an electrical resistance furnace. The melting temperature was

maintained at 780°C, while the alloys were grain-refined by adding 0.2%Ti as Al-5%Ti-1%B master alloy in rod form and modified by adding 200 ppm Sr in the form of an Al-10%Sr master alloy. Nickel, zirconium, manganese and scandium were added to the melts in the form of Al-20wt%Ni, Al-20wt%Zr, Al-25wt%Mn and Al-2wt%Sc master alloys, respectively, as was the case with the casting of the tensile test samples. For the purpose of determining the reactions taking place during solidification, part of the molten metal was also poured into an 800 g capacity graphite mold preheated to 650°C so as to obtain near-equilibrium solidification conditions at a cooling rate of 0.35 °C s⁻¹. A high sensitivity Type-K (chromel-alumel) thermocouple, insulated using a double-holed ceramic tube, was attached to the centre of the graphite mold. The temperature-time data was collected using a high speed data acquisition system linked to a computer system that recorded the data every 0.1 second, as shown in Figure 3.7 and Figure 3.8.

From this data, the cooling curves and the corresponding first derivative curves for a number of selected alloys were plotted so as to identify the main reactions occurring during solidification with the corresponding temperatures; the various phases which constituted the microstructure of each alloy were expected to be revealed as well.

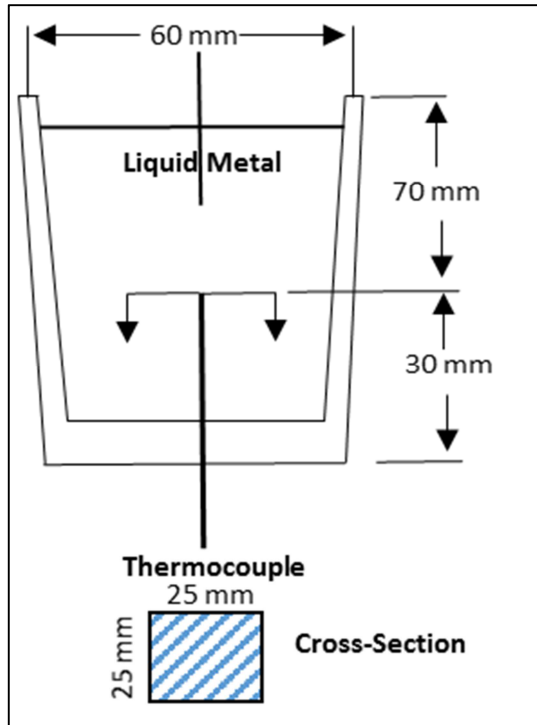


Figure 3.7 Schematic drawing showing the graphite mold used for thermal analysis.



Figure 3.8 Thermal analysis set-up.

3.6.2 Optical Microscopy

Samples for metallography were sectioned from the tensile-tested bars of selected conditions alloy studied, approximately 10 mm below the fracture surface, as shown in

Figure 3.9. The samples were individually mounted and then subjected to grinding and polishing procedures to produce a mirror-like surface. The mounting of the samples in bakelite was carried out using a Struers LaboPress-3 machine, while the grinding and polishing procedures were carried out using a TegraForce-5 machine, as shown in Figure 3.10. The grinding procedures were applied using silicon carbide (SiC) abrasive papers in a sequence of 120 grit, 240 grit, 320 grit, 400 grit, 800 grit and 1200 grit sizes. It should be noted that the word “grit” is used to represent a measure of fineness for abrasive materials and that water was used as a lubricant in this stage.

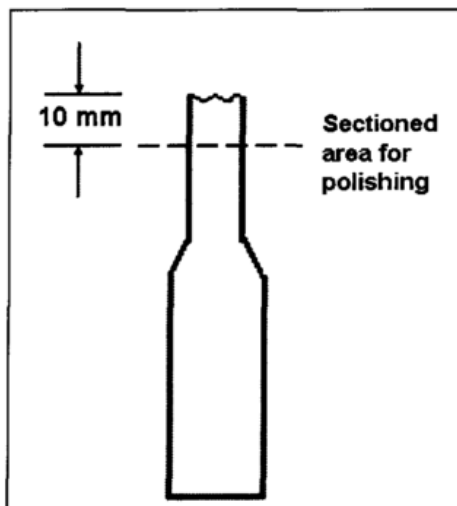


Figure 3.9 Diagram showing the sectioned area for analysis of tensile samples using optical microscopy.

Polishing was carried out using Struers diamond-suspension, with a diamond particle size of $6\ \mu\text{m}$, as the first step of the polishing process followed by further polishing through the application of a finer suspension containing a smaller diamond particle size of $3\ \mu\text{m}$. The lubricant used for this polishing stage is a Struers DP-lubricant. The final stage of polishing was carried out using a Mastermet colloidal silica suspension, SiO_2 , having a particle size of $0.6\ \mu\text{m}$. Water was used as lubricant throughout the final polishing stage,

after which the samples displayed a mirror-like surface and were ready for microstructural examination.

The microstructures of the polished sample surfaces were examined using an Olympus PMG3 optical microscope linked to a Clemex Vision P image-analysis system, as shown in Figure 3.11.



Figure 3.10 Struers LaboPress-3 and TegraForce-5 machines for mounting and polishing of metallography samples.



Figure 3.11 Clemex Vision PE 4.0 image analyzer-optical microscope system.

3.6.3 Scanning Electron Microscopy

Scanning electron microscopy (SEM) and field-emission scanning electron microscopy (FESEM) techniques were used to examine the characteristics of the hardening precipitates under various heat treatment conditions for the 354 alloys. The purpose of using these techniques of microscopic analysis was mainly to assess the distribution, size and density of the hardening precipitates in the casting structure under the various aging temperatures and times involved. The SEM used in the current study was a JEOL 840A scanning electron microscope attached to an EDAX Phoenix system designed for image acquisition and energy dispersive x-ray spectroscopy (EDS). The SEM was operated at a voltage of 15 kV, with a maximum filament current of 3 micro amperes. Figure 3.12 shows a photograph of the SEM used. The FESEM provides clear and less electrostatically distorted high resolution images even at low voltages; it produces images of 2.1 nm resolution at 1 kV and of 1.5 nm resolution at 15 kV. The FESEM used in this study was the Hitachi-S-4700 FEGSEM shown in Figure 3.13.



Figure 3.12 Scanning electron microscope system used in this study.



Figure 3.13 Field emission scanning electron microscope used in this study.

CHAPTER 4

MICROSTRUCTURE CHARACTERIZATION AND

POROSITY FORMATION

CHAPTER 4

MICROSTRUCTURE CHARACTERIZATION AND POROSITY FORMATION

4.1 INTRODUCTION

This chapter is divided into two main parts. The first part presents the results obtained on the effect of different alloying element additions such as iron, copper, magnesium, zirconium, nickel, manganese, and scandium, individually and/or in combination on the microstructure and phases precipitated during solidification of the 354 aluminum alloys studied using the thermal analysis technique which provides close-to-equilibrium cooling rate conditions. The second part of this chapter presents the porosity formation observed in these same alloys. The alloy samples investigated in this part include the as-cast and solution heat-treated conditions, covering both one and multi-step solution heat treatments.

For purposes of recapitulation, Section 3.2 lists the Alloy Codes and corresponding additives of the 354 alloys presented in this chapter.

4.2 THERMAL ANALYSIS

From the thermal analysis data, the solidification curve and the first derivative curve were plotted for each alloy condition. These curves and the corresponding optical microstructures are presented in Figure 4.1 through Figure 4.14. The reactions expected to occur (marked 1 through 8 in the thermal analysis plots) are listed in Table 4.1, and were

identified with reference to the atlas of Backerud et al. [121] on the solidification of aluminum foundry alloys. The four main reactions observed correspond to the formation of the α -Al dendrite network (peak 1), followed by the precipitation of the Al-Si eutectic (peak 2), and the precipitation of the copper intermetallic phases (peaks 6 and 7).

Table 4.1 Suggested main reactions occurring during solidification of 354-type alloys [122].

Reaction	Suggested Temperature Range (°C)	Suggested Precipitated Phase
1- Al	600-597	- Formation of α -Al dendritic network
2- Al-Si, β -Fe and α -Fe	560-558	- Precipitation of Al-Si eutectic phase - Precipitation of post-eutectic β -Al ₅ FeSi phase - In case of presence of Mn, precipitation of α -Al ₁₅ (Mn,Fe) ₃ Si ₂ phase
3- Fe-Ni	555-556	- Precipitation of Al ₉ FeNi phase
4- Mg-Si	540-538	- Precipitation of Mg ₂ Si phase
5- π -phase	525-523	- Transformation of β -Al ₅ FeSi phase to π -Al ₈ Mg ₃ FeSi ₆ phase
6- Al-Cu-Ni	523-520	- Precipitation of Al ₃ CuNi phase
7- Al-Cu	500-496	- Formation of eutectic Al-Al ₂ Cu phase
8- Q-phase	485-489	- Precipitation of Q-Al ₅ Mg ₈ Cu ₂ Si ₆ phase

The mechanism involved in Al₂Cu precipitation was proposed by Samuel et al. [123] as follows: (a) during the first stages of solidification, the formation of the α -Al dendritic network is associated with the segregation of Si and Cu in the melt, ahead of the progressing dendrites; (b) when the solidification temperature approaches the eutectic temperature, Si particles precipitate, leading to a local concentration of Cu in the remaining areas, and because of this segregation, the Al₂Cu phase more often than not precipitates in

the block like form rather than in the fine eutectic form. Magnesium also led to the precipitation of the $\text{Al}_5\text{Mg}_8\text{Cu}_2\text{Si}_6$ and Mg_2Si phases, and to the splitting of the copper phase formation temperature range into two explicit peaks representing the precipitation of Al_2Cu and $\text{Al}_5\text{Mg}_8\text{Cu}_2\text{Si}_6$ phases.

4.2.1 Alloy R (354 + 0.25%Zr)

Figure 4.1 shows the solidification curve and its first derivative obtained from the thermal analysis of Alloy R *i.e.*, 354 alloy with 0.25 wt% Zr addition. Several reactions take place during the course of solidification, as marked by the different numbers on the first derivative curve. These numbers correspond to the reactions listed in Table 4.1. As may be seen from the figure, alloy R starts to solidify at 598°C (Reaction 1) with the development of the α -Al dendritic network, followed by the precipitation of the Al-Si eutectic (Reaction 2) at 560°C , the Mg_2Si phase (Reaction 4) at 540°C , and the transformation of β -phase into π - $\text{Al}_8\text{Mg}_3\text{FeSi}_6$ phase (Reaction 5) at 525°C ; following which the Al_2Cu and Q- $\text{Al}_5\text{Mg}_8\text{Cu}_2\text{Si}_6$ phases precipitate as the last reactions (Reactions 7 and 8) at 498°C and 488°C , respectively, toward the end of solidification. In Zr-containing alloys, Al_3Zr particles may appear in various forms as square, rectangular or rounded. These particles act as nucleation sites for Zr- and Sc-rich intermetallics. As a result of the low cooling rate of the thermal analysis castings, and a Zr content of 0.25 wt%, all Zr-containing alloys are located in the L + Al_3Zr region of the Al-Zr phase diagram during the melting stage. Thus the coarse Al_3Zr particles observed in the microstructure come directly from the master alloy added to the melt. These particles do not dissolve in the melt and provide nucleation sites for the formation of Zr-, Sc-, and Ti-intermetallics from the melt during solidification [124,125]. Apart from the α -Al dendrites and the eutectic Si particles

observed in the interdendritic regions, $(Al, Si)_3(Ti, Zr)$ phase particles may also be observed in the optical micrograph of the corresponding sample, as shown in Figure 4.2.

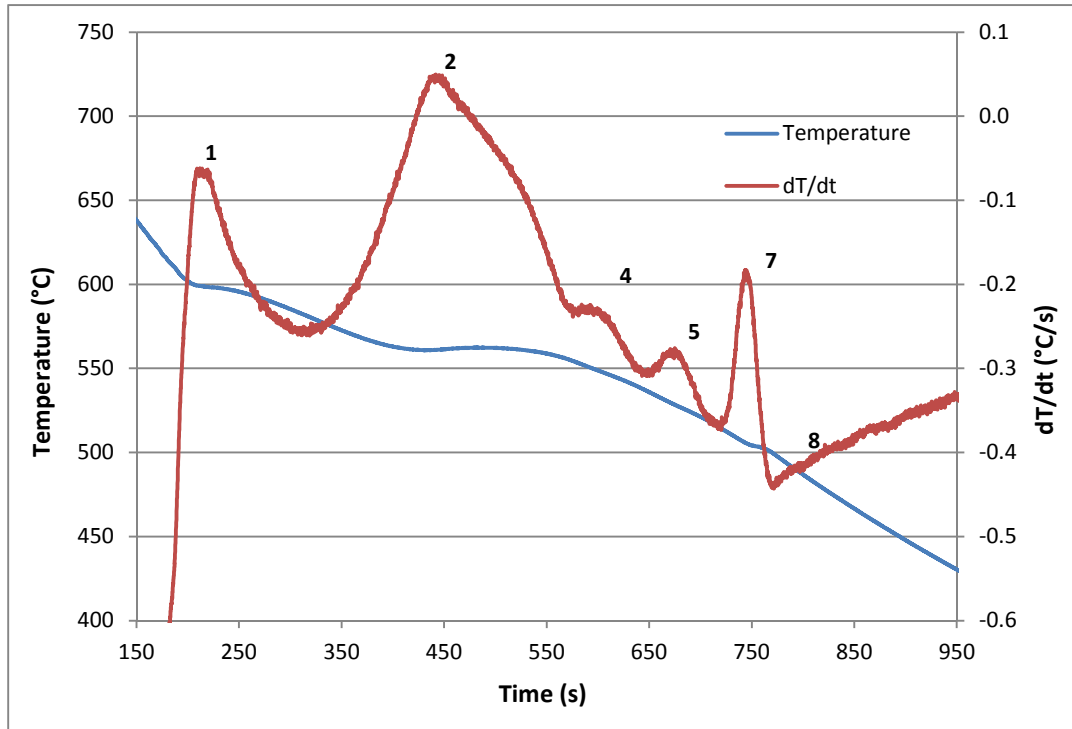


Figure 4.1 Temperature-time plot and first derivative obtained from the thermal analysis of Alloy R (354 + 0.25% Zr).

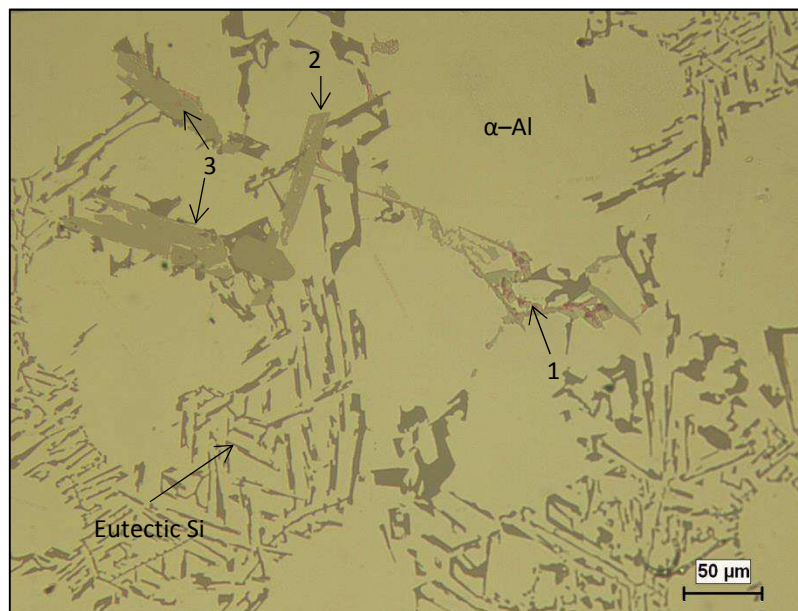


Figure 4.2 Optical microstructure of R (354 + 0.25% Zr) alloy sample obtained from the thermal analysis casting (cooling rate $0.35^{\circ}C/s$), showing the different phases present in the alloy: 1- Al_2Cu ; 2- $AlMgCuSi$; 3- $AlZrTi$.

4.2.2 Alloy S (354 + 0.25%Zr + 2%Ni)

The thermal analysis results for Alloy S *i.e.*, 354 alloy containing 2 wt% Ni + 0.25 wt% Zr are plotted in Figure 4.3. The presence of Ni results in the precipitation of Ni-containing phases, represented by the Reactions 3 and 6 as noted on the first derivative curve. In addition, due to the presence of Zr and Fe in Alloy S, another precipitate is formed, namely, AlSiNiZrFe besides the AlFeNi phase.

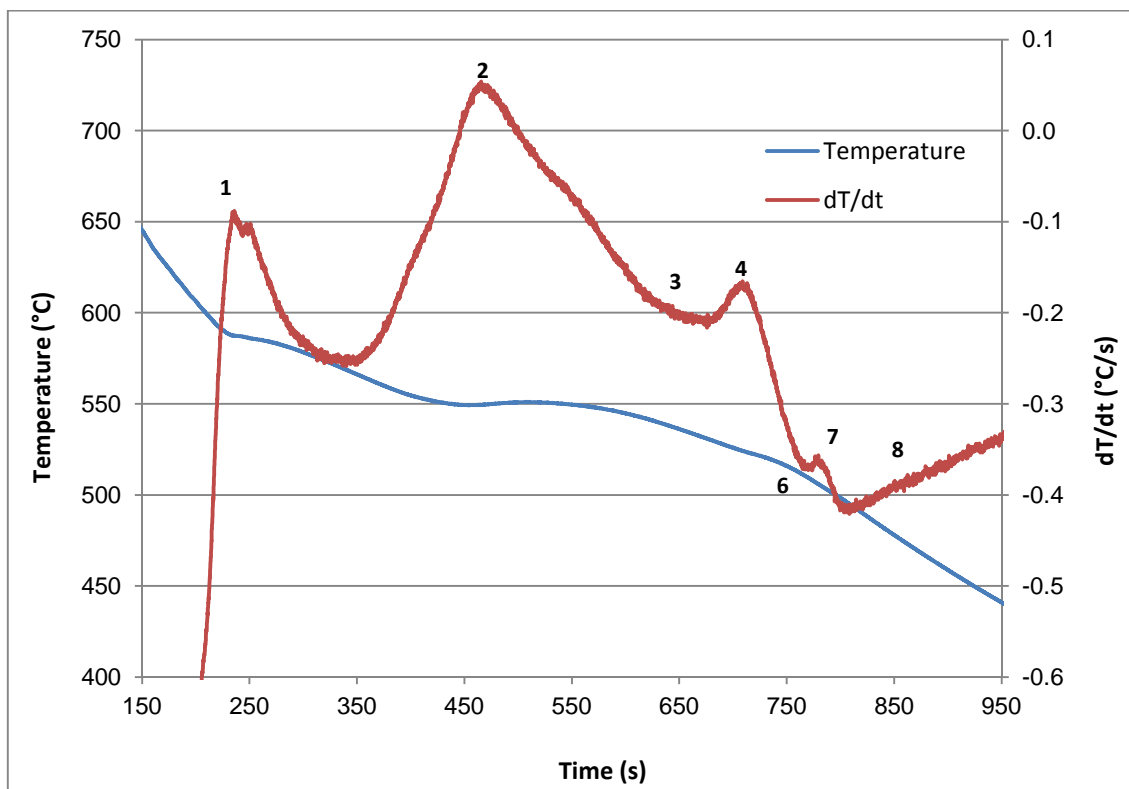


Figure 4.3 Temperature-time plot and first derivative from the thermal analysis of Alloy S (354 + 2% Ni + 0.25% Zr).

The presence of the Q-Al₅Mg₈Cu₂Si₆ and Mg₂Si phases under the low solidification rate conditions of the thermal analysis experiment primarily depends on the Mg content. Although the Q-phase and Mg₂Si phase reactions were observed in the first derivative curve of alloy R, the proportion of Mg₂Si formed increased as the Mg level increased, as evidenced by Figures 4.3 and 4.4 in the case of Alloy S. It is also interesting to note from

Figure 4.4 that, in alloy S, the Al_3CuNi phase is observed situated adjacent to the Al_2Cu phase and both phases are located at the limits of the dendritic $\alpha\text{-Al}$ phase; this observation is in agreement with the fact that the reactions noted in the thermal analysis curves, namely Reactions 6 and 7, appear consecutively.

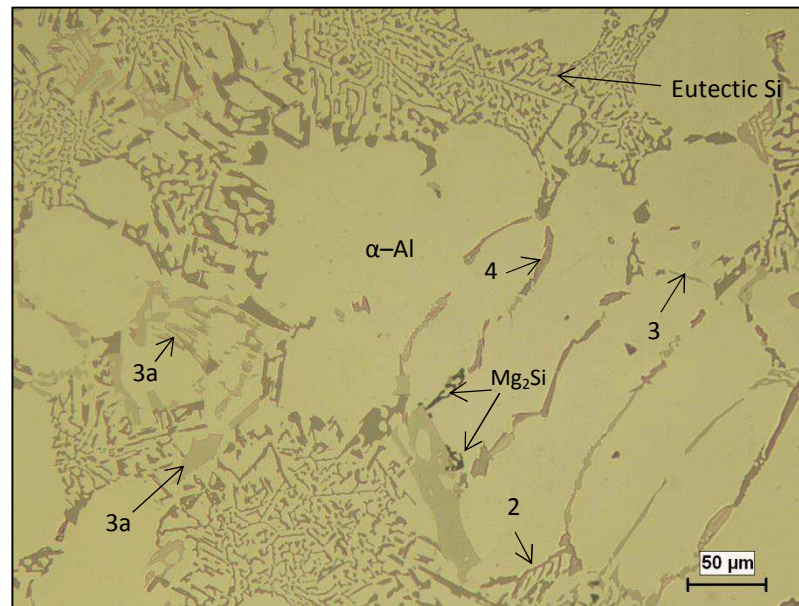


Figure 4.4 Optical microstructure of Alloy S (354 + 2% Ni + 0.25% Zr) sample obtained from the corresponding thermal analysis casting (cooling rate 0.35°C/s), showing the different phases present in the alloy: 2- AlCuNi ; 3- AlNiFe ; 3a- AlSiNiZr-Fe ; 4- Al_2Cu .

4.2.3 Alloy T (354 + 0.25%Zr + 4%Ni)

The solidification curve of Alloy T which, similar to alloy S, contains 0.25 wt% Zr but with a higher Ni content of 4 wt%, as obtained from its temperature-time data is shown in Figure 4.5 along with its first derivate plot. Apart from the $\alpha\text{-Al}$ dendrites and the eutectic Si particles observed in the interdendritic regions, other phases may also be observed in the optical micrograph of the corresponding thermal analysis sample of alloy T namely the Ni-containing AlFeNi and AlCuNi phases, as shown in Figure 4.6. It is interesting to note the larger sizes of AlFeNi and AlCuNi phase particles observed in

this case, when compared to those seen in Figure 4.3 for the S alloy sample with its lower Ni content of 2 wt%.

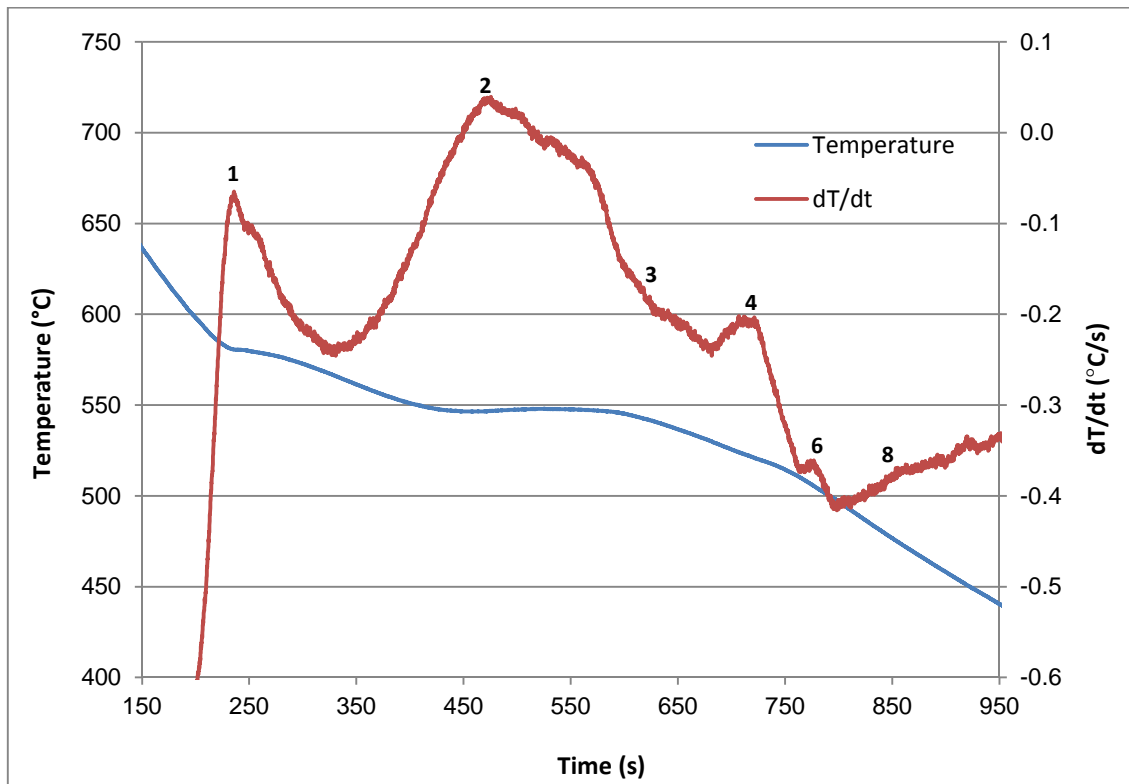


Figure 4.5 Temperature-time plot and first derivative from the thermal analysis of Alloy T (354 + 4% Ni + 0.25% Zr).

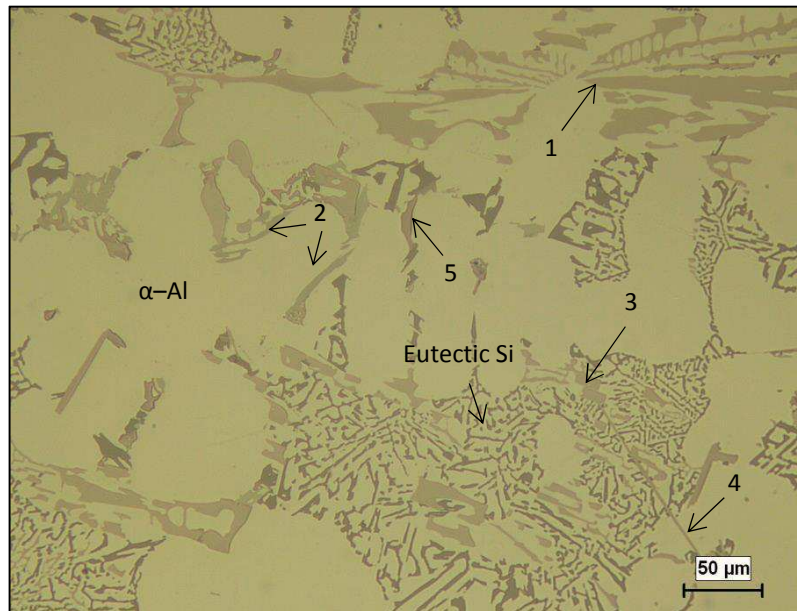


Figure 4.6 Optical microstructure of Alloy T (354 + 4% Ni + 0.25% Zr) sample obtained from the corresponding thermal analysis casting (cooling rate 0.35°C/s), showing the different phases present in the alloy: 1-AlCuNi; 2- AlNiFe; 3- AlTiZr; 4- β -AlFeSi; 5- Al₂Cu.

4.2.4 Alloy U (354 + 0.25%Zr + 0.75%Mn)

Figure 4.7 shows the solidification curve and its first derivative obtained for Alloy U, namely 354 alloy containing 0.75 wt% Mn and 0.25 wt% Zr addition. The reactions which occur during solidification are marked by the peaks 1, 2, 4, 5, 7 and 8. As this alloy contains no Ni addition, Reactions 3 and 6 are not observed. It is interesting to note the broad width of peak #2 indicating that it encompasses other reactions besides the Al-Si eutectic reaction.

During solidification, iron, together with other alloying elements partly goes into solid solution in the matrix and partly forms intermetallic compounds, including the platelet-like β -Al₅FeSi and the Chinese script-like α -Al₁₅(Mn,Fe)₃Si₂ phases. The latter is less detrimental to the alloy properties than the β -Al₅FeSi phase because of its compact form, so that Mn is generally added to alloys containing Fe to “neutralize” the harmful

effect of the β -Al₅FeSi intermetallic phase. If high iron and manganese levels are present in the alloy, and the cooling rate is low, the α -Al₁₅(Fe,Mn)₃Si₂ phase will precipitate as a primary phase, in the form of coarse particles termed “sludge,” having polygonal or star-like morphologies which are not harmful to the alloy.

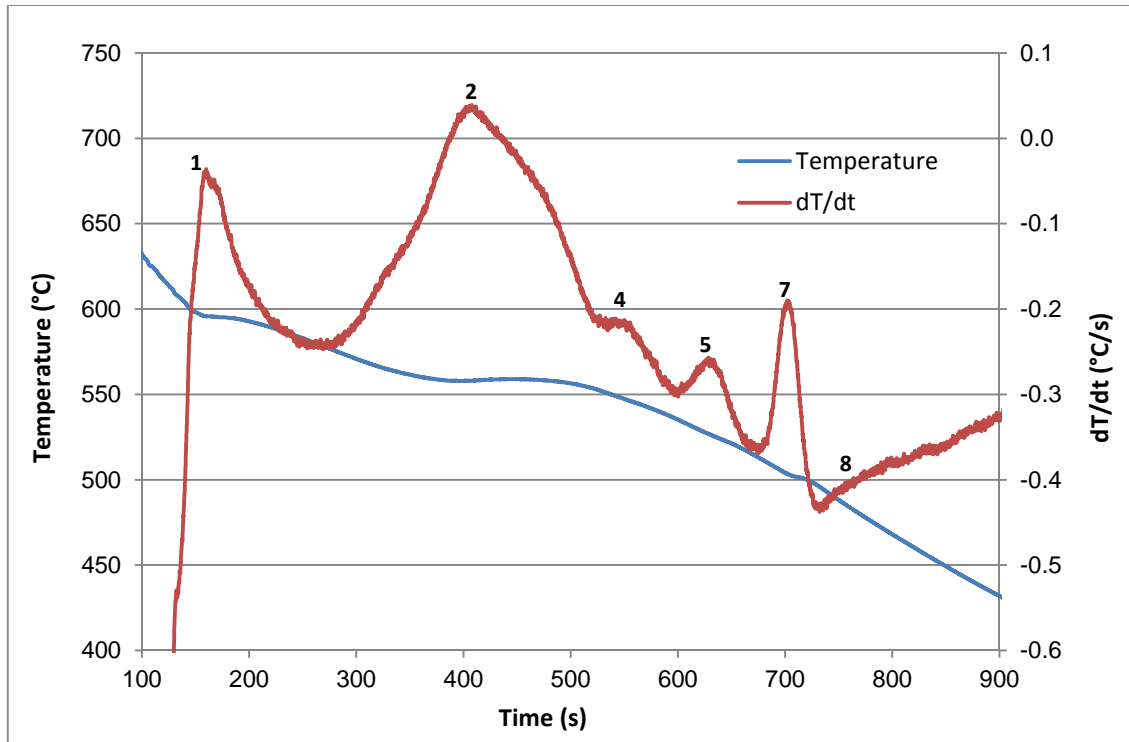


Figure 4.7 Temperature-time plot and first derivative from the thermal analysis of Alloy U (354 + 0.75% Mn + 0.25% Zr).



Figure 4.8 Optical microstructure of Alloy U (354 + 0.75% Mn + 0.25% Zr) sample obtained from the thermal analysis casting (cooling rate 0.35°C/s), showing the different phases present in the alloy: 2- Al₂Cu; 3- AlSiMnFe.

The optical micrograph of Figure 4.8 taken from the corresponding thermal analysis casting sample shows that the Mn addition in Alloy U helps in reducing the detrimental effect of the β -iron phase by replacing it with the less-detrimental Chinese script α -Al₁₅(Fe,Mn)₃Si₂ phase and sludge particles. The precipitation of the α -Fe script phase within the α -Al dendrite actually strengthens the alloy matrix, as reported by Wang et al. [3].

4.2.5 Alloy V (354 + 0.25%Zr + 0.75%Mn + 2%Ni)

The solidification curve of Alloy V which contains 0.75 wt% Mn and 0.25 wt% Zr additions similar to alloy U, but also 2 wt% Ni, obtained from its temperature-time data is shown together with its first derivate plot in Figure 4.9. Apart from the α -Al dendrites and the eutectic Si particles observed in the interdendritic regions, other phases observed in the optical micrograph of the corresponding alloy sample are the α -Al₁₅(Fe,Mn)₃Si₂ script phase, the Ni-containing AlNi and AlCuNi phases, as well as

small particles of Mg_2Si and the Al_2Cu phase, as shown in Figure 4.10. Again, in this case also, the α -Fe script phase is observed to precipitate within the α -Al dendrite, indicating its primary nature.

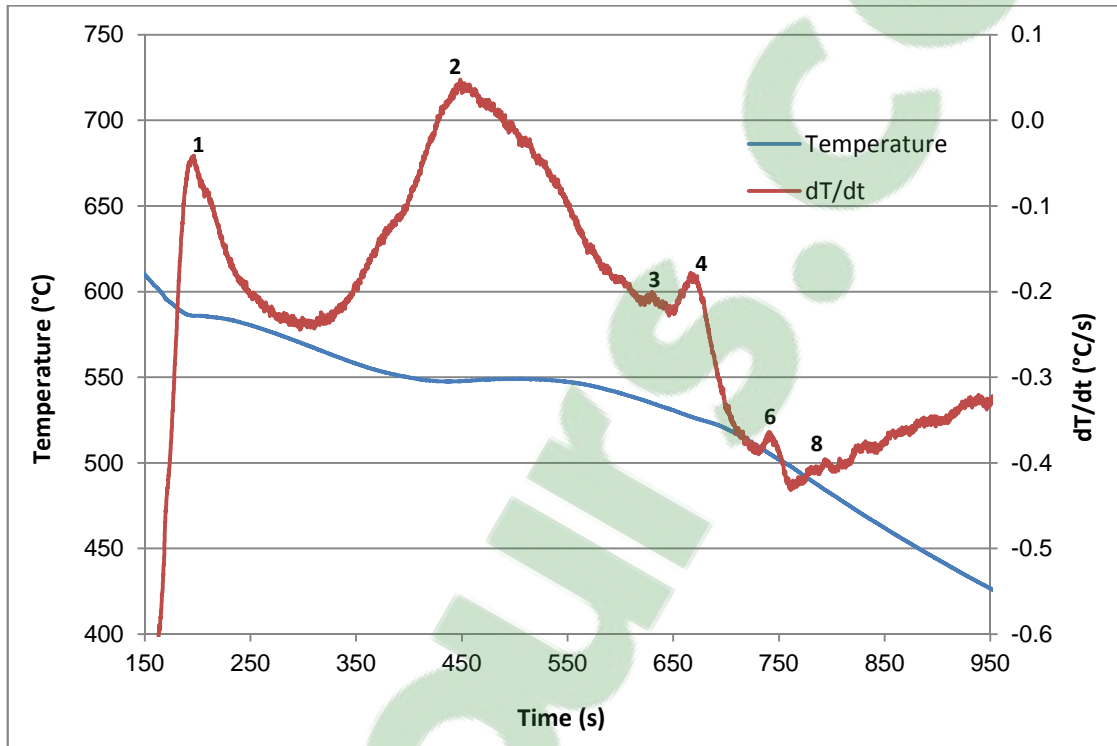


Figure 4.9 Temperature-time plot and first derivative from the thermal analysis of Alloy V (354 + 0.75% Mn + 2% Ni + 0.25% Zr).

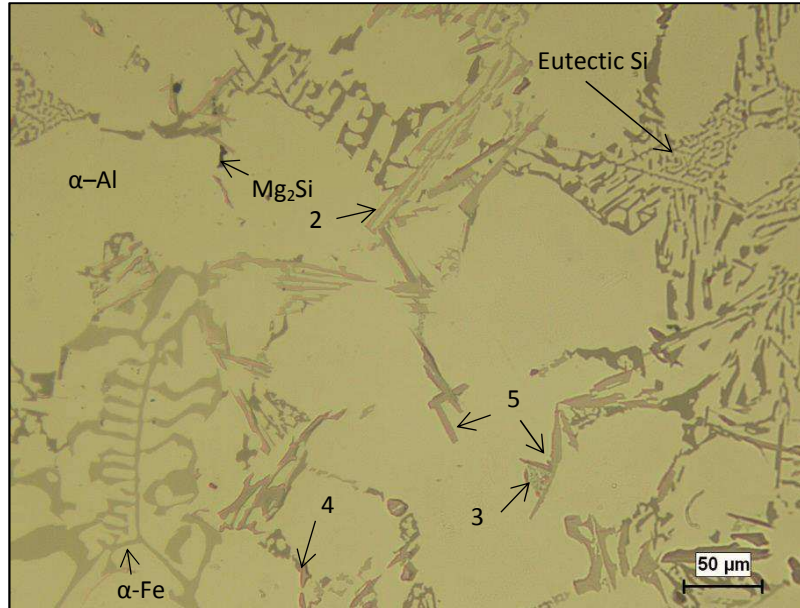


Figure 4.10 Optical microstructure of Alloy V (354 + 0.75% Mn + 2% Ni + 0.25% Zr) sample obtained from the thermal analysis casting (cooling rate 0.35°C/s), showing the different phases present in the alloy: 2- AlNiCu; 3- AlFeNiCu; 4- Al₂Cu; 5- Zr-rich phase.

4.2.6 Alloy Z (354 + 0.25%Zr + 0.15%Sc)

The solidification curve of Alloy Z, *i.e.* 354 alloy containing 0.15 wt% Sc + 0.25 wt% Zr, and its first derivate plot are shown in Figure 4.11. The addition of transition elements Zr and Sc, together with the presence of Ti, refine the α -Al grain size by transforming the morphology from dendritic to a non-dendritic type, which leads to a significant reduction in the size of intermetallic compounds such as the Al₂Cu and α -Fe that are subsequently formed during solidification. Besides the α -Al dendrites and the eutectic Si particles, other phases may also be observed, as shown in the corresponding optical micrograph of Figure 4.12 such as the (Al,Ti)(Sc,Zr) phase and the Al₂Cu phase.

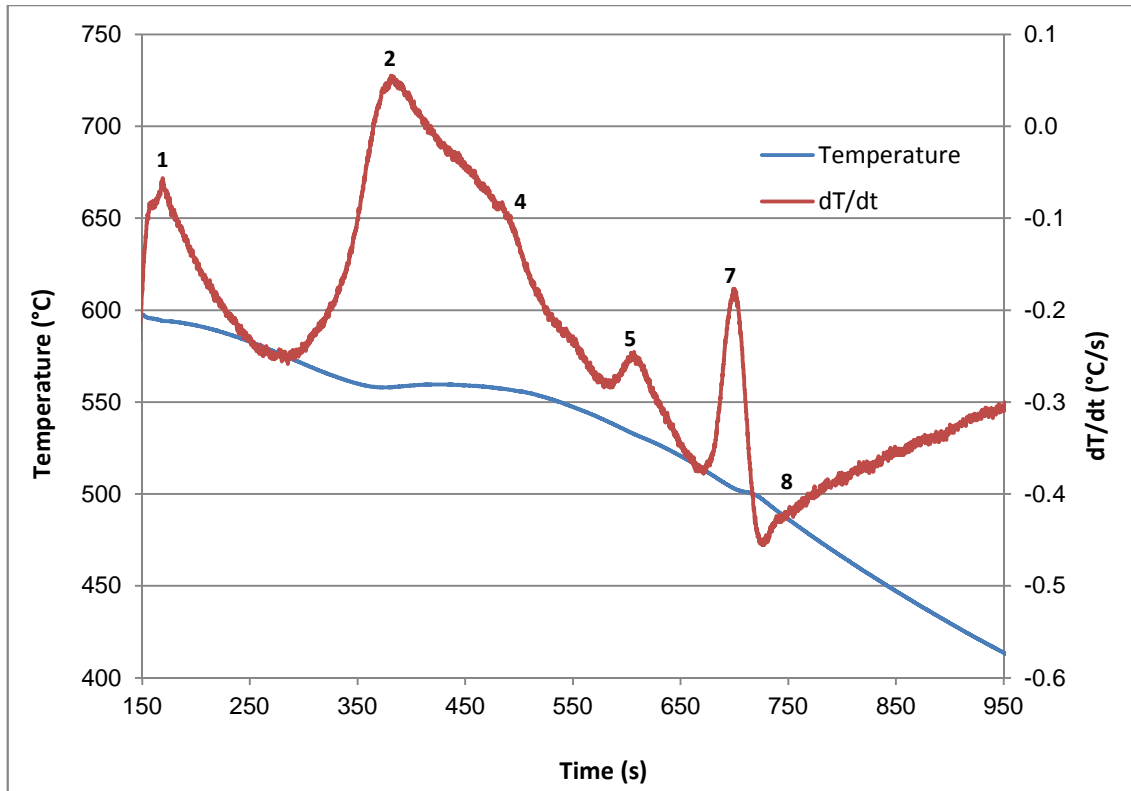


Figure 4.11 Temperature-time plot and first derivative from the thermal analysis of Alloy Z (354 + 0.15% Sc + 0.25% Zr).

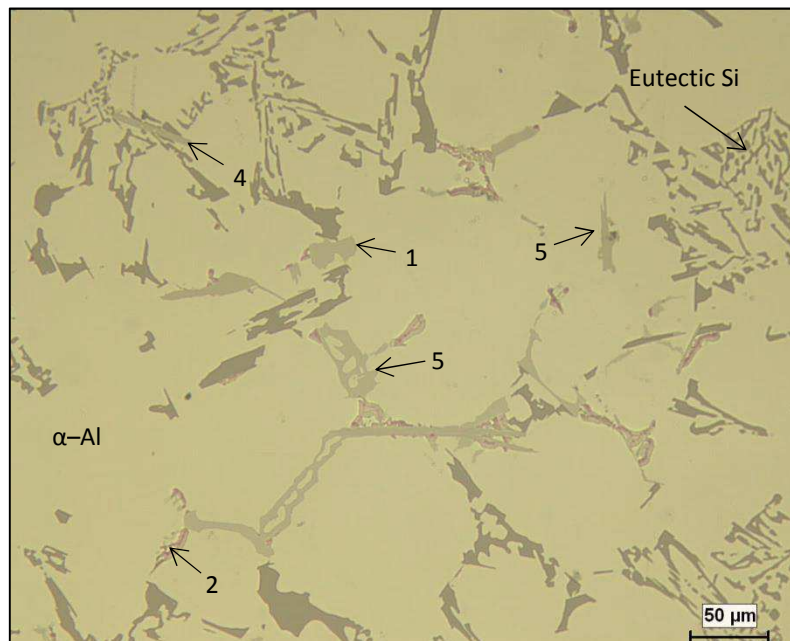


Figure 4.12 Optical microstructure of Alloy Z (354 + 0.15% Sc + 0.25% Zr) sample, obtained from the thermal analysis casting (cooling rate 0.35°C/s), showing the different phases present in the alloy: 1- (Al,Ti)(Sc,Zr); 2- Al_2Cu ; 4- $\beta\text{-AlFeSi}$; 5- (Al,Si)(Sc,Zr,Ti).

When both Sc and Zr are present in the alloy, zirconium atoms replace some of the scandium atoms in the Al_3Sc unit cell, and its chemical formula might be more accurately written as $\text{Al}_3\text{Sc}_{1-x}\text{Zr}_x$ [126], where x is a variable that depends on the content of Zr in the alloy. The star-like $\text{Al}_3(\text{Sc,Zr})$ phase has a L1_2 type structure which is characterized by a structural and dimensional matching with the aluminum matrix [126,127]. Also, as its temperature of formation is higher than that of the α -Al phase, it can be used as a potent grain refiner for a wide range of aluminum alloys because of its high efficiency in nucleating α -Al grains. Nabawy [124] reported that in the presence of 0.2 wt% Ti, the $\text{Al}(\text{Sc,Zr})$ phase changed to an $\text{Al}(\text{Sc,Zr,Ti})$ phase in Al-2%Cu alloys. In the present case, EDS results showed the presence of $(\text{Al,Si})(\text{Sc,Zr,Ti})$ and $(\text{Al,Ti})(\text{Sc,Zr})$ phase particles.

4.2.7 Alloy L (398 + 0.25%Zr + 0.15%Sc)

As mentioned in Chapter 1, the effect of Zr and Sc additions on the strength of cast aluminum alloy 398 (Al-16%Si alloy) were investigated at room and high temperatures for the purposes of examining how the properties of the 354 alloys investigated in this study stand with respect to the 398 alloy, an alloy developed by NASA and reported to give superior high temperature properties [9]. The 398 alloy containing 0.15 wt% Sc and 0.25 wt% Zr additions (coded Alloy L) could then be used for direct comparison with the 354 alloy containing the same Sc and Zr additions - Alloy Z, presented in the previous section.

The solidification curve obtained for Alloy L and its first derivative plot are shown in Figure 4.13. As may be seen from this figure, the alloy starts to solidify at 570°C , with the formation of the α -Al dendritic network (Reaction 1), at a temperature lower than that observed in the case of the 354 alloys, followed by precipitation of the Al-Si eutectic

(Reaction 2) at 560°C, the Mg_2Si phase (Reaction 4) at 540°C, and the transformation of the β -phase into $\pi-Al_8Mg_3FeSi_6$ phase (Reaction 5) at 525°C. The Al_2Cu and $Q-Al_5Mg_8Cu_2Si_6$ phases precipitate as the last reactions at 498°C and 488°C, respectively, towards the end of solidification. The optical micrograph of Figure 4.14 taken from the corresponding alloy sample shows some of the phases observed in the microstructure, including the presence of the $(Al,Ti)(Sc,Zr)$ phase as in the case of Alloy Z.

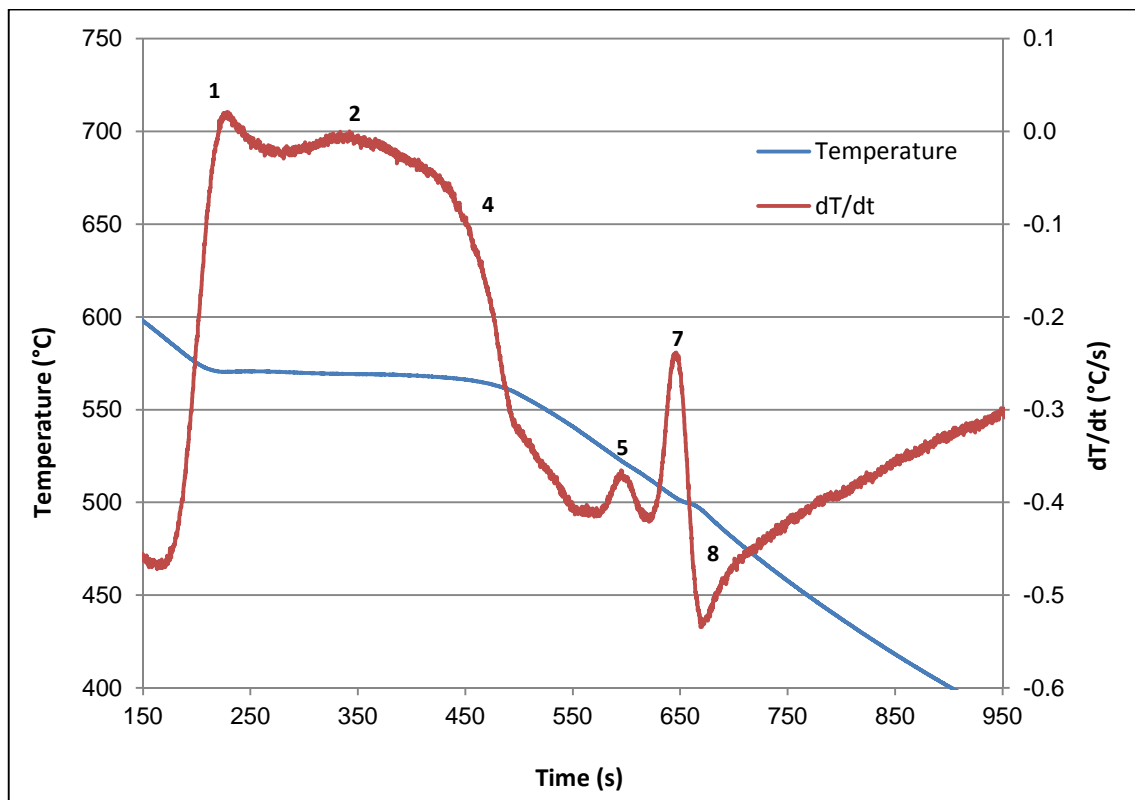


Figure 4.13 Temperature-time plot and first derivative from the thermal analysis of Alloy L (398 + 0.15% Sc + 0.25% Zr).

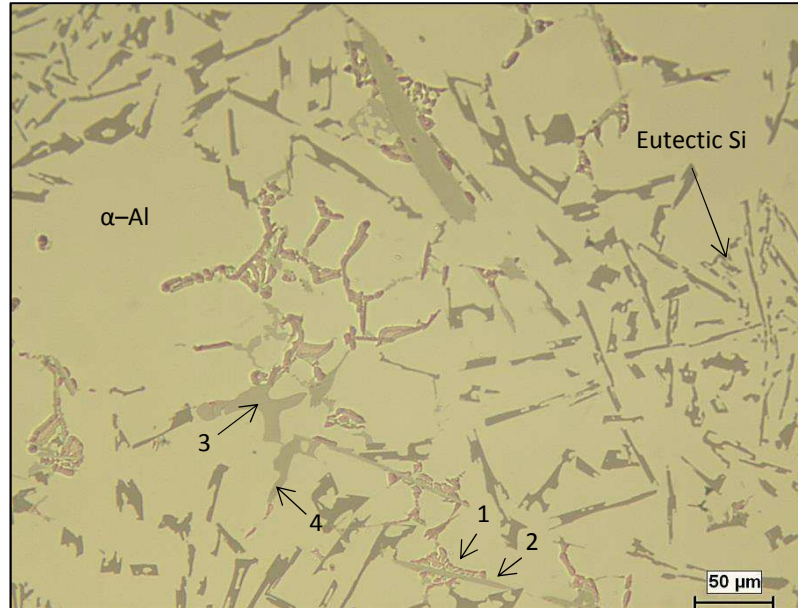


Figure 4.14 Optical microstructure of Alloy L (398 + 0.15% Sc + 0.25% Zr) sample obtained from the thermal analysis casting (cooling rate 0.35°C/s), showing the different phases present in the alloy: 1- Al₂Cu; 2- β-AlFeSi; 3- (Al,Si)(Sc,Zr); 4- π-AlMgFeSi.

4.3 POROSITY FORMATION DUE TO INCIPIENT MELTING

Solution heat treatment is carried out to maximize the concentration of hardening elements such as Mg and Cu in solid solution, to homogenize the casting, and to alter the structure of the eutectic silicon particles in order to improve the mechanical properties. In Al-Si-Cu-Mg alloys, control of the solution treatment process is very critical because, if the solution heat treatment temperature exceeds the melting point, there is localized melting at the grain boundaries and the mechanical properties are reduced. In this study, the alloys were heat treated using two different solution heat treatment processes: one step and multi-step solution treatments. The multi-step solution heat treatment is carried out at three different temperatures consecutively, for different solution times, *viz.*, 5 hours at 495°C, then 2 hours at 515°C, and then 2 hours at 530°C. A main consequence of incipient melting in Al-Si-Cu-Mg alloys is the melting of the Al₂Cu phase. As reported by de la Sablonnière and Samuel [128], the Al₂Cu intermetallic may melt at 525 °C, so that when

the temperature of the multi-step solution heat treatment reaches 530°C, or when local heating occurs at any point in the sample, it is expected that the Al₂Cu phase will melt, causing the formation of porosity and, in turn, a deterioration in the mechanical properties.

In the present study, all alloy melts were degassed to minimize the hydrogen level before casting. The only variable factor with respect to the cast samples would be the temperature, depending on the solution heat treatment conditions. Hence, any relatively significant changes in the porosity characteristics could be reasonably attributed to the melting of the copper phase(s) resulting from the changes in the temperature variable. Therefore, porosity measurements were carried out to monitor the incipient melting that resulted in the alloys studied, corresponding to the various solution heat treatments. The porosity characteristics resulting from incipient melting were examined and quantified using an optical microscope-Clemex Vision PE 4.0 image analysis system. Ten fields were examined for each alloy sample, at 200x magnification. The porosity parameters measured were the average area percent porosity (percentage porosity over a constant sample surface area), and the average pore area, total pore area (SUM) and the pore count. These values are listed in Table 4.2.

As may be seen from Table 4.2, the as-cast samples for all alloys show minimum porosity, whereas after solution heat treatment, the porosity values increase. In general, compared to the one step or SHT 1 treatment, the multi-step solution treatment leads to somewhat higher porosity values for the 354 alloys, whereas for Alloy L (398 + Zr + Sc), the one-step solution heat treatment results in a higher porosity value. This trend may be noted more clearly in the column showing the SUM or total area of the pores measured in each sample.

It is worthwhile mentioning here that while these measurements provide quantitative results *per se*, they should be considered in a qualitative light overall, when discussing the influence of such porosity (resulting from incipient melting) on the mechanical properties of these alloys, which will be presented in the next chapter.

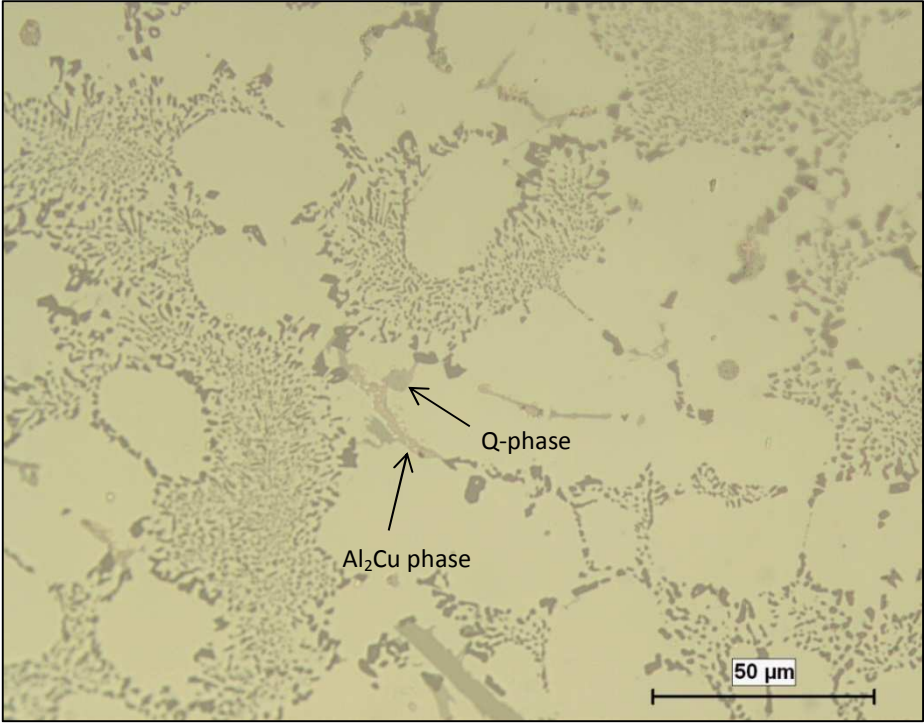
The microstructures of the alloys studied were examined at high magnification (500x) to highlight some of the interesting features observed with respect to the incipient melting-related porosity observed in the as-cast, SHT 1 and SHT 2 samples corresponding to each alloy, as well as the effect of the progress of solution heat treatment on the micro-constituents themselves.

Table 4.2 Porosity measurements for Alloys R, S, T, U, V, Z and L.

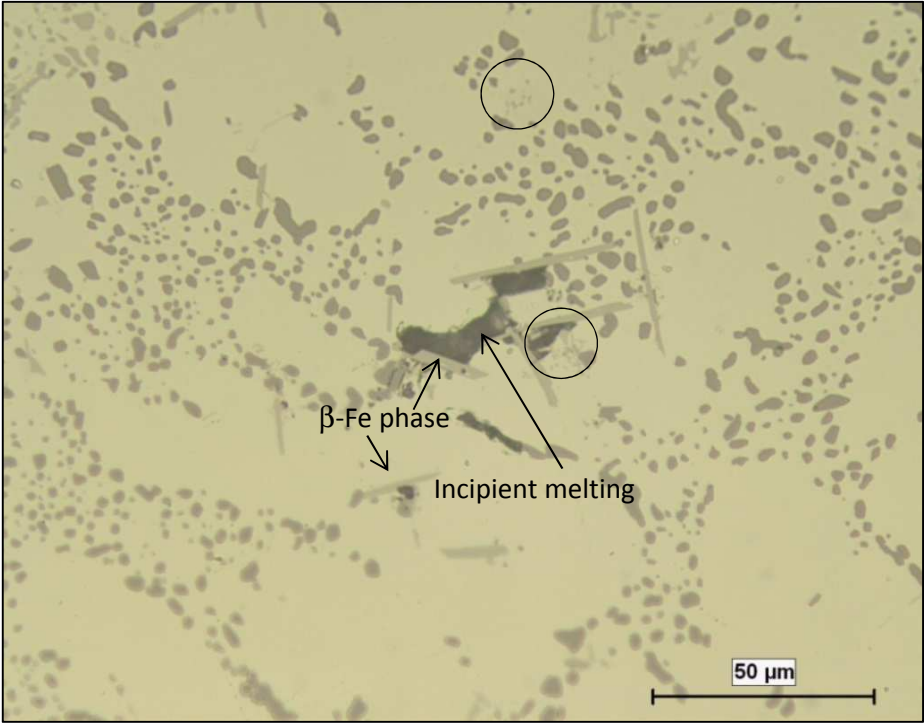
Alloy Code	Condition	Area (%)		Pore Area (μm^2)			
		Mean	SD	Mean	SD	SUM	Count
R	As Cast	0.012	0.005	0.614	0.14	183	317
	SHT 1	0.063	0.018	4.45	4	1105.8	388
	SHT 2	0.067	0.035	12.45	7.36	1483.5	127
S	As Cast	0.024	0.048	1.98	2.25	221.2	226
	SHT 1	0.075	0.032	8.98	7.38	1639.4	498
	SHT 2	0.087	0.038	3.5	2.88	1920.8	760
T	As Cast	0.0082	0.006	2.13	1.76	180.1	79
	SHT 1	0.0629	0.0344	7.35	6.18	1378.1	268
	SHT 2	0.1	0.037	4.5	2.96	2214.2	693
U	As Cast	0.02	0.021	2.08	8.35	441.2	212
	SHT 1	0.09	0.045	22	38.4	1959.2	89
	SHT 2	0.087	0.054	6.81	19.3	1913	281
V	As Cast	0.011	0.011	1.16	2.61	238	206
	SHT 1	0.078	0.055	5.59	25.1	1710.9	306
	SHT 2	0.097	0.071	6.32	19.5	2130	337
Z	As Cast	0.021	0.019	2.81	7.44	461.2	164
	SHT 1	0.088	0.159	20	35	1939.5	97
	SHT 2	0.099	0.063	16.3	38.6	2168.5	133
L	As Cast	0.009	0.0056	2.09	3.33	198.9	95
	SHT 1	0.105	0.042	5.23	21.2	2305.8	441
	SHT 2	0.086	0.029	6.64	21.6	1886.6	284

Figure 4.15(a) displays an optical micrograph of the as-cast Alloy R sample, taken at 500x magnification, showing an overview of the sample surface, comprising the α -Al dendrites, modified eutectic Si regions, the β -Al₅FeSi phase as well as the Al₂Cu phase. Small particles of the π -Fe phase and the Q-copper phase are also seen. Upon solution heat treatment of the sample (one-step solution treatment), spheroidization of the Si particles is clearly noted and also some areas where incipient melting of the Al₂Cu phase has occurred, adjacent to β -Al₅FeSi phase platelets, as seen in Figure 4.15(b). This is to be expected, since the eutectic Al₂Cu phase is generally observed to precipitate along the sides of the β -Fe platelets. Dissolution of the Cu-phases is also observed, as highlighted by the circled areas in Figure 4.15(b).

When the as-cast sample is subjected to the multi-step solution treatment – involving higher solution temperatures and longer durations, an increased amount of incipient melting is expected to occur, as may be noted in Figure 4.15(c). Coarsening of the Si particles is also observed, with larger particles growing bigger at the expense of smaller ones, in accordance with the Ostwald ripening phenomenon [129].



(a) – R-As-cast



(b) – R-SHT 1



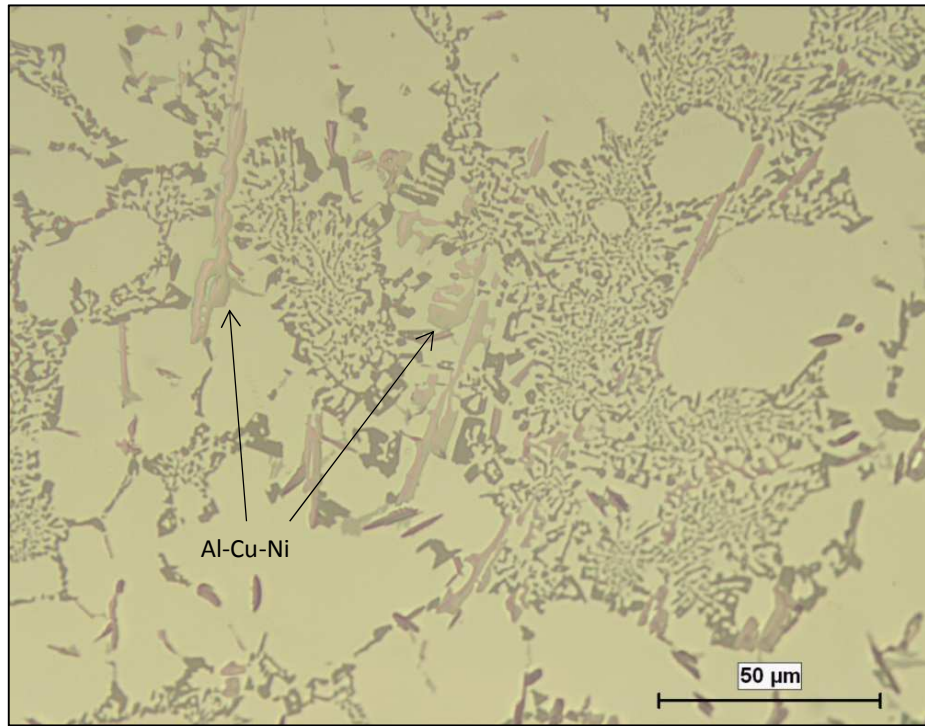
(c) – R-SHT 2

Figure 4.15 Optical micrographs of alloy R (354 + 0.25%Zr) showing the microstructures observed in (a) as cast, (b) SHT-1 and (c) SHT-2 tensile test samples (500x). Circled areas in (b) highlight dissolution of Cu-phases.

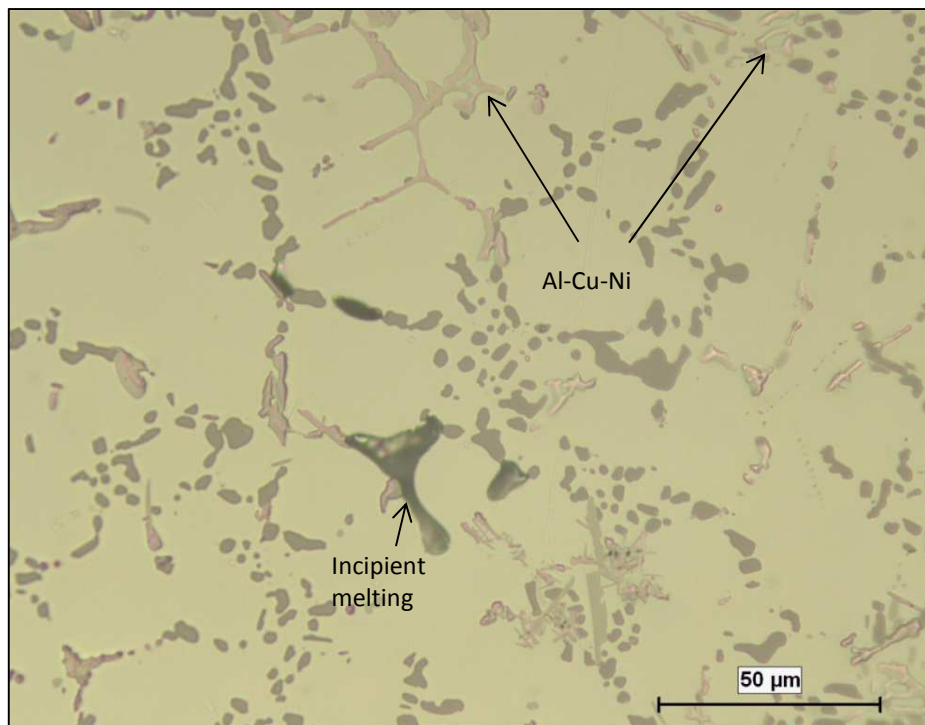
Compared to the base alloy R, in the case of Alloy S which contains 0.25 wt% Ni + 2 wt% Ni, the as-cast microstructure displays several Al-Cu-Ni particles, in script-like form, Figure 4.16(a). After solution heat treatment, a certain amount of incipient melting is observed, as well as the dissolution of Cu-phase and Al-Cu-Ni particles, as evidenced respectively by the small sized pink particles observed across the matrix and the smaller sizes of the Al-Cu-Ni particles in Figure 4.16(b). In Figure 4.16(c), very fine needles of Al-Cu-Ni observed in the circled area show the persistence of these Ni-containing particles even after long solution treatment times.

Figures 4.17 through 4.20 similarly display optical micrographs of the as-cast and solution heat-treated samples for the remaining 354 alloys, showing the occurrence of incipient melting and other interesting microstructural features in each case. Note the

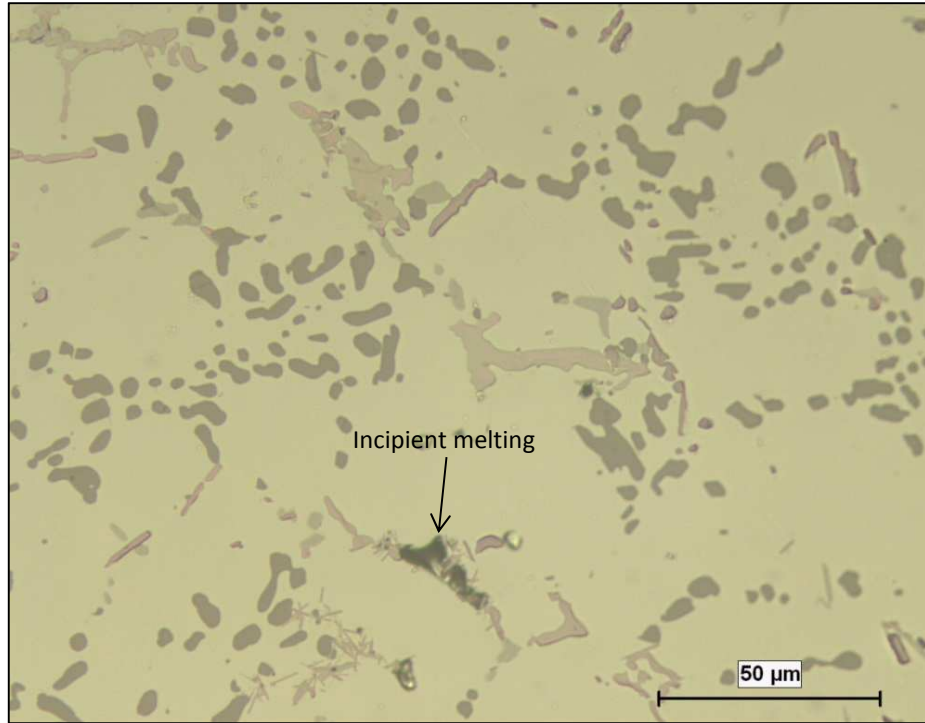
profusion of the Al-Cu-Ni phase in Alloy T, which persists even after solution treatment SHT-2.



(a) – S-As-cast

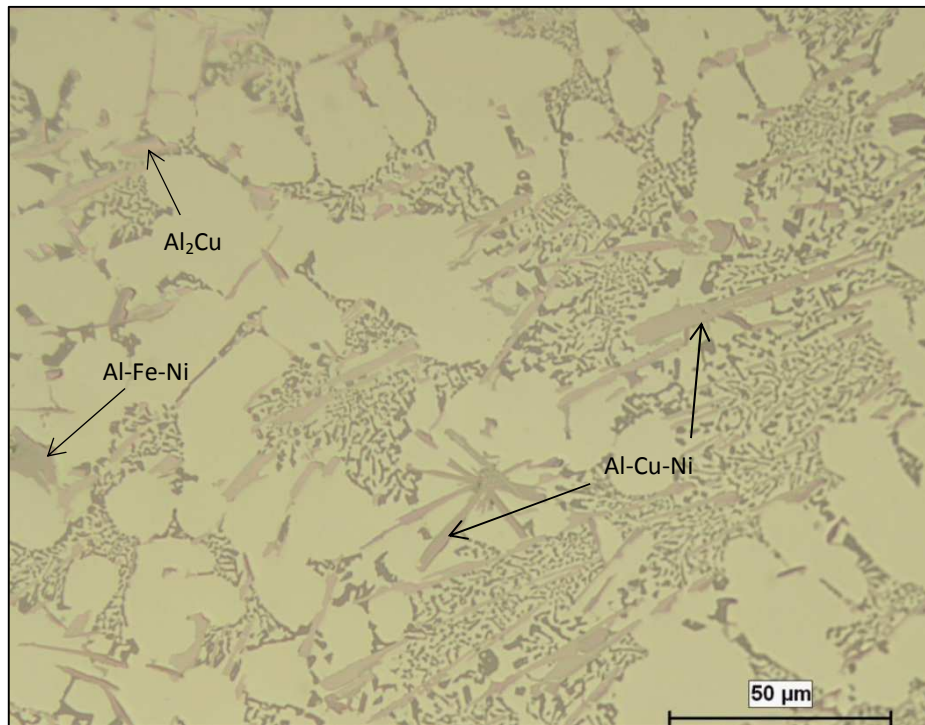


(b) – S-SHT 1

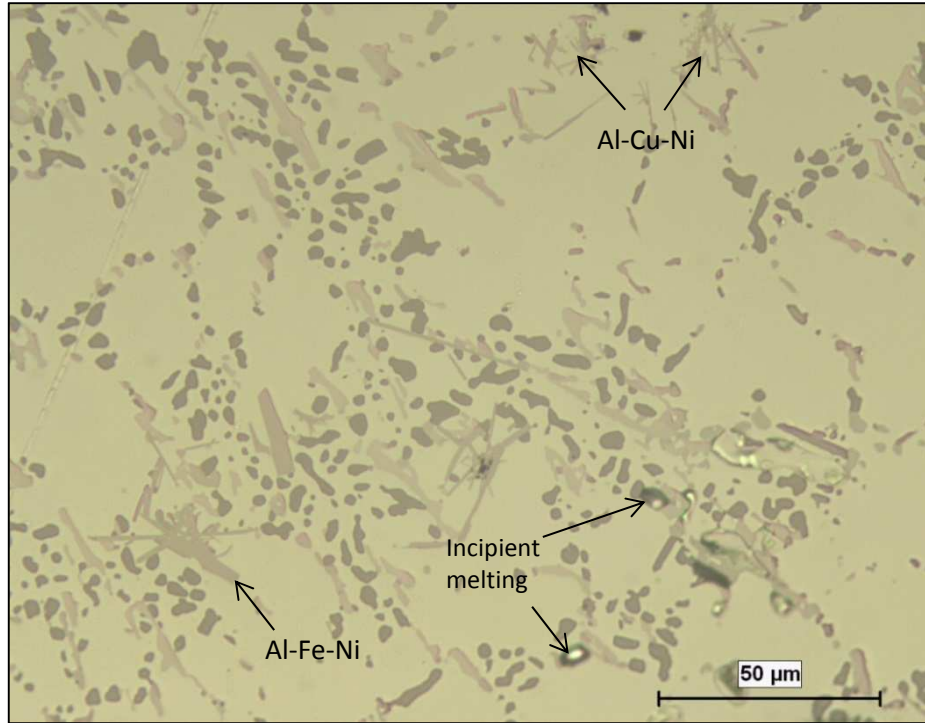


(c) – S-SHT 2

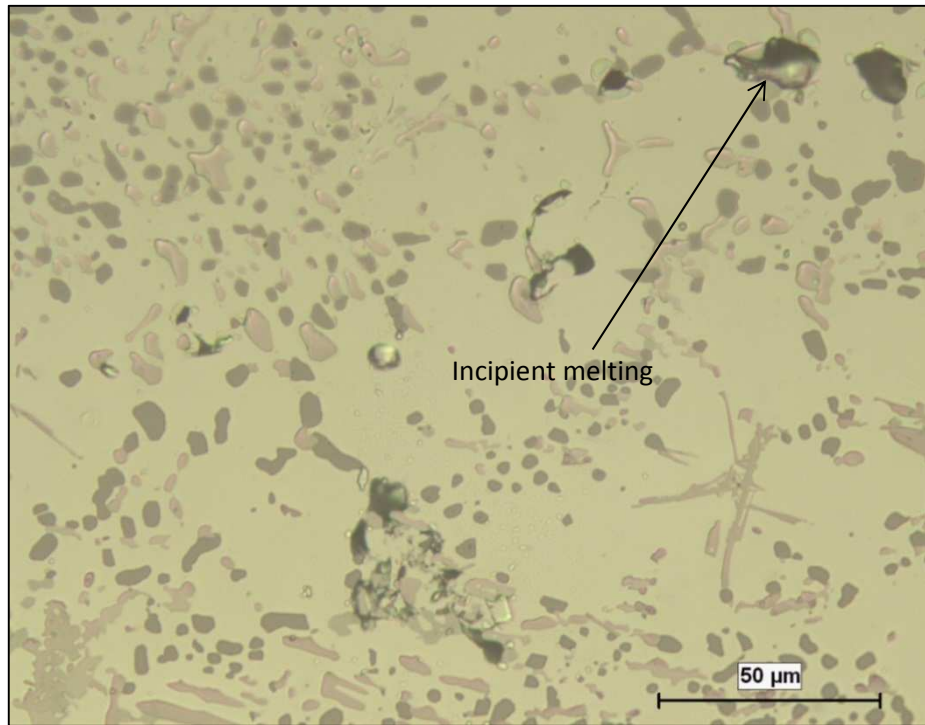
Figure 4.16 Optical micrographs of Alloy S (354 + 0.25% Zr + 2% Ni) showing the microstructures observed in (a) as cast, (b) SHT-1 and (c) SHT-2 tensile test samples (500x).



(a) – T-As-cast

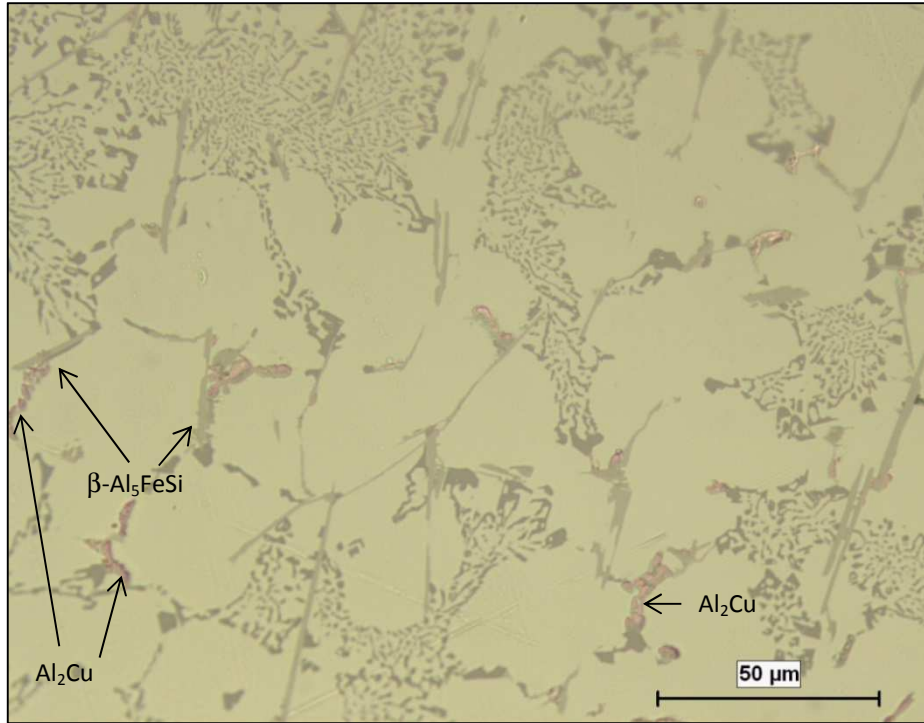


(b) – T-SHT 1

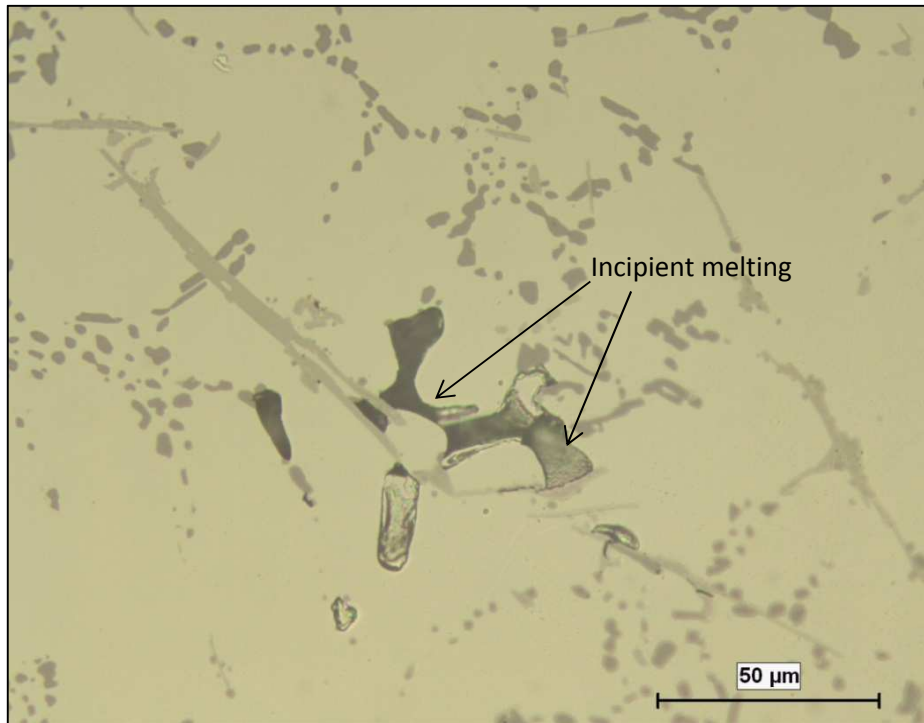


(c) – T-SHT 2

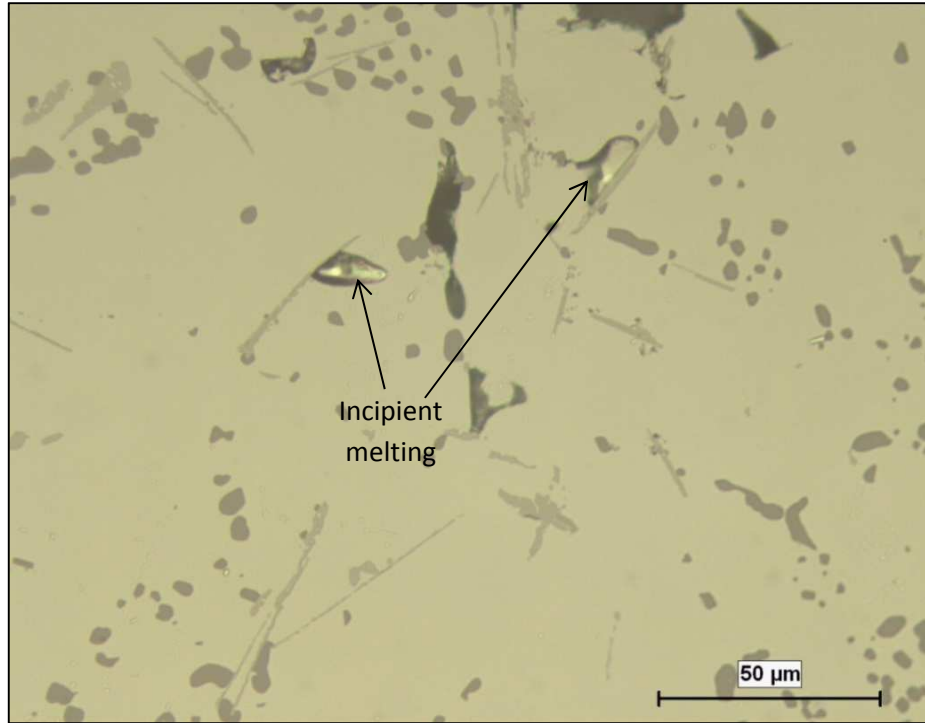
Figure 4.17 Optical micrographs of Alloy T (354 + 0.25%Zr + 4%Ni) showing the microstructures observed in (a) as cast, (b) SHT-1 and (c) SHT-2 tensile test samples (500x).



(a) – U-As-cast

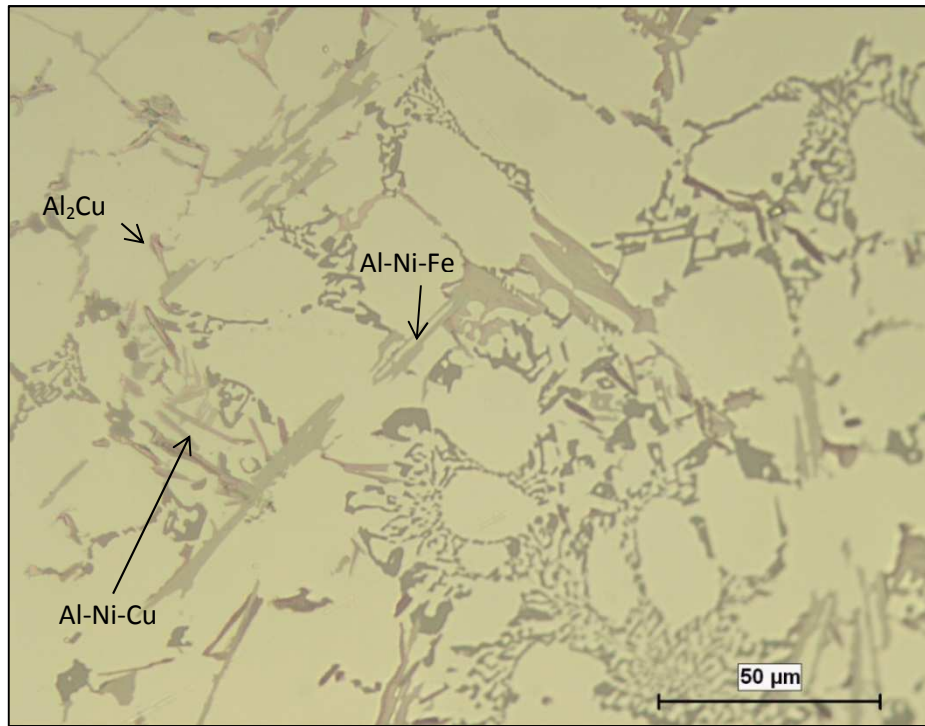


(b) – U-SHT 1

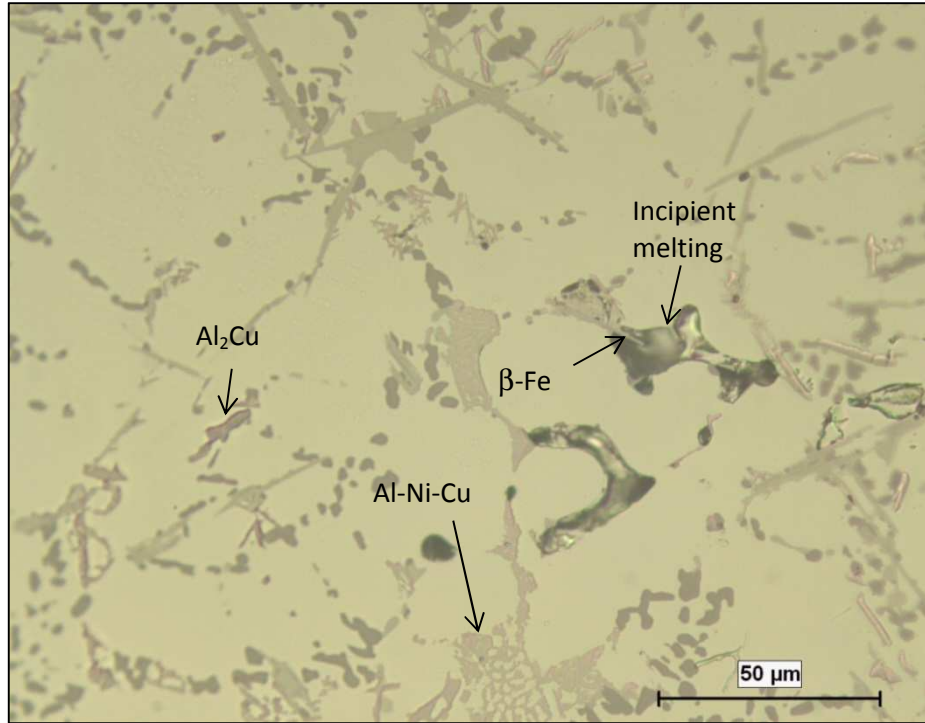


(c) – U-SHT 2

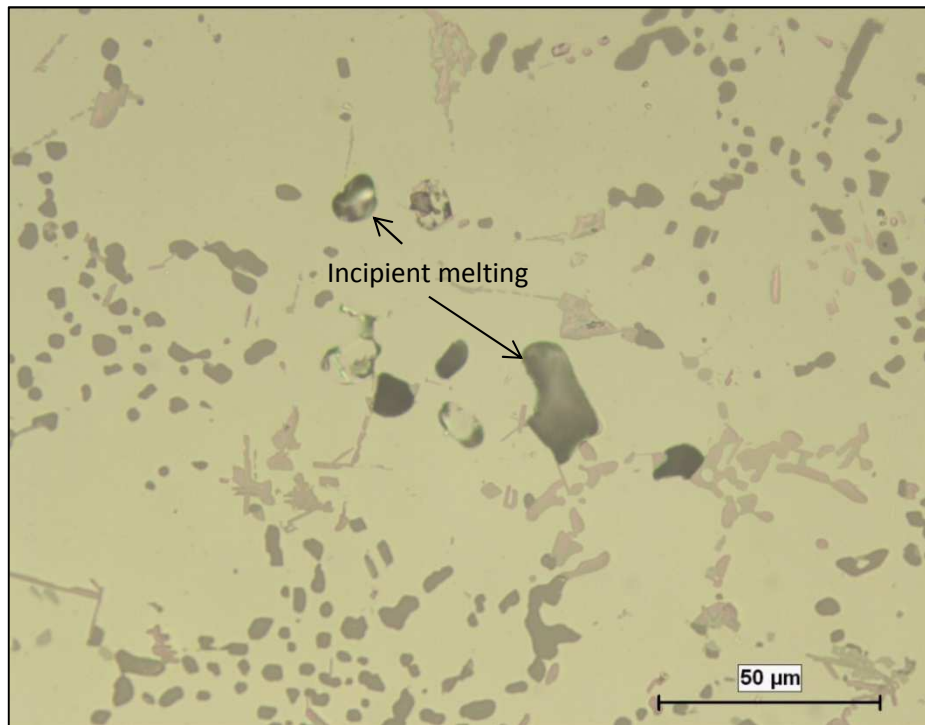
Figure 4.18 Optical micrographs of Alloy U (354 + 0.25%Zr + 0.75%Mn) showing the microstructures observed in (a) as cast, (b) SHT-1 and (c) SHT-2 tensile test samples (500x).



(a) – V-As-cast

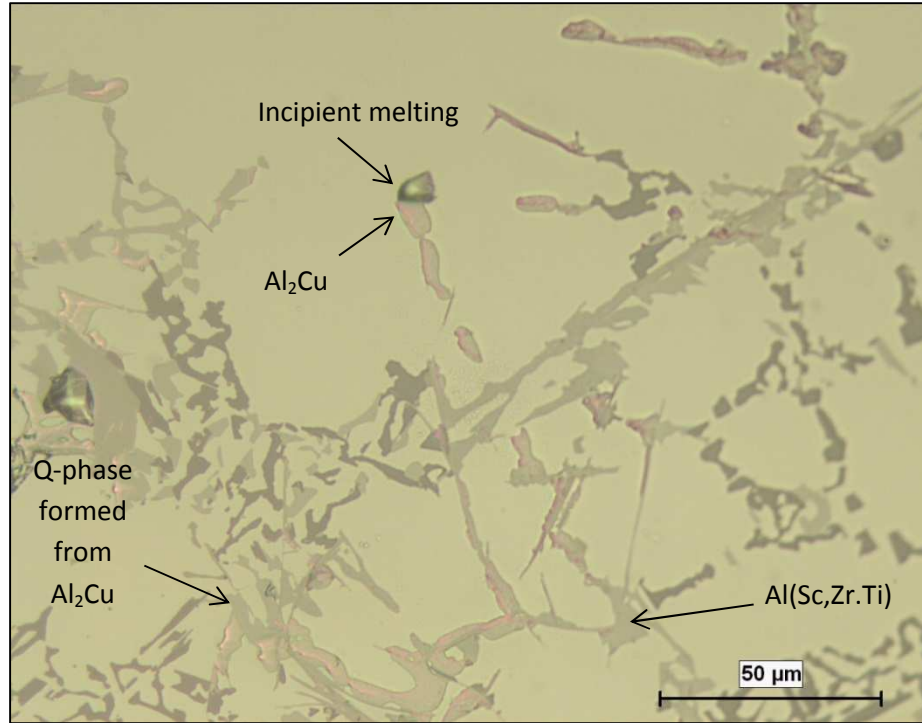


(b) – V-SHT 1

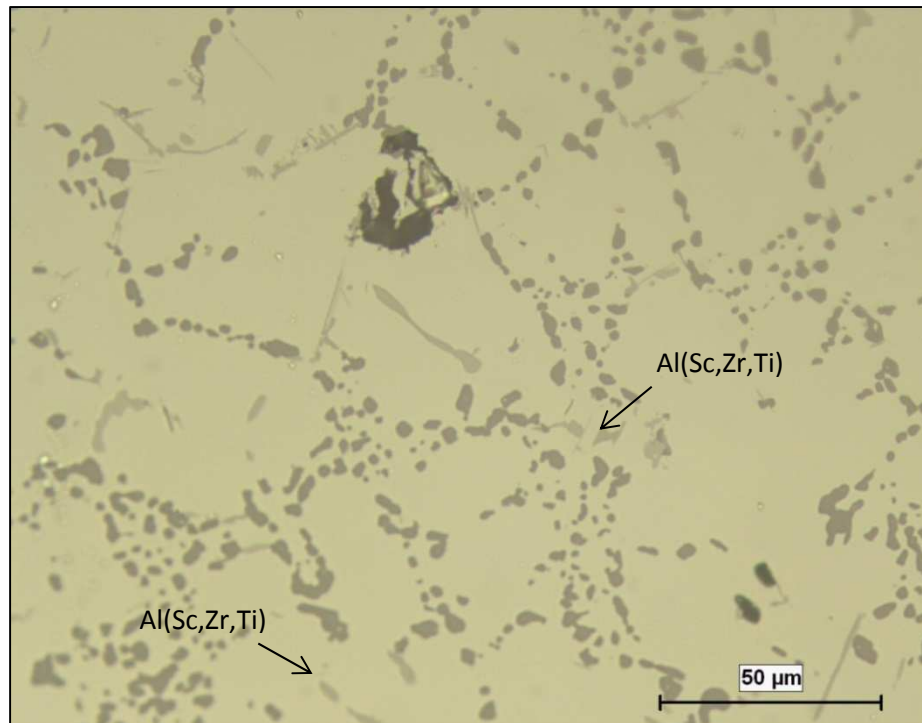


(c) – V-SHT 2

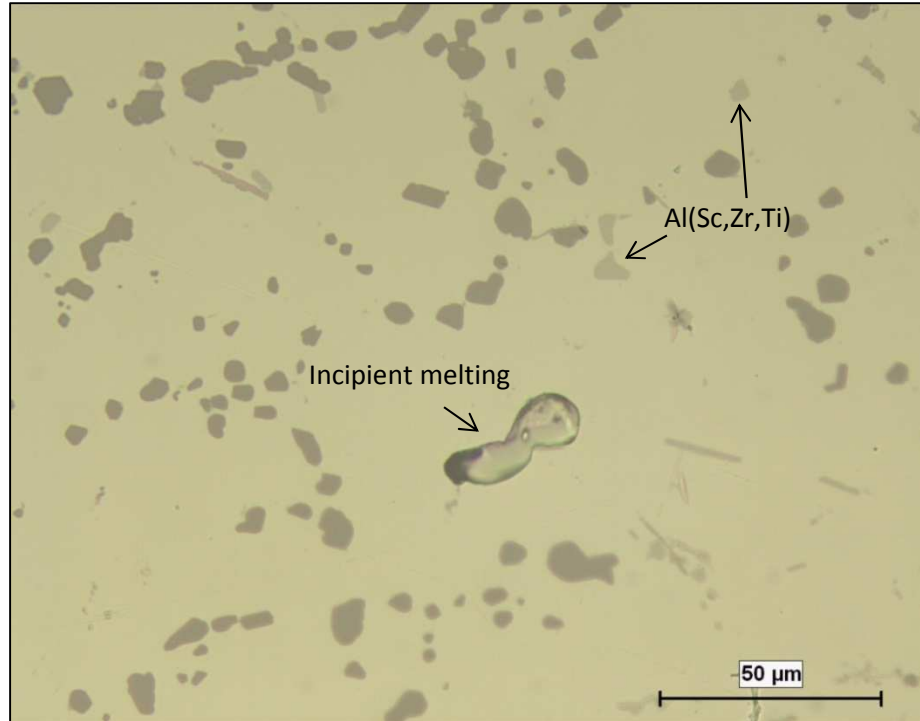
Figure 4.19 Optical micrographs of Alloy V (354 + 0.25%Zr + 0.75%Mn + 2%Ni) showing the microstructures observed in (a) as cast, (b) SHT–1 and (c) SHT–2 tensile test samples (500x).



(a) – Z-As-cast



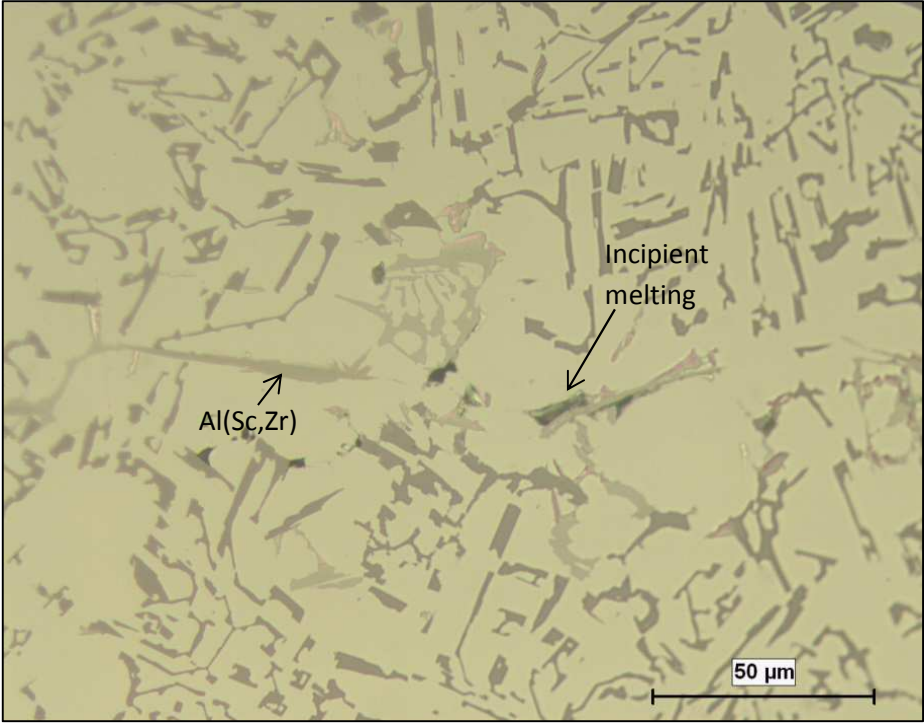
(b) – Z-SHT 1



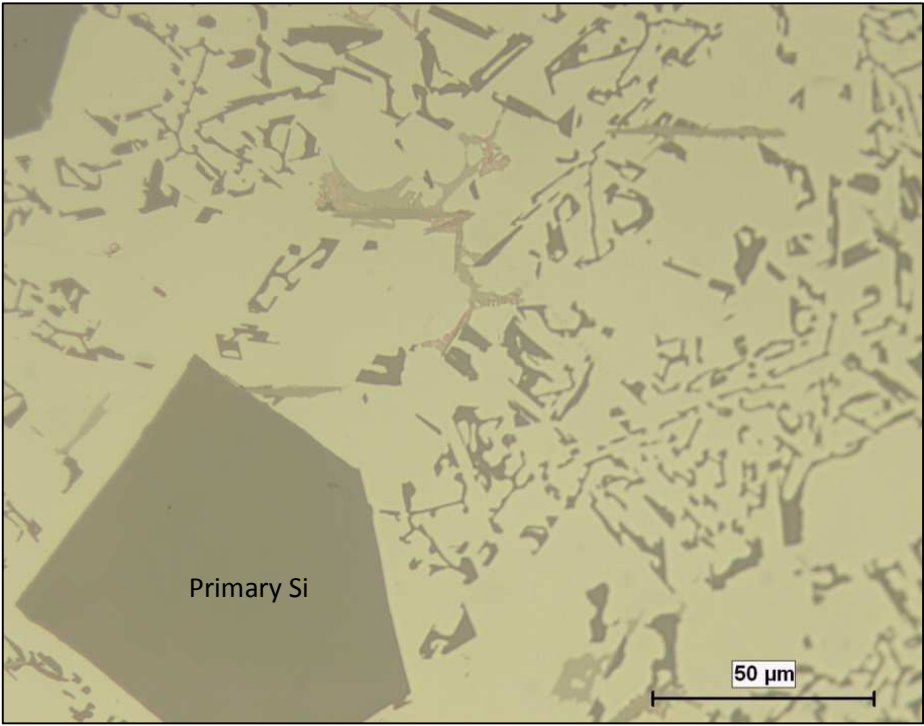
(c) – Z-SHT 2

Figure 4.20 Optical micrographs of Alloy Z (354 + 0.25%Zr + 0.15%Sc) showing the microstructures observed in (a) as cast, (b) SHT–1 and (c) SHT–2 tensile test samples (500x).

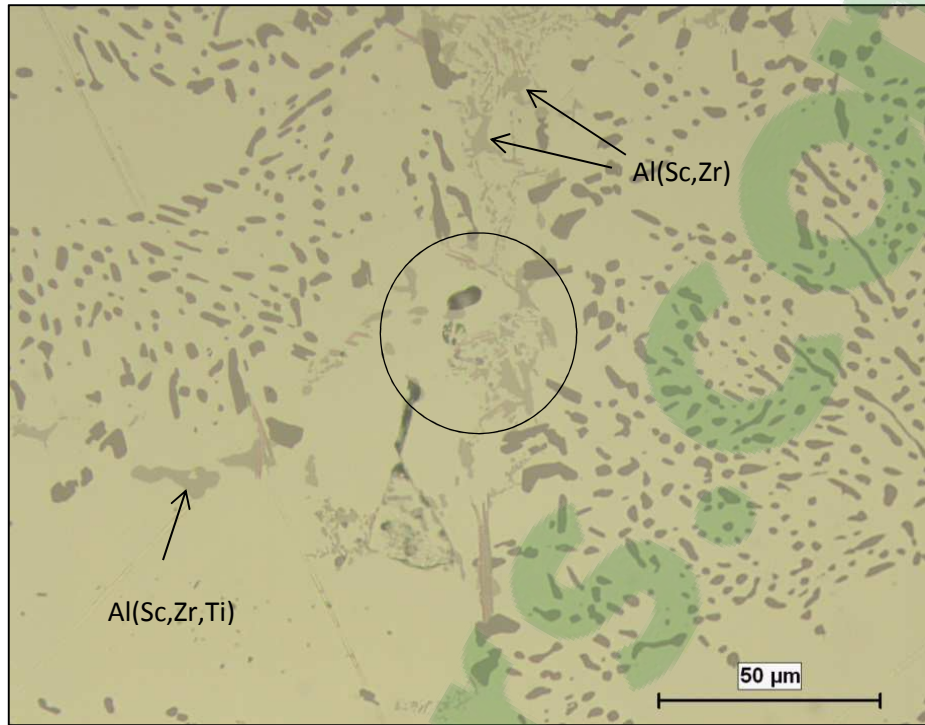
Figure 4.21 shows the microstructures of the (a, b) as-cast, (c) SHT 1 and (d) SHT 2 samples for Alloy L. Obviously, as the L alloy is an hypereutectic alloy with 16 wt% Si, primary Si particles are also observed in the microstructure, as may be seen from Figures 4.21(b) and (d). The presence of these primary Si particles is expected to affect the mechanical properties of the alloy when compared to Alloy Z which exhibits only the eutectic Si phase. A small amount of incipient melting is observed in the as-cast sample as seen in Figure 4.21(a).



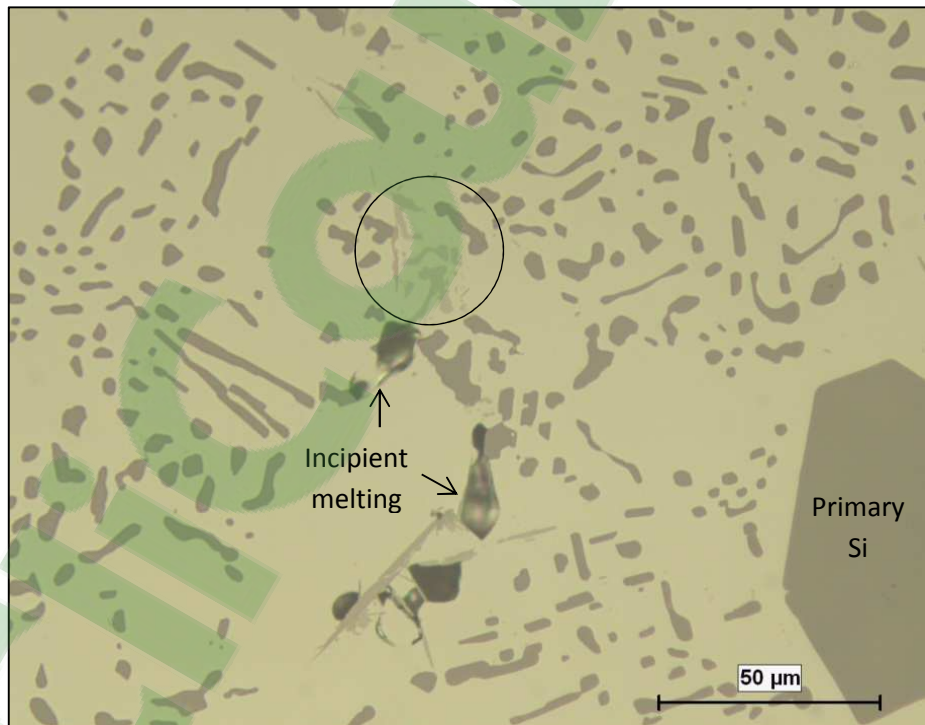
(a) – L-As-cast



(b) – L-As-cast



(c) – L-SHT 1



(d) – L-SHT 2

Figure 4.21 Optical micrographs of Alloy L (398 + 0.25%Zr + 0.15%Sc) showing the microstructures observed in (a, b) as cast, (c) SHT-1 and (d) SHT-2 tensile test samples at 500X magnification. Circled areas in (c) and (d) highlight dissolution of phases.

CHAPTER 5

ROOM AND HIGH TEMPERATURE TENSILE

PROPERTIES

CHAPTER 5

ROOM AND HIGH TEMPERATURE TENSILE PROPERTIES

5.1 INTRODUCTION

This chapter presents and analyzes the tensile test results obtained at room and high temperature (250°C) concerning the influence of metallurgical parameters on the tensile properties of 354 casting alloys. As mentioned in previous chapters, tensile tests were also carried out on the 398 alloy (reported to give superior high temperature properties [9]) for purposes of comparison with the performance of the 354 alloys studied. The parameters investigated were the effect of alloying element additions of zirconium, nickel, manganese and scandium, and the influence of different heat treatment conditions.

In order to understand and compare the alloy properties in relation to the various alloying elements as well as determine the effect of the additions made in relation to the heat treatment conditions applied, quality charts, color contour maps and multiple line charts were generated for presenting the tensile test data. The tensile properties and the quality index values pertaining to each alloy/heat treatment condition will be correlated to the corresponding microstructural features and constituents for the purposes of interpreting the results obtained.

Plots of ΔP will also be presented. Such plots represent the difference in a property (P) value obtained for a specific alloy composition/heat treatment condition with respect to that obtained for a base alloy. In the present case, the ΔP values will be plotted taking the

R alloy (354 + 0.25wt%Zr) in the as-cast condition as the base or reference line. The ΔP plots of the UTS, YS and percent elongation values obtained will be generated for selected alloys relative to the values obtained for the base alloy.

5.2 ROOM TEMPERATURE TENSILE PROPERTIES (AS-CAST AND SOLUTION HEAT-TREATED CONDITIONS)

The solution treatment temperature for the 354 casting alloys was selected by a critical selection process because of the high copper content (1.8% Cu) of the alloys. Two solution heat treatment processes were considered suitable based on the extensive investigations carried out by Northwood et al. [130], Sokolowski et al. [131] and Wang et al. [31] of the effect of solution treatment temperature on the tensile properties, namely, single and multi-step solution heat treatments.

Table 5.1 lists the tensile properties obtained for the as-cast and solution heat-treated alloys. The one step solution heat treatment (designated SHT 1) for the 354 alloys was carried out at 495°C for 5 hours while the multi-step solution heat treatment (designated SHT 2) was carried out at three different temperatures: 495 °C , 515 °C and 530 °C for specific times of 5, 2 and 2 hours, respectively. The subsequent increase in solution temperature in the second and third steps improved the strength of the castings compared to the as-cast condition. The tensile properties of R, S, T, U, V and Z alloys in the one-step solution heat-treated condition showed an increase of 10-40 MPa in the UTS, and up to 2.5% in percent elongation in comparison with the as-cast condition, while the yield strength (YS) decreased in the case of alloys R (354 + 0.25% Zr), S (354+2%Ni + 0.25%Zr), U (354+0.75%Mn + 0.25%Zr) and Z (354+0.15%Sc + 0.25%Zr), but showed a slight increase in alloys T (354+4%Ni + 0.25%Zr) and V (354+0.75%Mn+2%Ni +

0.25%Zr). The multi-step solution heat treatment displayed higher tensile properties than those achieved with SHT 1 or in the as-cast condition. The ultimate tensile strength of the given alloys in the multi-step solution heat-treated condition, increased by as much as 70 MPa, and by 3% for the percent elongation in comparison with the as-cast and SHT 1 conditions, while the yield strength remained almost the same. This increase in the mechanical properties is related to the changes occurring in the morphology of the silicon particles during solution heat treatment, so that they become more rounded, resulting in a decrease in their aspect ratio and density [36]. The change in ductility may be explained as follows: in the as-cast condition, the brittle acicular silicon particles serve as stress concentrators since they are harder than the matrix. Such particles tend to promote crack propagation during load application thereby decreasing the ductility of the alloy. The effect of solution heat treatment on the spheroidization of the Si particles increases with the progress of solution treatment at the specified solution temperature, and the ductility increases correspondingly.

The main purpose of solution heat treatment is to maximize dissolution of hardening elements in solid solution; it also leads to the fragmentation and dissolution of undissolved phases such as Fe-intermetallics and fragmentation and spheroidization of the eutectic Si particles so that a homogeneous structure is achieved, leading to improvement in the ductility and the quality of Al-Si cast alloys [39] [132].

From the tensile test data shown in Table 5.1, quality index or Q values were calculated and are also listed in the table. Quality charts were then generated for evaluating the influence of the metallurgical parameters involved on the tensile properties and quality of the 354 aluminum alloys investigated.

Table 5.1 Mean values for UTS, YS, %El for alloys R, S, T, U, V, Z and L subjected to different heat treatment conditions and tested at ambient temperature; Q values obtained using Equation 1

Identification		UTS (MPa)	YS (MPa)	%El (%)	Q (MPa)
R	As Cast	312.41	230.39	2.15	362.37
	SHT1	351.34	209.41	7.38	481.52
	SHT2	381.25	224.55	8.77	522.71
S	As Cast	294.33	209.66	1.70	328.87
	SHT1	305.56	192.12	3.49	387.05
	SHT2	331.97	217.98	3.73	417.70
T	As Cast	300.29	204.31	1.51	327.07
	SHT1	312.32	207.09	2.22	364.35
	SHT2	324.33	222.62	2.25	377.17
U	As Cast	297.56	217.23	1.86	338.05
	SHT1	324.97	213.55	3.44	405.40
	SHT2	339.12	231.03	3.66	423.57
V	As Cast	273.59	202.20	1.29	289.99
	SHT1	299.79	206.64	1.99	344.68
	SHT2	299.27	217.53	1.75	335.79
Z	As Cast	316.01	244.36	1.67	349.42
	SHT1	343.86	240.20	3.65	428.17
	SHT2	331.08	243.79	3.13	405.43

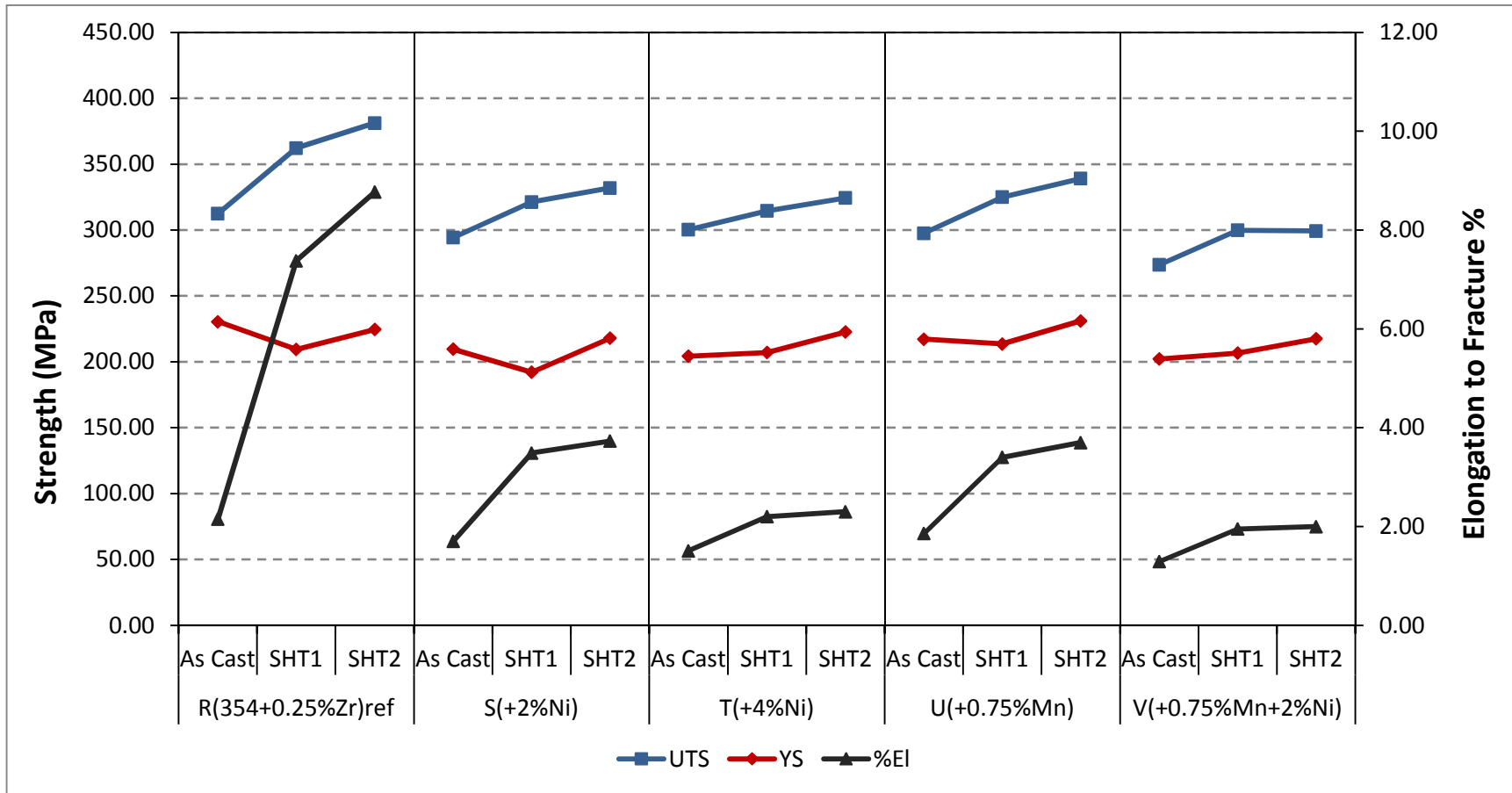


Figure 5.1 Mean values for UTS, YS, % El for Alloys R, S, T, U and V in the as-cast and SHT 1 and SHT 2 solution heat-treated conditions.

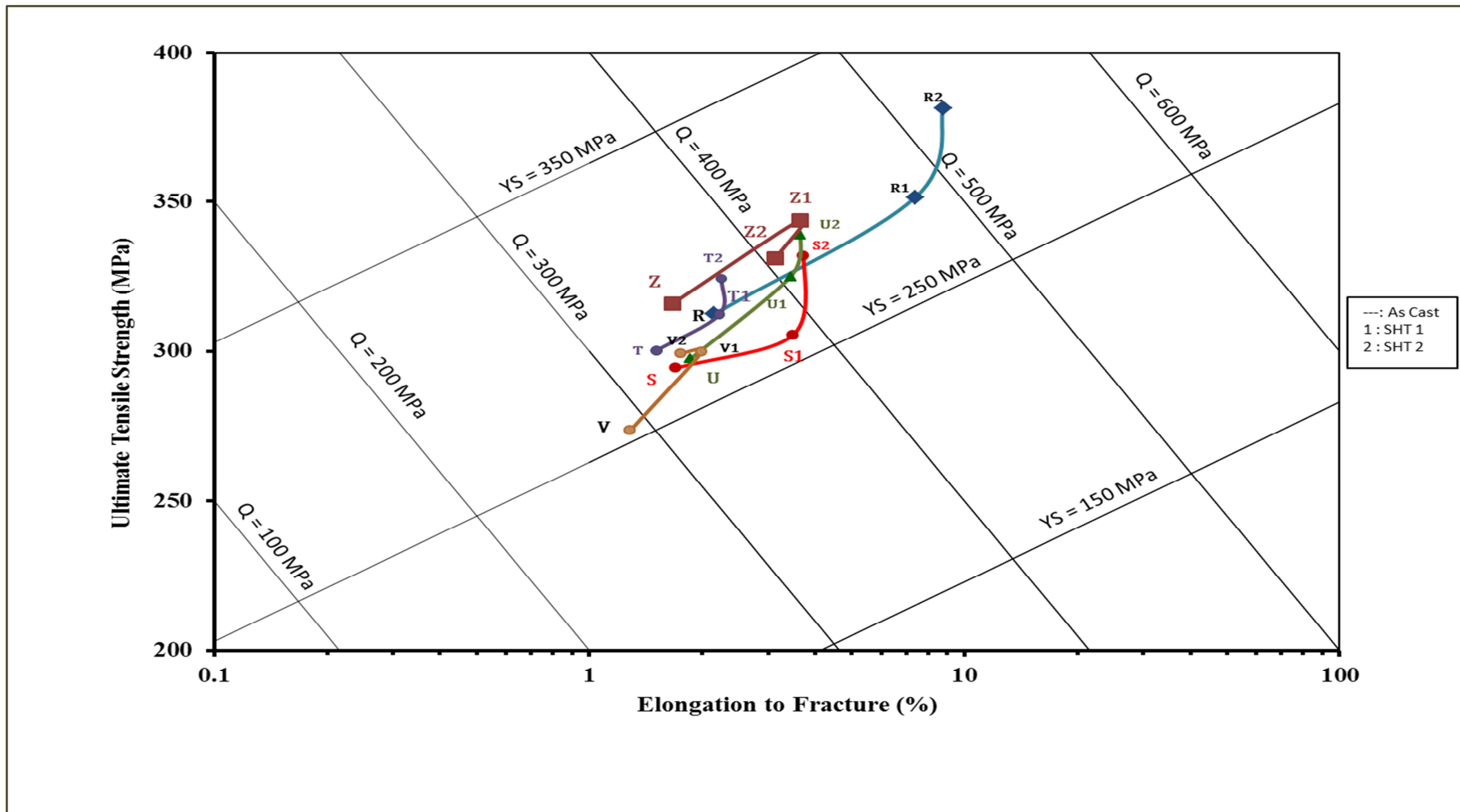


Figure 5.2 Quality chart showing relationship between UTS and percent elongation for the 354 alloys investigated in the as-cast and SHT 1 and SHT 2 solution heat treated conditions.

5.3 INFLUENCE OF ALLOYING ADDITIONS AND HEAT TREATMENT CONDITIONS

Figures 5.3 and 5.4 respectively show the tensile properties of the 354 alloys obtained under various heat-treatment conditions and different alloying element additions, tested without and after 200 h stabilization at 250 °C. The T6 heat treatment condition, which comprises the one step solution heat treatment of 495 °C/5h, followed by quenching and aging at 180°C/8h, increases the alloy strength (UTS and YS) while maintaining more or less the same ductility as that observed in the as-cast case. After T62 treatment, Alloy U (containing 0.75wt% Mn + 0.25wt% Zr) showed the maximum increase in tensile properties, followed by Alloy R (containing only 0.25wt% Zr). In the case of Alloy U, the UTS and YS values increased by ~100 MPa and ~160 MPa, respectively. As may be seen in Figure 5.3, without stabilization, after T5 treatment, the UTS of the alloy is decreased by adding alloying elements to the base alloy R, while no significant change in tensile properties is observed after T7 treatment, compared to the as-cast condition.

Figure 5.4 shows the tensile properties of alloys tested at room temperature after stabilization at 250°C for 200h, for the various heat treatment conditions. The best tensile properties are obtained with the T6 heat treatment. The figure reveals that the alloy performs well with the addition of Mn to the base alloy R. With the use of stabilization, the strengths of the alloys improve after T5 treatment whereas the ductility is lowered. No significant change in the alloy strength is observed with the use of T6, T62 and T7 treatments, while the ductility is improved compared to the T5 condition, with the T62-treated alloys displaying the highest values in each case.

Table 5.2 Mean values of UTS, YS, %El obtained at room temperature (without stabilization) for Alloys R, S, T, U and V subjected to different heat treatment conditions; Q and Probable YS values were obtained using Eqns 1 and 2

Mean values of UTS (MPa) and El (%) used to obtain Q and YS						
Q = UTS + 150log (%El) - Eq. 1 PYS = UTS - 60log (%El) + 13 - Eq 2						
Identification		UTS (MPa)	YS (MPa)	Total Strain (%El)	Q (MPa) (Eq.1)	PYS(MPa) (Eq.2)
R (354+0.25%Zr)	As Cast	312.41	230.39	2.15	362.37	305.42
	T5	336.35	298.21	1.08	341.36	347.34
	T6	374.26	333.56	1.35	393.81	379.44
	T62	393.41	353.24	1.31	411.00	399.37
	T7	340.30	284.19	2.18	391.07	332.99
S (354+0.25%Zr+2%Ni)	As Cast	294.33	209.66	1.70	328.87	293.52
	T5	290.01	265.53	0.80	275.47	308.82
	T6	332.10	322.52	0.79	316.74	351.24
	T62	356.06	353.66	0.76	338.18	376.21
	T7	318.08	281.41	1.12	325.46	328.13
T (354+0.25%Zr+4%Ni)	As Cast	300.29	204.31	1.51	327.07	302.58
	T5	277.71	244.61	0.80	263.17	296.52
	T6	353.51	342.79	0.78	337.32	372.98
	T62	371.40	370.00	0.71	349.09	393.32
	T7	271.96	238.82	0.90	265.10	287.71
U (354+0.25%Zr+0.75%Mn)	As Cast	297.56	217.23	1.86	338.05	294.36
	T5	263.33	238.29	0.81	249.60	281.82
	T6	357.21	345.69	0.84	345.85	374.75
	T62	397.19	373.79	1.01	397.84	409.93
	T7	280.86	234.92	1.36	300.89	285.85
V(354+0.25%Zr+0.75%Mn+2%Ni)	As Cast	273.59	202.20	1.29	289.99	280.04
	T5	244.56	227.46	0.67	218.47	268.00
	T6	284.18	283.40	0.55	245.23	312.76
	T62	335.53	335.00	0.65	307.47	359.76
	T7	257.40	228.22	0.90	250.54	273.15

Table 5.3 Mean values of UTS, YS, %El obtained at room temperature (after 200h/250°C stabilization) for Alloys R, S, T, U and V subjected to different heat treatment conditions; Q and Probable YS values were obtained using Eqns 1 and 2

Mean values of UTS (MPa) and El (%) used to obtain Q and YS						
Q = UTS + 150log (%El) - Eq. 1 PYS = UTS - 60log (%El) + 13 - Eq 2						
Identification		UTS (MPa)	YS (MPa)	Total Strain (%El)	Q (MPa) (Eq.1)	PYS (MPa) (Eq.2)
R(354+0.25%Zr)	As Cast	216.63	130.19	3.04	289.06	200.66
	T5	244.63	138.20	3.17	319.79	227.57
	T6	254.03	152.84	5.39	363.77	223.13
	T62	288.08	176.47	7.42	418.64	248.86
	T7	275.54	164.25	6.20	394.40	241.00
S(354+0.25%Zr+2%Ni)	As Cast	263.48	167.82	1.88	304.69	259.99
	T5	278.92	191.77	1.73	314.63	277.63
	T6	267.80	173.25	2.64	331.09	255.48
	T62	279.33	171.09	3.99	369.41	256.27
	T7	276.25	178.03	3.02	348.17	260.48
T(354+0.25%Zr+4%Ni)	As Cast	259.91	166.37	1.55	288.46	261.49
	T5	298.32	203.78	1.57	327.72	299.56
	T6	293.4	197.99	1.86	333.39	290.19
	T62	294.4	181.47	2.84	362.5	280.16
	T7	283.31	187.24	1.88	323.98	279.63
U(354+0.25%Zr+0.75%Mn)	As Cast	274.67	186.92	2.22	326.62	266.89
	T5	318.1	213.16	2.38	374.59	308.51
	T6	315.7	202.48	3.94	404.62	292.57
	T62	286.46	172.23	4.53	384.87	260.09
	T7	283.87	175.58	3.68	368.75	262.92
V(354+0.25%Zr+0.75%Mn+2%Ni)	As Cast	297.02	198.23	1.60	327.64	297.77
	T5	300.34	216.96	1.42	322.99	304.28
	T6	291.88	190.04	2.35	347.62	282.59
	T62	296.74	192.29	2.75	362.64	283.38
	T7	282.83	180.13	2.33	337.93	273.79

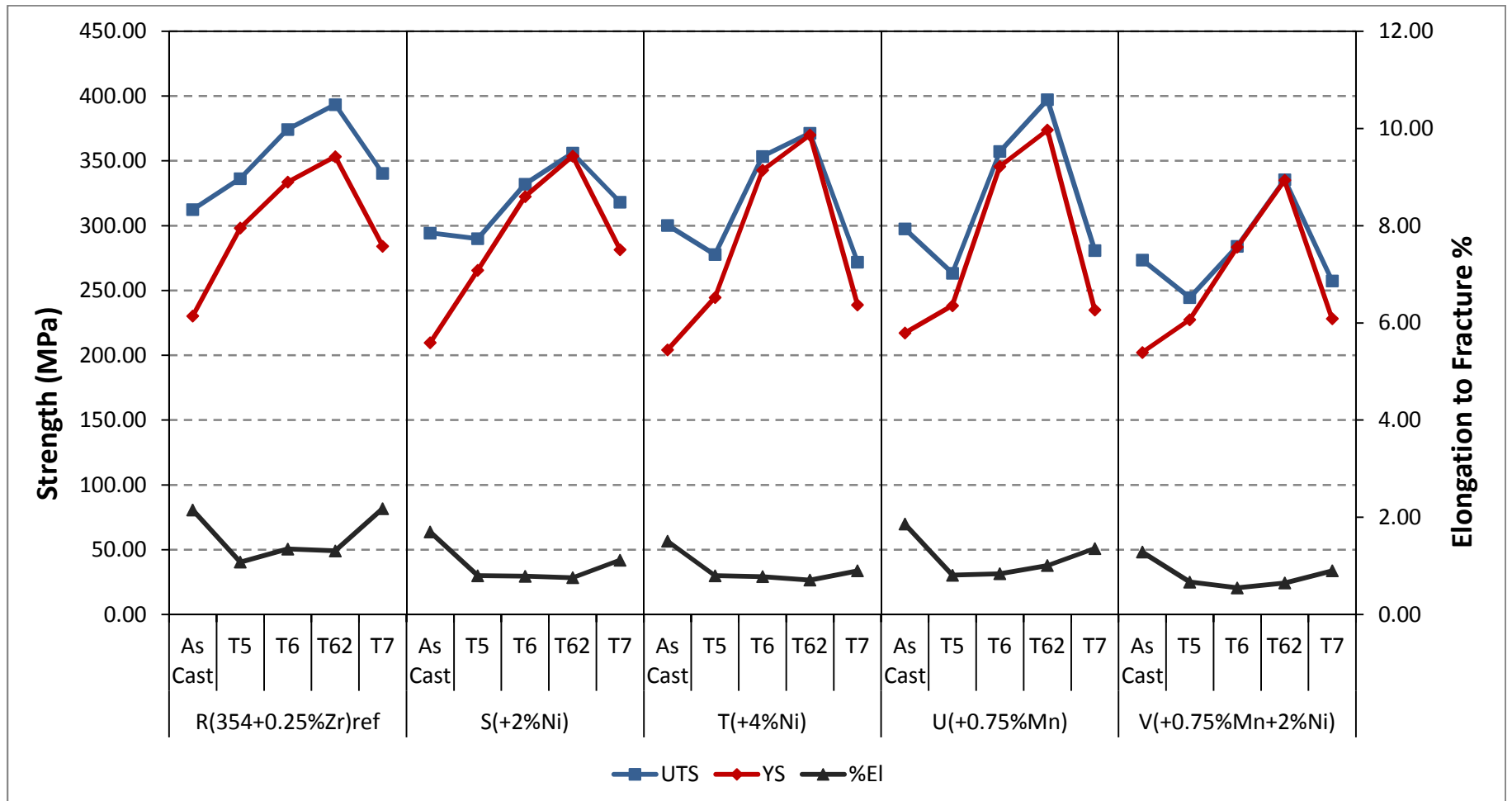


Figure 5.3 Mean values for UTS, YS, % EI for Alloys R, S, T, U and V obtained under the given heat treatment conditions (without stabilization).

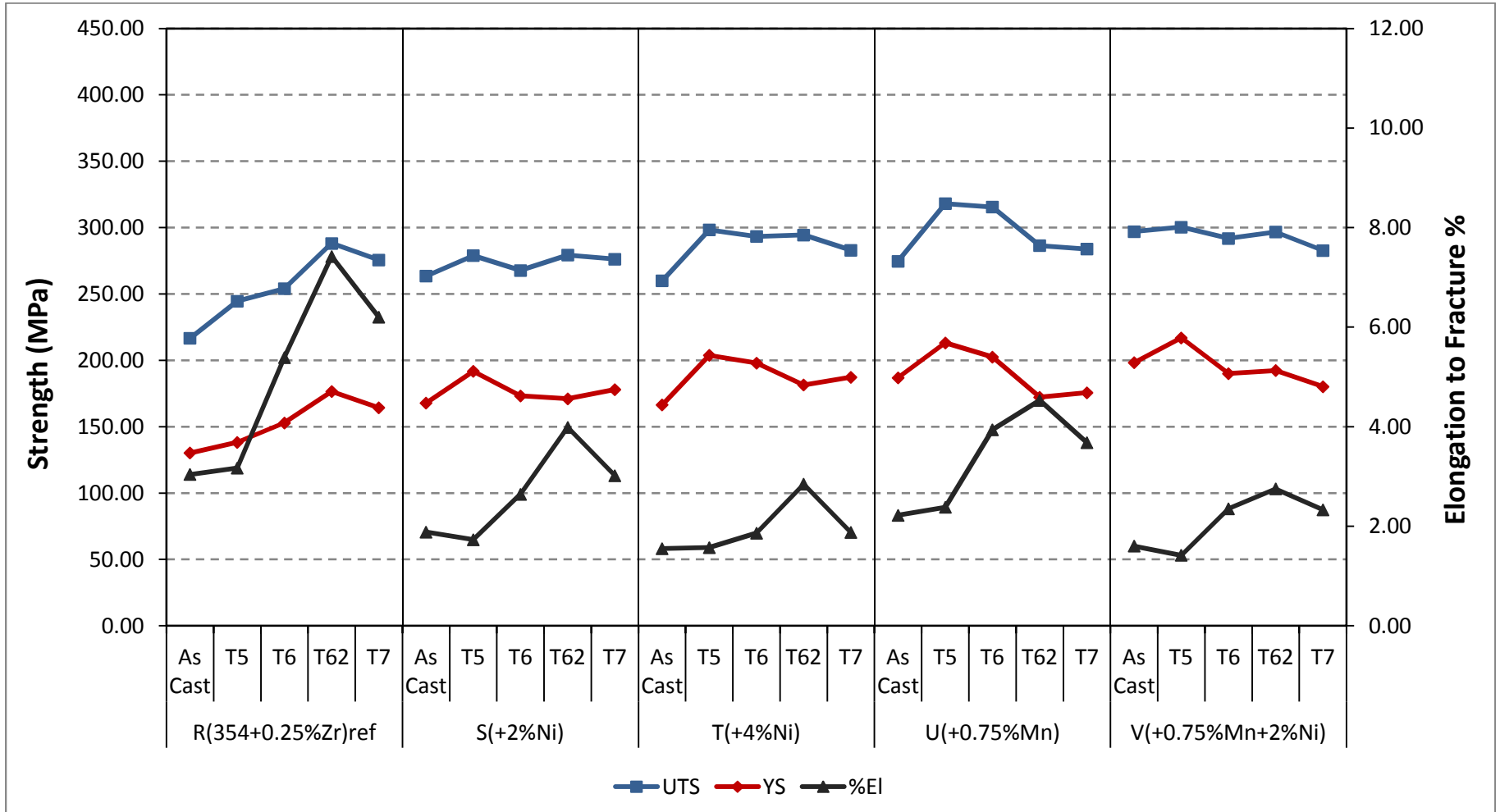


Figure 5.4 Mean values of UTS, YS, % El for Alloys R, S, T, U and V obtained under the given heat treatment conditions (after 200 hours stabilization at 250°C).

Color-contour maps are 2D vector plots that display a field of vectors in x, y coordinates where both direction and magnitude are represented. It is a tool that can help to present the tensile results obtained in a different way, whereby one can observe how the properties vary with different heat treatment conditions, according to the change in color and magnitude of the contour regions. Each contour line represents a specific value of the property being considered. As an example, Figures 5.5 and 5.6 show the quality index (Q) and probable yield strength (YS) color-contour maps for Alloys R, S, T, U and V tested at room temperature, without and after 200 hours stabilization at 250°C, respectively. Quality index (Q) and probable yield strength (PYS) values were obtained using Equations 1 and 2, and are plotted as a function of heat treatment conditions and alloying additions.

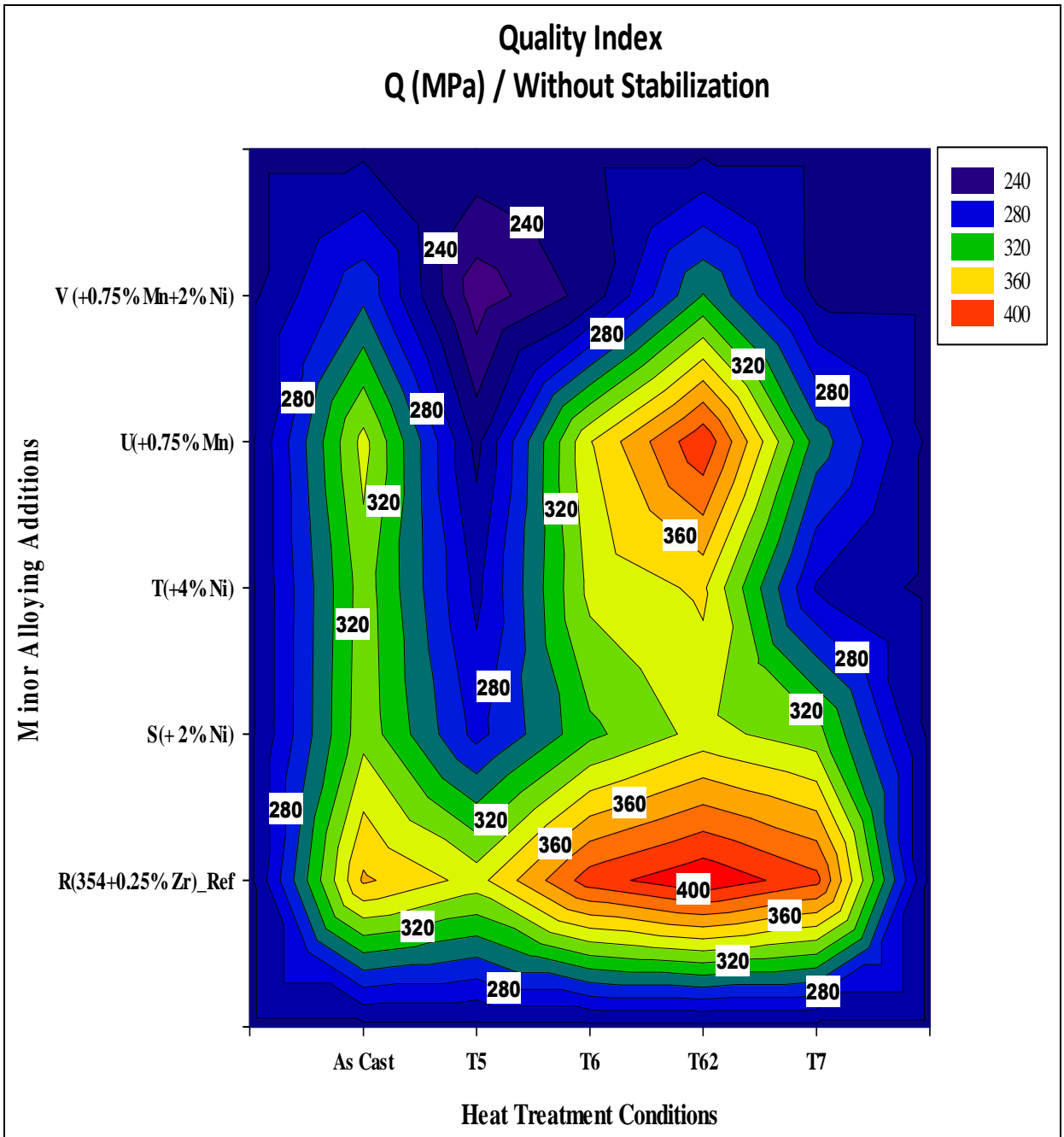
As may be seen from Figure 5.5, the tensile performance of the as-cast base alloy R is improved after the application of different heat treatments. After T5 treatment, the quality of the alloy decreases with the addition of alloying elements to the base alloy R. For T6 and T62 heat treatments, the tensile properties decrease with the addition of Ni, but increase in the case of Alloy U when Mn is added. The figure also reveals that Alloy R shows the best quality index values after T62 treatment, i.e., 411 MPa and 418.64 MPa without, and with 200 hours stabilization, respectively, followed by Alloy U which displays a Q value of 397.84 MPa after T62 treatment (with no stabilization) and 404.62 MPa following T6 treatment and 200 h stabilization at 250°C before testing.

Figure 5.6 shows the probable yield strength (YS) color-contour maps for Alloys R, S, T, U and V. Figure 5.6(a) reveals that, in the absence of stabilization, the yield strength of the base alloy R does not change to any great extent with alloying additions. With 200 h

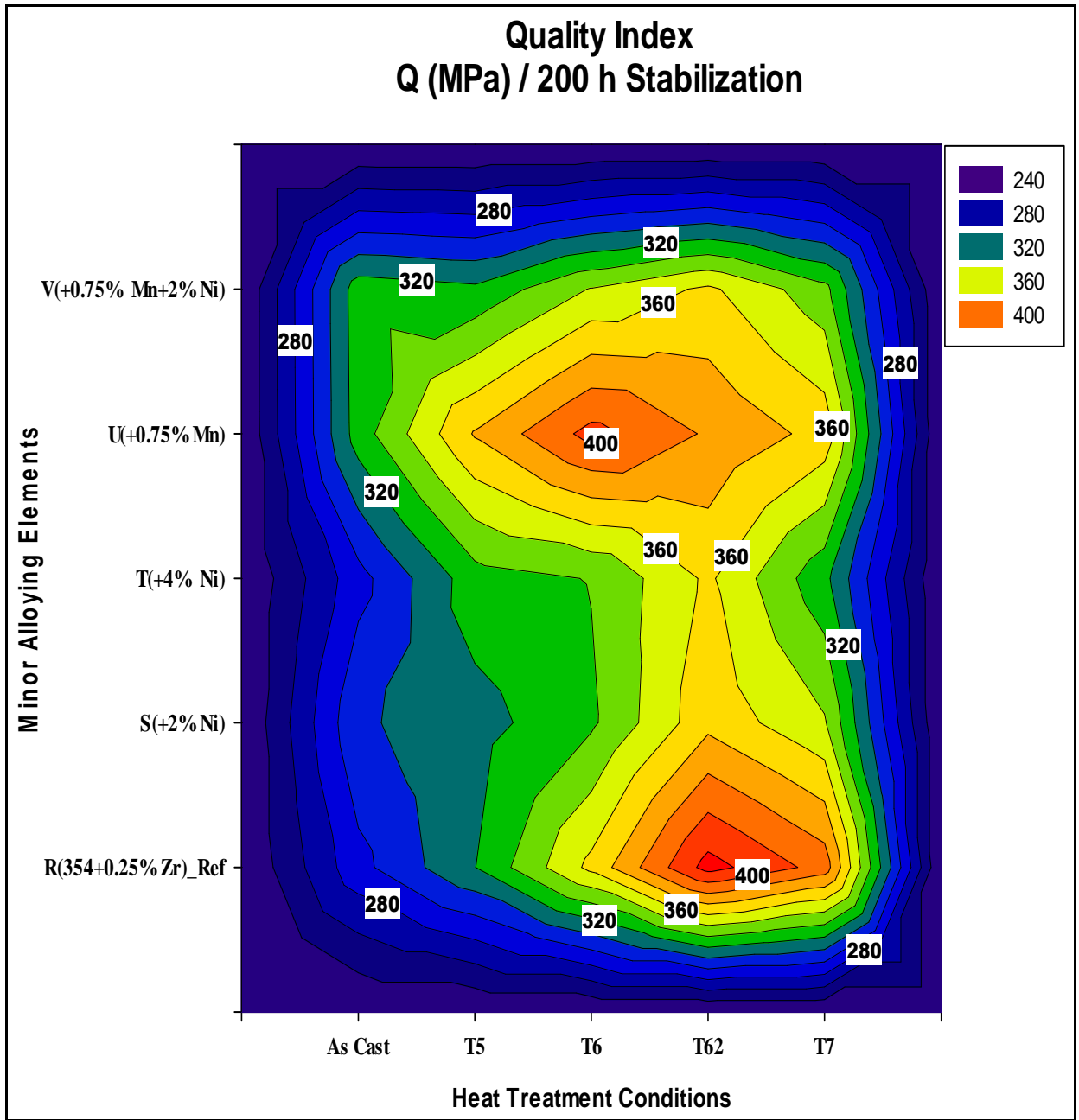
stabilization at 250 °C, however, the yield strength increases with both addition of alloying elements and the heat treatments applied to Alloy R, as seen from Figure 5.6(b).

The ultimate tensile strength (UTS) is normally used for the specification and quality control of the casting, while the ductility of the casting, expressed as percent elongation to fracture, is usually used as an indicator of casting quality because of its sensitivity to the presence of any impurity or defect in the cast structure. On the other hand, yield strength does not represent the quality of the casting since it is a material property which is not affected by the level of defects or impurities present in the casting, but is influenced, rather, by the movement of dislocations in the casting structure, and depends on the resistance expected by the hardening precipitates to the movement of dislocations. [123] In general, therefore, quality charts provide a simple tool for estimating and recommending the appropriate processing conditions to obtain specified properties and hence to facilitate the selection of castings to meet these specifications.

As may be seen in Figures 5.5 and 5.6, the more colored contours observed in the case of Alloys R, S and U are indicative of the fact that the mechanical quality shows an increase in the range of values both without and with 200 hours stabilization.

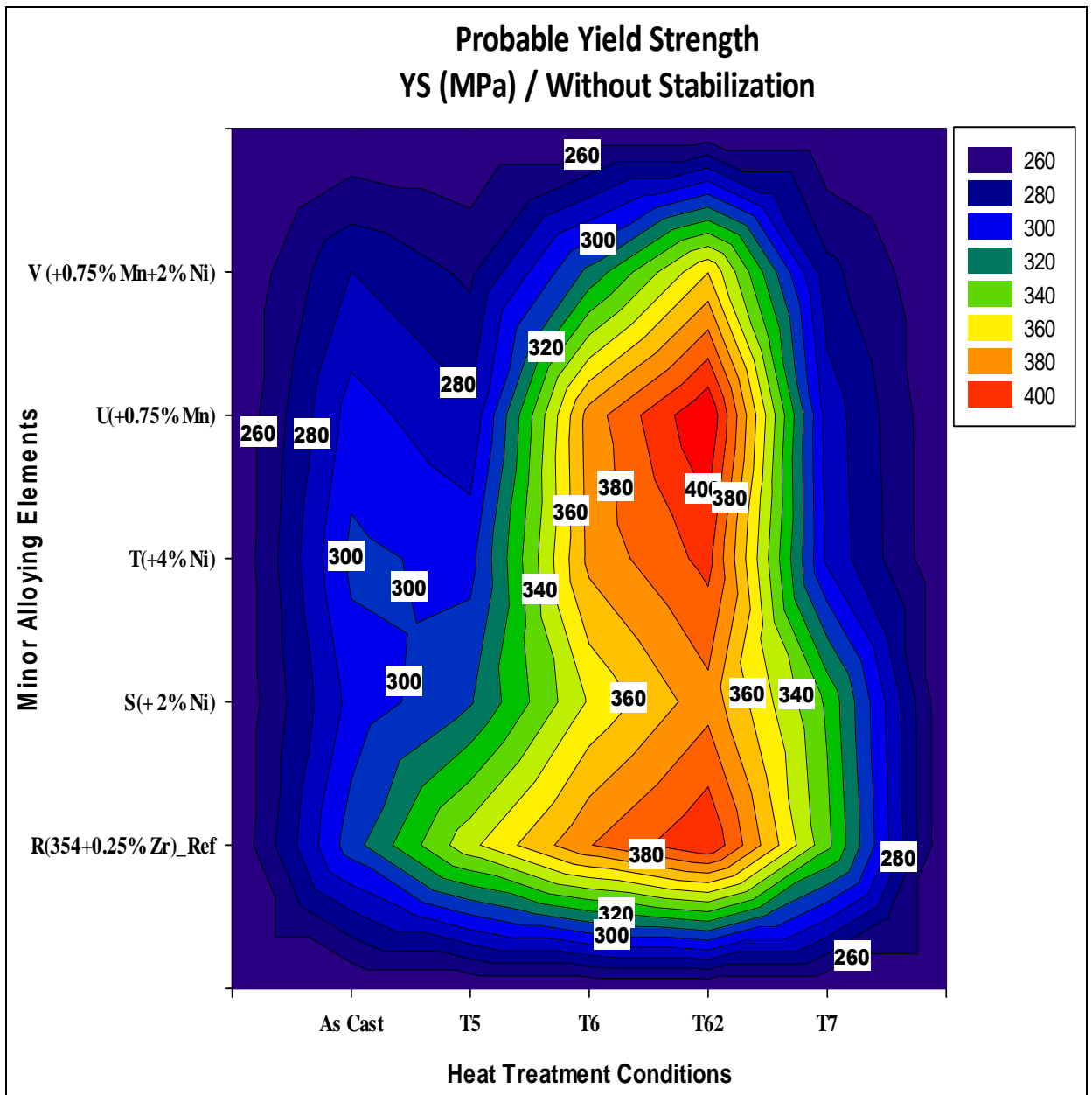


(a)



(b)

Figure 5.5 Quality index-color contour charts for Alloys R, S, T, U and V obtained from room temperature tensile testing data: (a) without stabilization, and (b) after 200 h stabilization at 250°C



(a)

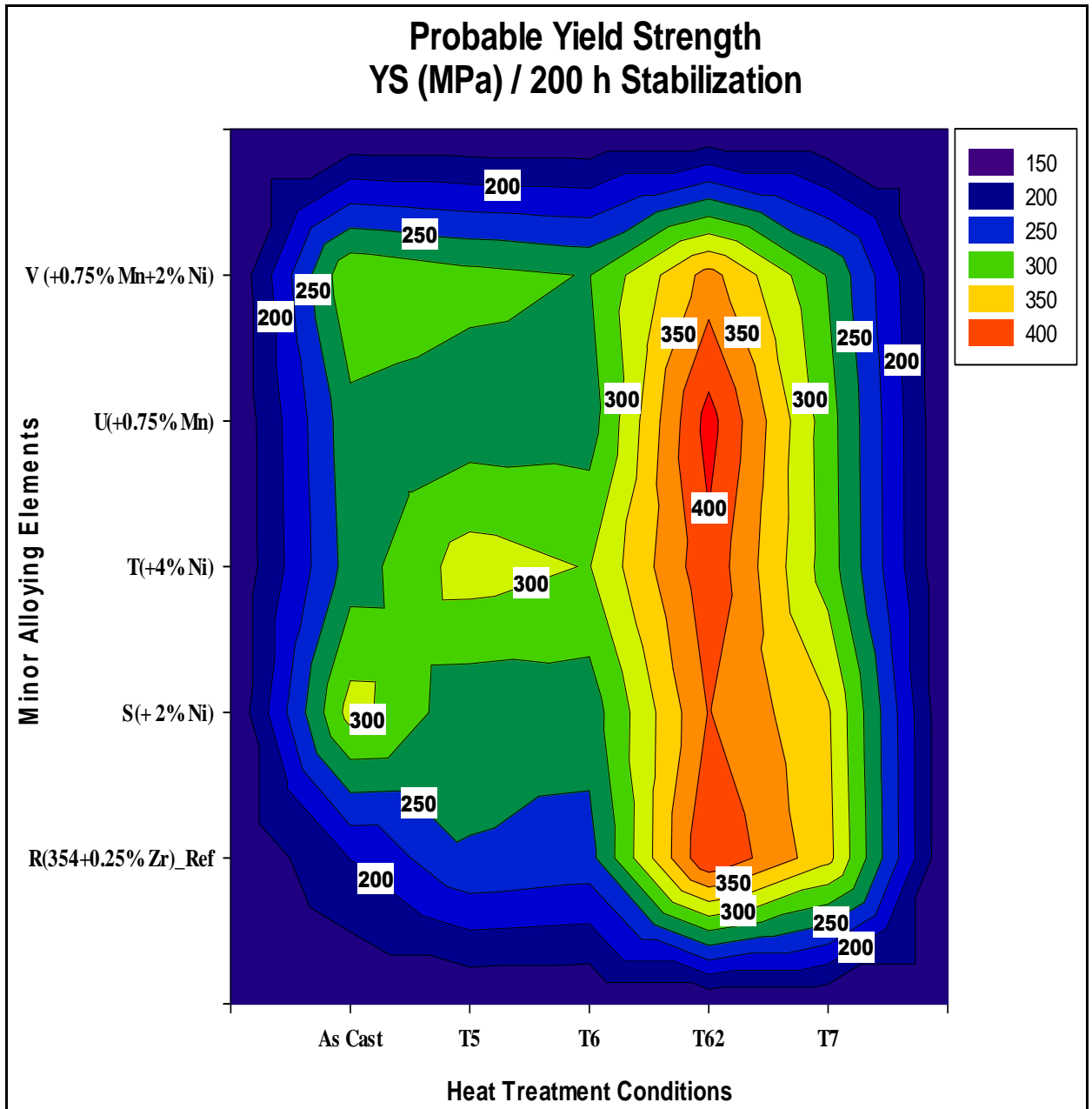


Figure 5.6 Probable yield strength-color contour charts for Alloys R, S, T, U and V obtained from room temperature tensile testing data: (a) without stabilization, and (b) after 200 h stabilization at 250°C.

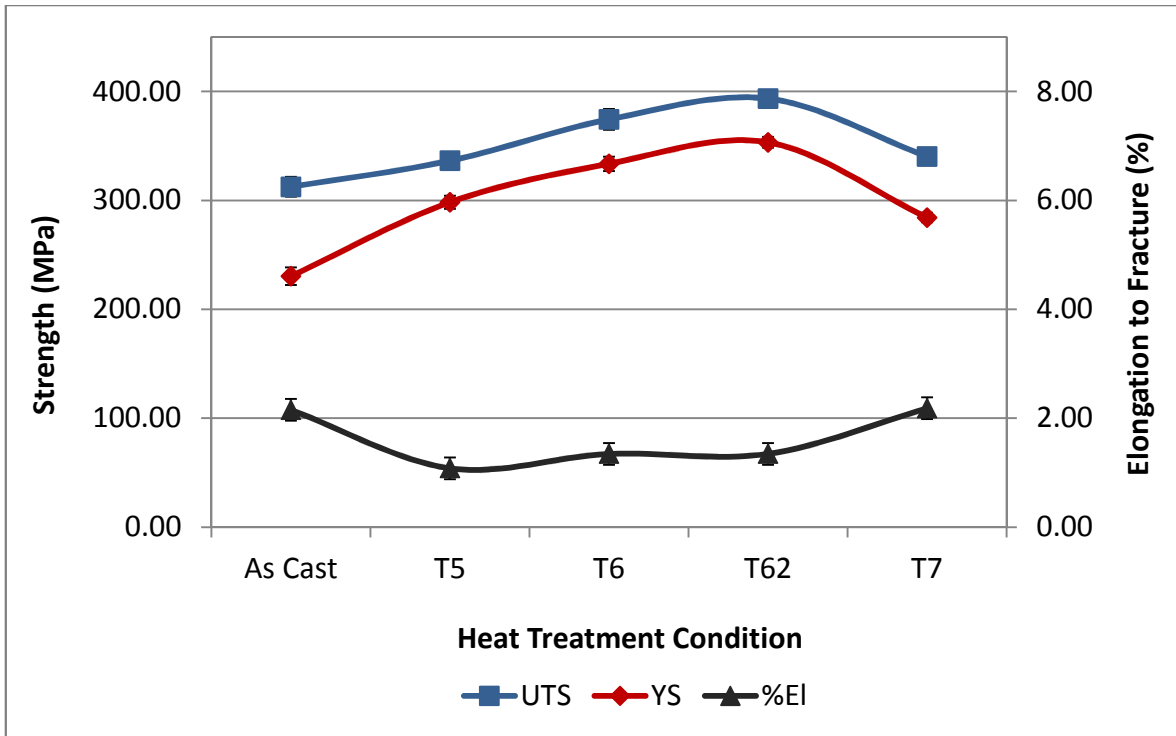
5.4 TENSILE PROPERTIES OF ALLOYS R, S AND U AT ROOM TEMPERATURE

Tensile tests at room and at high temperature were performed to know the effect of additions of zirconium, nickel, manganese and scandium on the mechanical performance of 354 cast aluminum alloy. As evidenced by the results presented in the previous section, Alloys R, S and U give best results for tensile properties. Therefore, these alloys were selected for testing at high temperature. Alloys Z and L which contain zirconium and scandium additions will also be compared with these alloys to determine the best alloys that are suitable for high temperature applications.

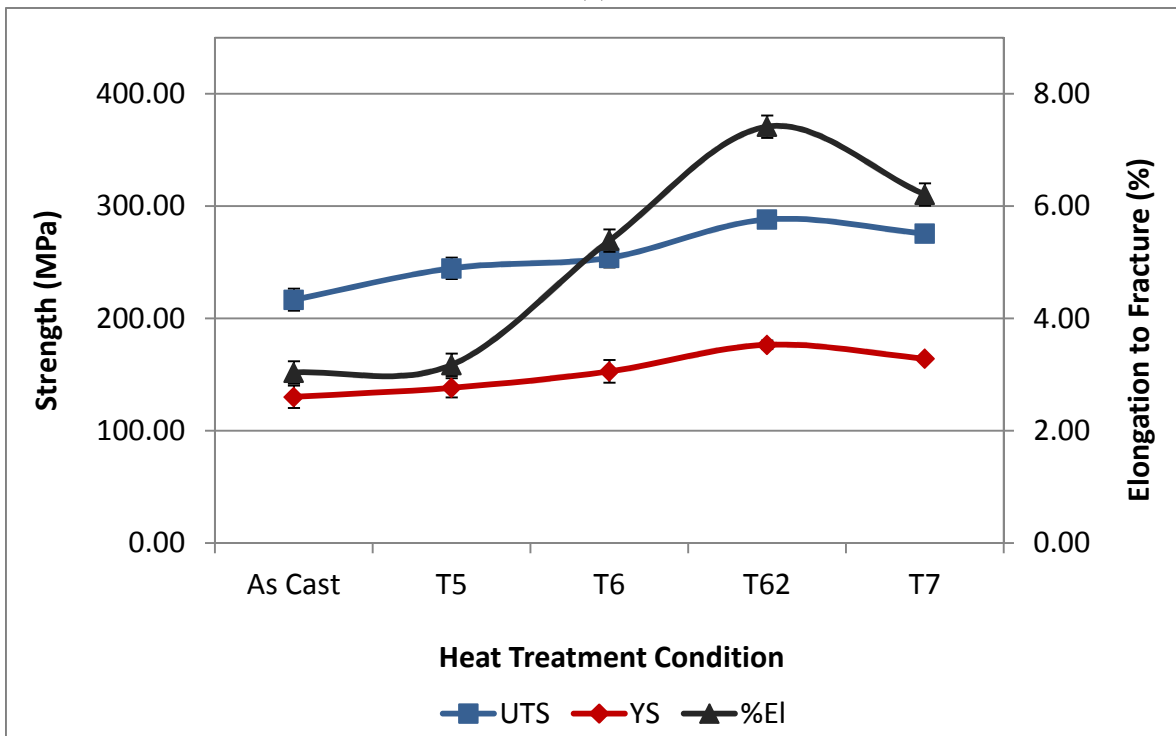
5.4.1 Alloy R (354 + 0.25wt% Zr)

Figure 5.7 shows the room temperature tensile properties obtained from Alloy R (containing 0.25wt% Zr) corresponding to various heat treatment conditions, without and after 200h@250°C stabilization prior to testing. Compared to the as-cast condition, heat treatment obviously affects the tensile performance of the alloy. As may be observed from Figure 5.7(a), without stabilization, the strength of the alloy increases with the heat treatments T6 and T62, in which the formation of coherent precipitates is the main source of strengthening in the R alloy, while it increases to a lesser extent after T5 and T7 heat treatments. With 200 h stabilization at 250°C, while lower strength values are obtained, the UTS and YS follow the same trend as in the case of Fig. 5.7(a) with respect to the heat treatment conditions applied, however, with a larger gap between them. In this case, also, highest strength is obtained with the T62 treatment. In addition, the alloy also exhibits high ductility, ~7% with this treatment.

The presence of Zr in the alloy would lead to the formation of Al_3Zr dispersoids which are known for persisting even at high temperatures. This will ensure that the alloy would maintain high strength values. The use of the T62 treatment, incorporating the two-step solution treatment, allows for maximum dissolution of the copper phases in the two stages of solution treatment. Such dissolution would further strengthen the alloy matrix. In general, if alloy strength is increased, the ductility correspondingly decreases, and vice versa. A high ductility implies that the hardening precipitates and particles observed in the matrix have undergone coarsening, larger particles growing at the expense of smaller ones, so that more of the ductile matrix is present between the hard precipitates, which will increase the ductility. Furthermore, the stabilization treatment would also contribute to this effect.



(a)



(b)

Figure 5.7 Mean values for UTS, YS, % El for Alloy R at the given heat treatment condition: (a) without, and (b) after 200 h stabilization at 250°C prior to testing.

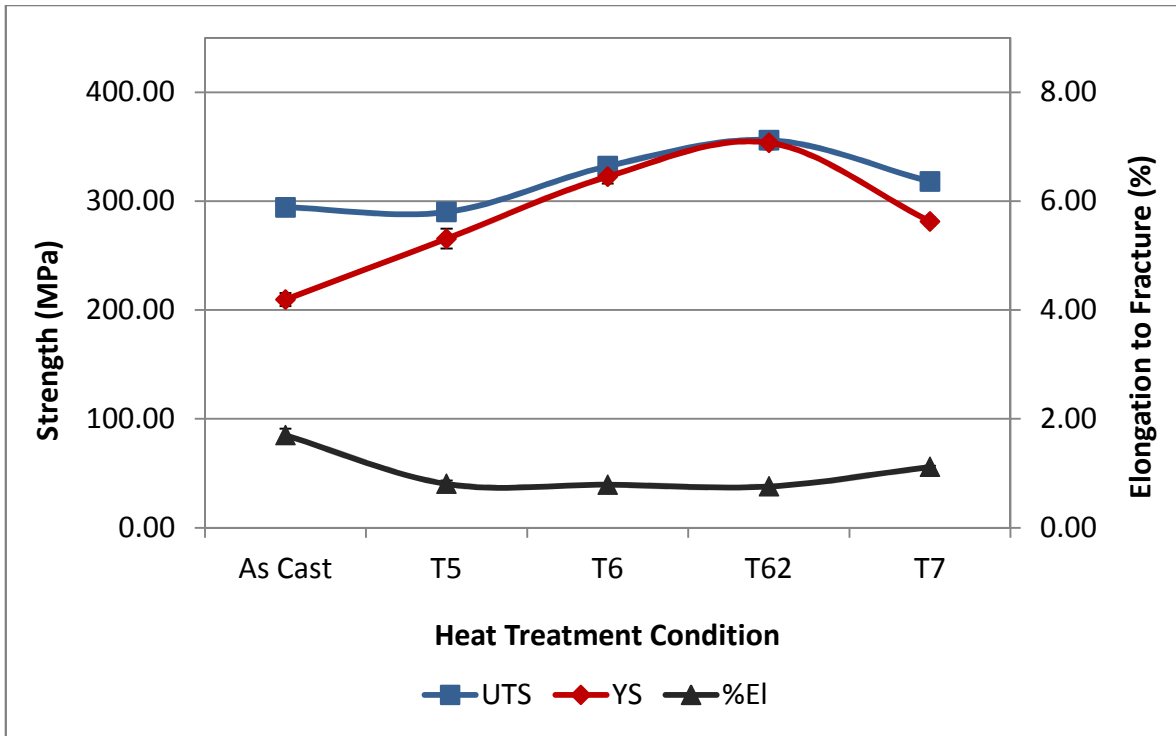
5.4.2 Alloy S (354 + 0.25wt% Zr + 2wt% Ni)

Figure 5.8 shows the tensile properties obtained from the S alloy (containing 0.25wt% Zr + 2wt% Ni) corresponding to the various heat treatment conditions applied. Without stabilization, T6 and T7 treatments improve the alloy UTS by ~25 MPa from its as-cast value, whereas there is a significant increase in YS, of about 80-100 MPa. As in the case of Alloy R, the T62 treatment produces the greatest improvement in both UTS and YS, whereas no change in UTS is noted after T5, except for the decrease in ductility to approximately half that in the as-cast case for T5, T6 and T62 heat treatments, with a slight increase for the T7 treatment, as expected, with the corresponding decrease in strength associated with alloy softening. Figure 5.8(b) reveals that with 200 h stabilization, the as-cast alloy strength (264 MPa UTS/~168 MPa YS) increases slightly by about 16 MPa UTS/~23 MPa YS after T5 treatment and then remains practically the same for the T6, T62 and T7 heat treatments. The ductility decreases or increases with the increase or decrease in UTS, ranging from ~1.7 to ~3%, with the exception of the T62-treated alloy, which exhibits the highest ductility of ~4%.

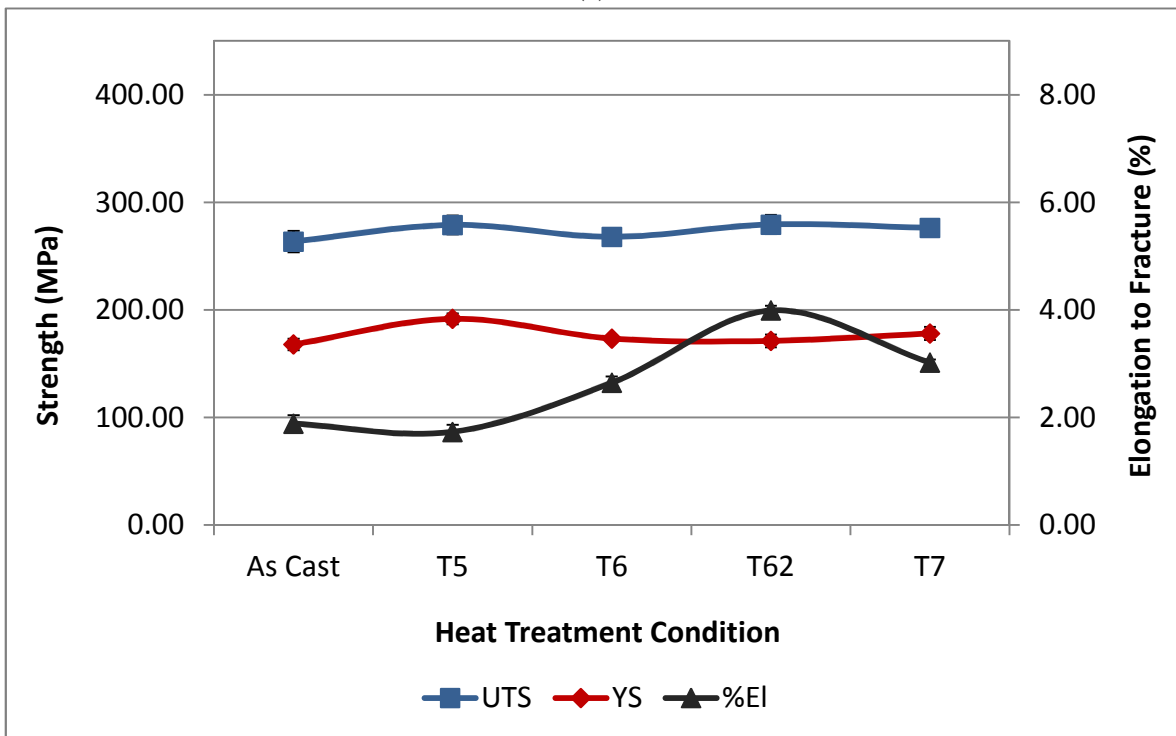
The presence of 2 wt% Ni in Alloy S leads to the formation of Al-Cu-Ni phase particles in addition to the Al₂Cu phase. The persistence of this phase after T6, T62 and T7 heat treatments would explain the increased strength observed in these cases, and would also account for the high YS values, as the Al-Cu-Ni particles would act as barriers to the movement of dislocations in the matrix.

The decrease in strength observed after the application of the stabilization treatment prior to testing, Figure 5.8(b), could be attributed to the effect of incipient melting of the copper phases, during the prolonged 200 h treatment at 250 °C, and the consequent

formation of porosity related to such melting. As the number of the hard Cu- or Cu-Ni-phase particles would decrease, the yield strength would also be significantly lowered. In this case, the increased ductility observed for the T62-treated alloy would be attributed to the effect of particle coarsening, as well, over the duration of the stabilization treatment.



(a)



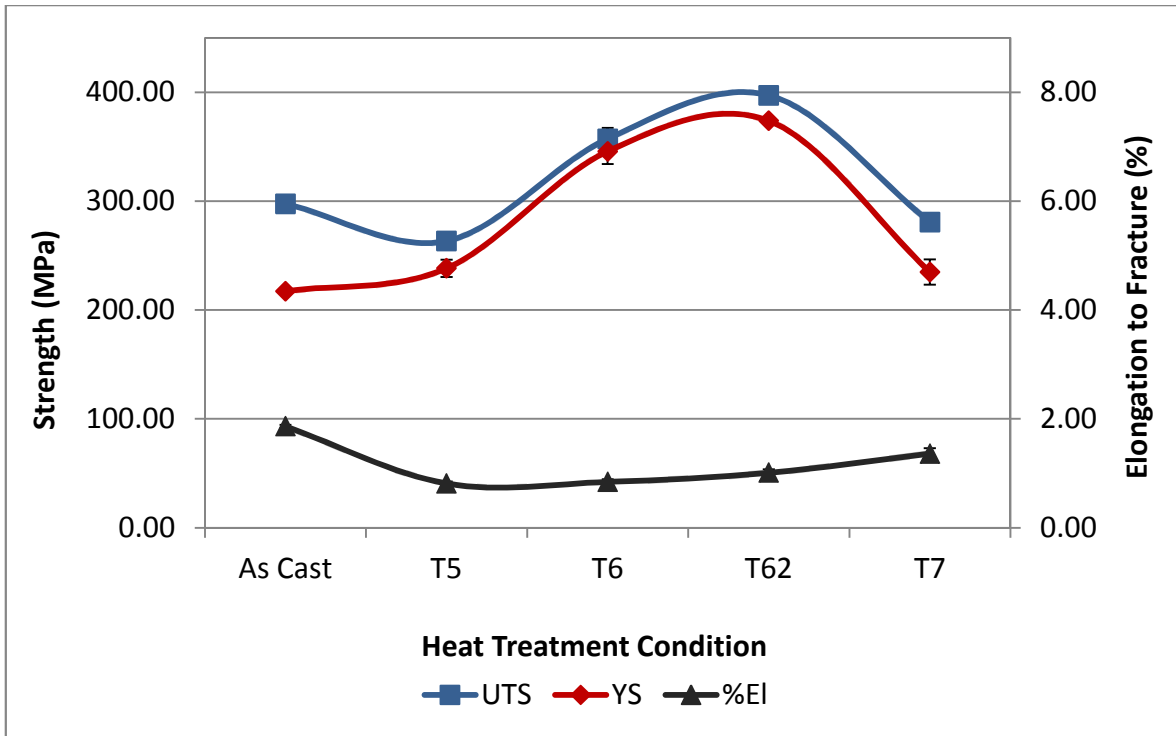
(b)

Figure 5.8 Mean values for UTS, YS, % EI for Alloy S at the given heat treatment condition: (a) without, and (b) after 200 h stabilization at 250°C prior to testing.

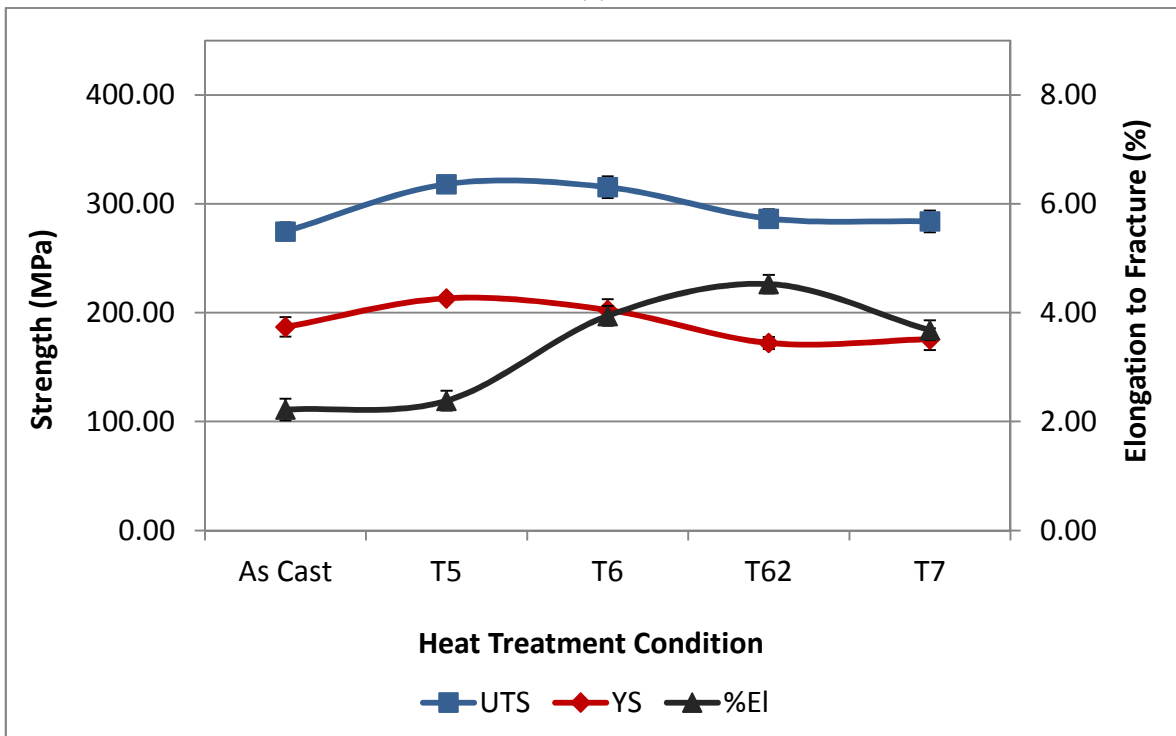
5.4.3 Alloy U (354 + 0.25wt% Zr + 0.75wt% Mn)

Figure 5.9 shows the room temperature tensile properties obtained for Alloy U subjected to the different heat treatment and stabilizing conditions. Compared to the as-cast condition, and without stabilization prior to testing, both T6 and T62 heat treatments increase the alloy strength by a significant amount compared to the T5 condition, with T62 corresponding to the peak aging condition, with strength values of ~397 MPa UTS and ~374 MPa YS, and T7 corresponding to the overaged condition where the strength values drop by ~120 MPa when softening of the alloy takes place. In association with the increase in UTS and YS values observed, the ductility decreases from 2% in the as-cast condition to ~1% for the T5, T6 and T62 heat-treated alloys, increasing to ~1.5% in the T7-treated alloy.

In contrast, after 200 h stabilization at 250 °C, the T62 and T6 display lower strength values, ranging from ~286 to 315 MPa UTS and from ~172 to 202.5 MPa YS, respectively, whereas the ductility in the T62 condition increases to almost double that of the as-cast value (*cf.* 4.53% with 2.22%). It may also be noted that T6- and T7-treated alloys exhibit practically the same ductility values, indicating that the T7 heat treatment conditions and the stabilization at 250 °C prior to testing were not sufficient to cause softening in the alloy.



(a)



(b)

Figure 5.9 Mean values for UTS, YS, % El for Alloy U at the given heat treatment condition: (a) without, and (b) after 200 h stabilization at 250°C prior to testing.

5.4.4 Quality charts for Alloys R, S and U - Room temperature tensile data

Quality charts were constructed from the tensile test data obtained for Alloys R, S and U subjected to the various heat treatments, and tested (a) without stabilization, and (b) after stabilization for 200 h at 250°C. Equations 1 and 2 were used to calculate the quality index (Q) values and plot the *iso-Q* lines and the *iso-YS* lines, respectively. Figure 5.10 presents the quality chart for Alloys R, S and U in which the points in the chart labelled 'T5', 'T6', etc. represent the values obtained without stabilization prior to testing, whereas 'T5.1', 'T6.1', etc. refer to values that were obtained when the alloys were stabilized before testing.

The contoured curves observed in the quality chart indicate how each type of heat treatment affects the performance of these alloys, and enables selection of the best compromise between strength and ductility required for a specific application. In the present case, the two sets of curves for each alloy also bring out certain salient facts. For example, the use of a stabilization treatment considerably improves the alloy quality, as is clearly seen in the case of Alloys S and U. The improvement in alloy quality is brought about by the shift towards higher ductility values exhibited by the stabilized alloys. With respect to heat treatment type, the T62 treatment provides the best results in terms of enhancing the alloy strength towards both higher *iso-YS* lines and UTS values. In the case of the base (reference) alloy R, higher alloy strengths are obtained without the stabilization treatment, whereas higher ductilities are obtained with stabilization. Here again, the T62 heat treatment provides the best results in terms of alloy quality.

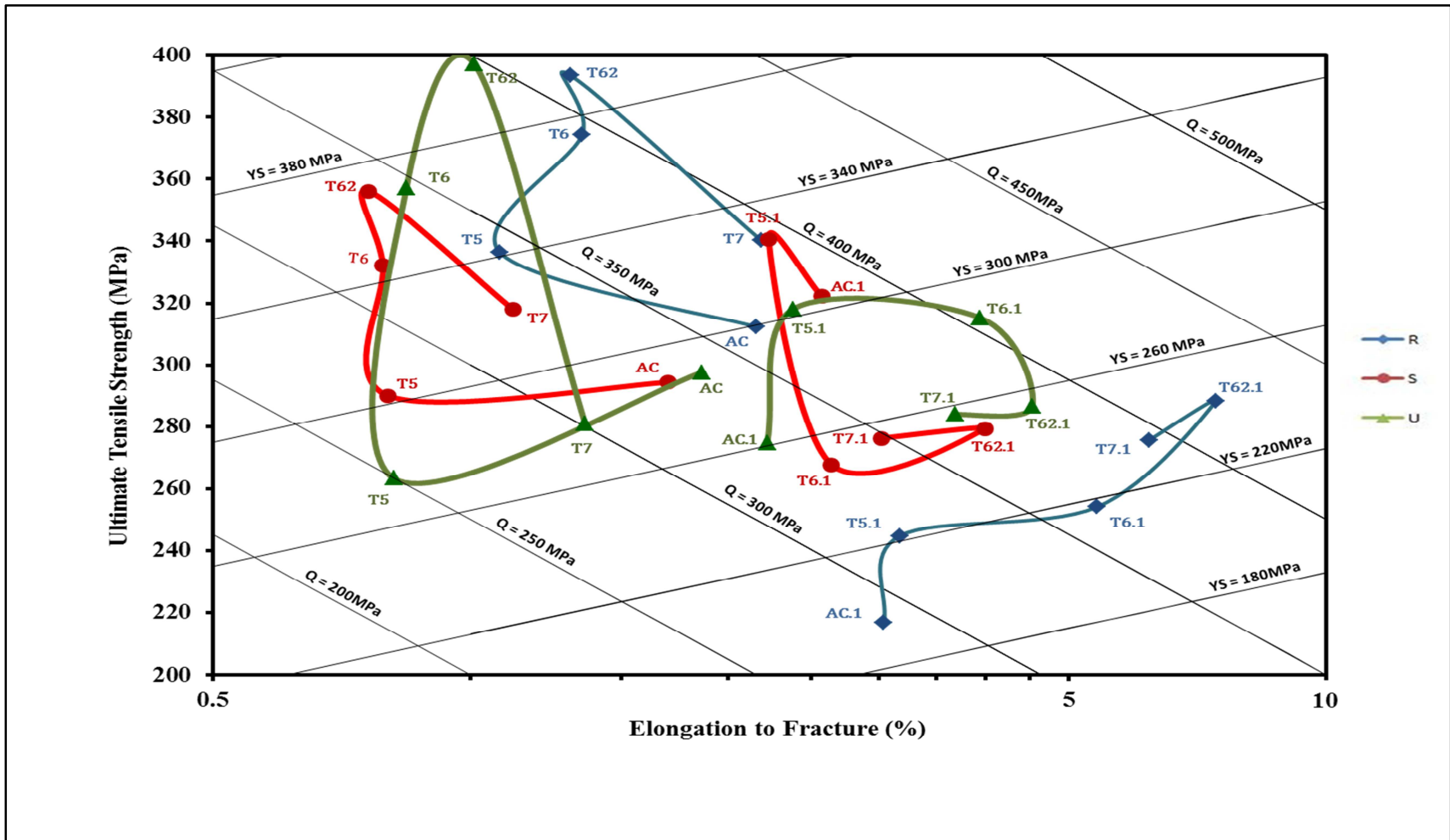


Figure 5.10 Quality charts showing UTS vs % El plots for Alloys R, S and U subjected to various heat treatment conditions, and tested at room temperature without and with 200 h stabilization at 250°C prior testing.

5.4.5 Effect of Zr and Sc addition to 354 and 398 alloys

In this section, the room temperature tensile properties of as-cast and T6-heat treated 354 alloys R, S and U will be compared with the tensile properties of another 354 alloy (Alloy Z, containing 0.25 wt% Zr and 0.15 wt% Sc) and the new aluminum alloy 398 (coded Alloy L, containing the same alloying additions as Alloy Z) to examine (i) the effect of a combined Zr and Sc addition in changing the behavior of the 354 alloy, and (ii) the feasibility of using the new alloy 398 with the same Zr and Sc additions as an alternative for similar high temperature applications.

Aluminum alloy 398 is an Al-Si hypereutectic alloy (containing 16 wt% Si) with a microstructure that consists of small polygonal primary silicon particles evenly distributed in an aluminum matrix. As mentioned previously, this alloy was originally developed by NASA as a high performance piston alloy to meet US requirements and tensile strength suitable for many applications at elevated temperatures - from 260°C to 370°C; this alloy has been reported to offer significant improvements in strength relative to most conventional aluminum alloys [9], [133]. It would be interesting, therefore, to compare the performance of the 354 alloy used in this study with that of 398 alloy.

To this effect, additions of 0.25wt% Zr + 0.15wt% Sc were made to each alloy (giving alloys Z and L) and their as-cast properties compared. It has been shown that Zr increases the resistance to aging when it is added to binary Al-Sc alloy [62]. Table 5.4 compares the tensile properties obtained for the five alloys when tested at room temperature without prior stabilization.

As may be seen from Table 5.4, for the as-cast condition, the strength of the alloy decreases with the addition of Ni in Alloy S, and Mn in case of Alloy U, but it remains almost the same in Alloy Z (containing Zr + Sc). Alloy L, however, or alloy 398 with the same Zr and Sc additions, gives the lowest strength values. After T6 heat treatment (incorporating SHT 1 solution treatment), the alloy strength is increased in each case. All alloys display an increase in UTS of approximately 30 MPa, 40 MPa and 60 MPa after heat treatment (T6), respectively. As may be observed from Table 5.4, Alloy R (containing 0.25wt% Zr) in the T6-SHT condition seems to be the best alloy with respect to mechanical properties at high temperature, since it displays the higher tensile properties taking into consideration the alloys tested in both as-cast and T6 conditions.

Table 5.4 Comparison of tensile properties of Alloys R, S, U, Z and L (tested at room temperature without stabilization).

	Room Temperature/No Stabilization									
	Alloy R (354 + 0.25% Zr)		Alloy S (354 + 0.25% Zr + 2%Ni)		Alloy U (354 + 0.25% Zr + 0.75% Mn)		Alloy Z (354 + 0.2 % Zr + 0.15% Sc)		New Alloy L (398 + 0.25%Zr + 0.15% Sc)	
Av.	As Cast	T6	As Cast	T6	As Cast	T6	As Cast	T6	As Cast	T6
UTS	312.41	374.26	294.33	332.10	297.56	357.21	316.01	357.94	234.7	260.37
SD	14.15	29.58	3.45	5.78	4.24	14.84	17.68	5.49	5.79	7.21
YS	230.39	333.56	209.66	322.52	217.23	345.69	244.36	342.25	204.33	260
SD	8.05	26.54	5.94	6.29	2.03	16.93	19.42	17.70	5.83	7.55
EI	2.15	1.35	1.70	0.79	1.86	0.84	1.67	0.90	0.78	0.44
SD	0.28	0.2	0.12	0	0.03	0.047	0.01	0.09	0.06	0.02

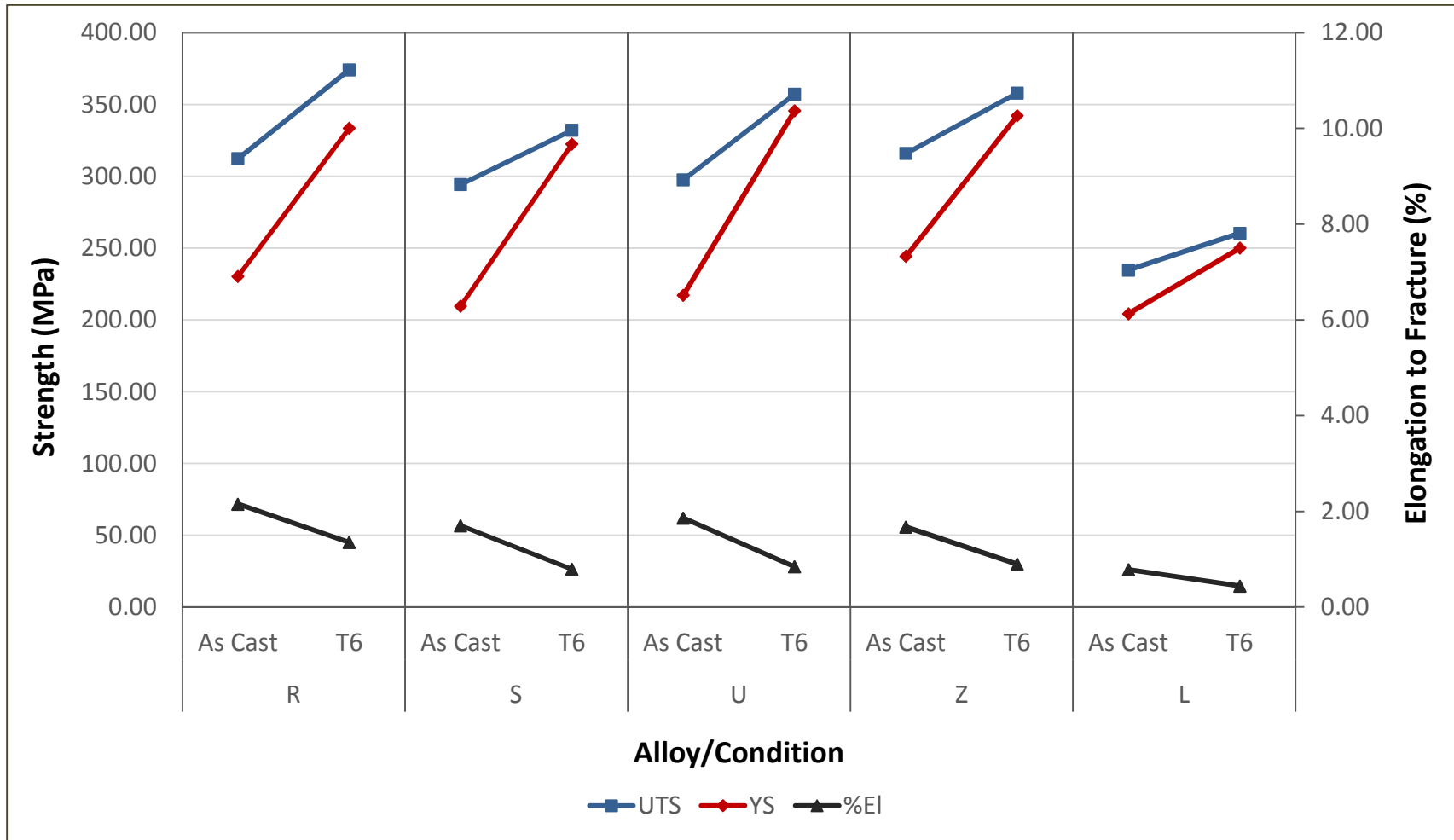


Figure 5.11 Comparison of tensile test data of Alloys R, S, U, Z and Alloy L listed in Table 5.4 (Room temperature tensile testing).

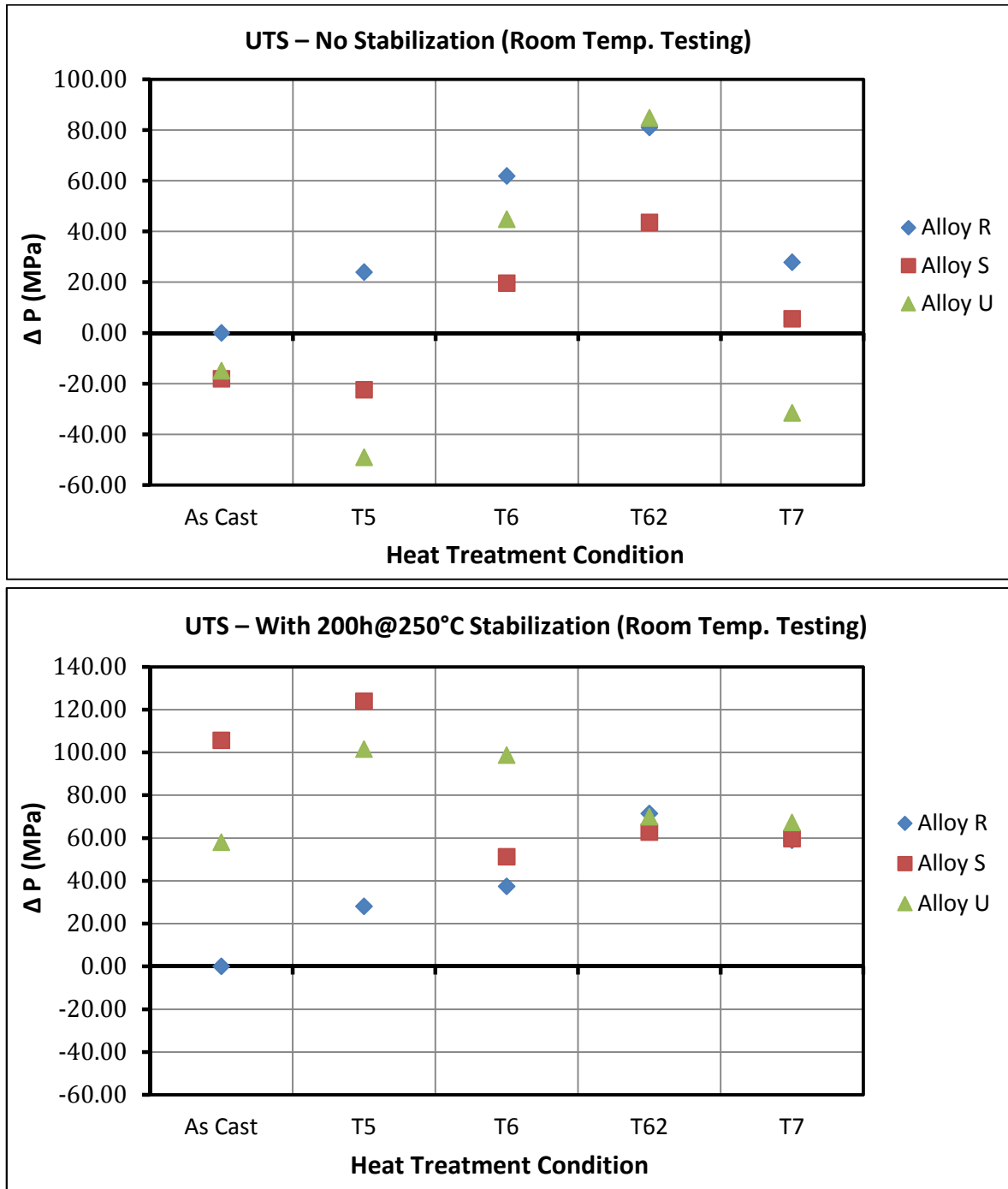
5.4.6 Statistical analysis

Figure 5.12 depicts the tensile properties obtained for Alloys R, S and U without and with 200 h stabilization at 250°C, relative to the values obtained for the as-cast R base alloy, i.e., subtracting the values obtained for the base alloy R in each case, and plotted as ΔP values on the Y-axis ($P = \text{Property} = \text{YS, UTS or \%El}$), with the X-axis representing the base line for alloy R. The use of this method provides an effective means of knowing how the various additions used and the different heat treatment conditions applied affect the properties of the 354 casting alloy.

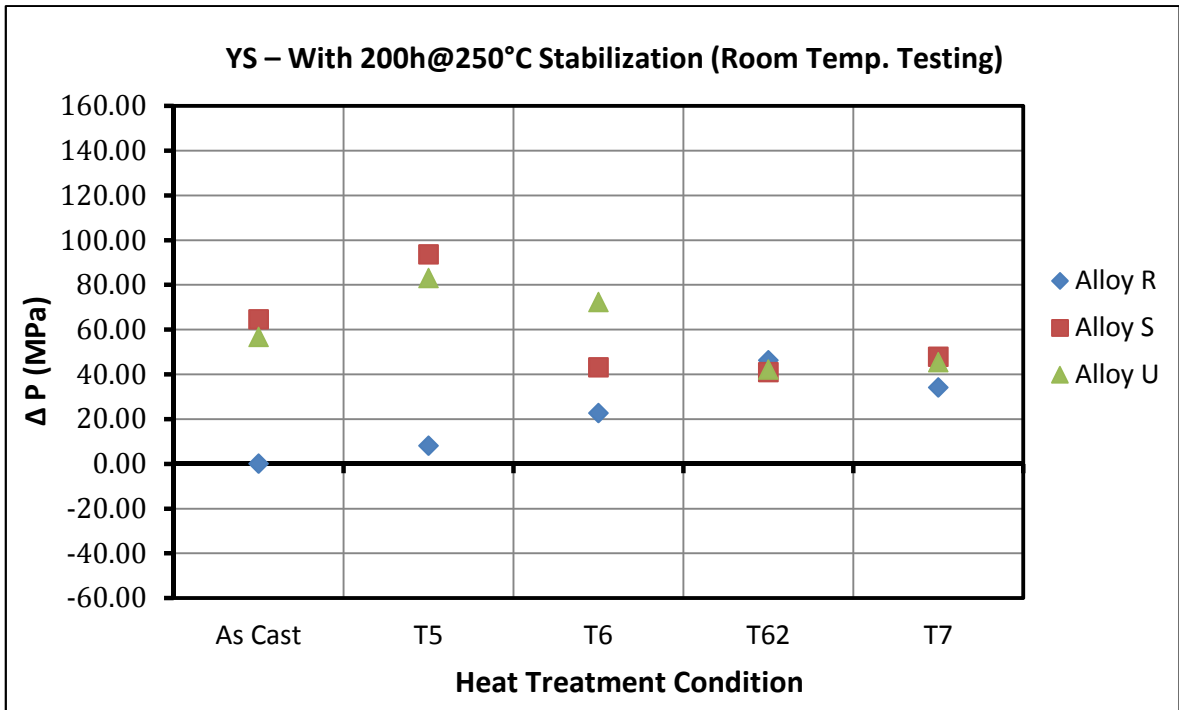
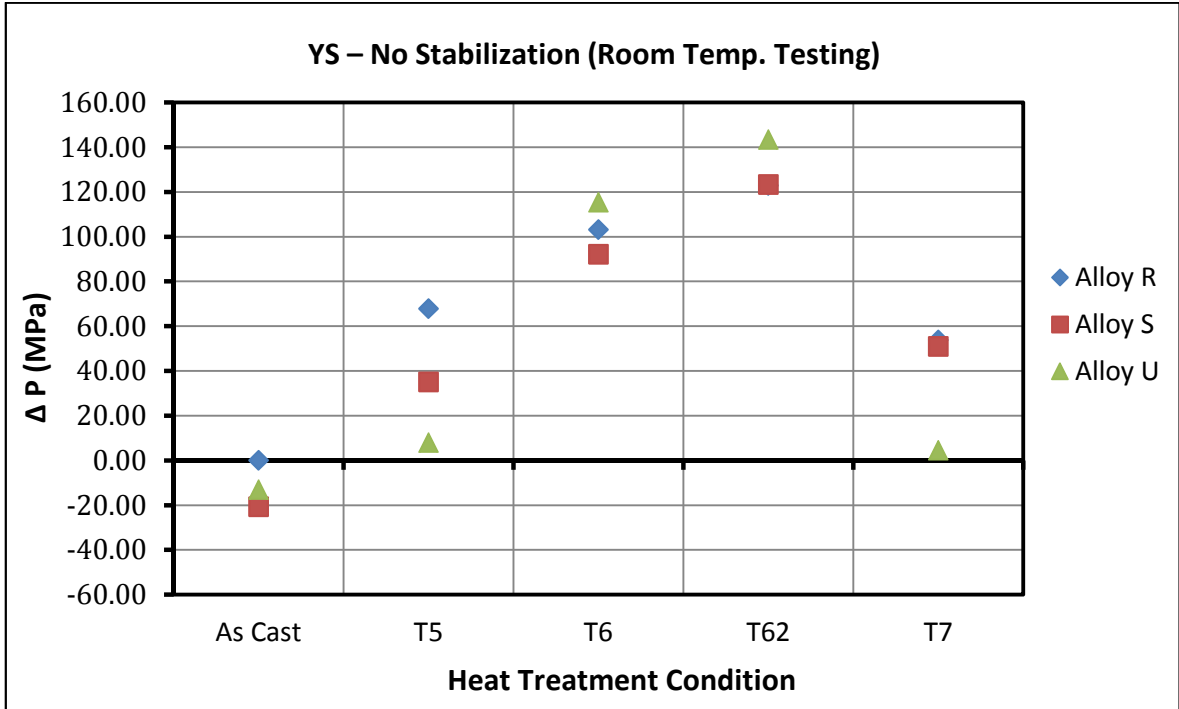
In general, as may be seen from Figure 5.12, additions of these elements improve the alloy properties, depending on the heat treatment applied. Without stabilization, T6 and T62 treatments provide the best improvements in ΔP_{UTS} and ΔP_{YS} values of all alloys; the increase in strength is reflected by a corresponding decrease in ductility, so that the $\Delta P_{\% \text{El}}$ values all lie below the reference baseline, exhibiting ductilities which are around 1% lower than that of the as-cast base alloy R. That the ΔP_{UTS} and ΔP_{YS} values for the R alloy improve for every type of heat treatment - evidently due to the addition of Zr - indicates the effectiveness of the Al-Zr-containing precipitates in maintaining the alloy strength.

With stabilization of 200 h at 250°C, an overall improvement in the ΔP_{UTS} and ΔP_{YS} values for all alloys is noted with respect to the as-cast base alloy R. Alloys S and U show the highest improvements in ΔP_{UTS} and ΔP_{YS} after T5 treatment, whereas after T6, ΔP_{UTS} drops considerably in the case of Alloy S, while for Alloy U it remains at the same level. The T62 and T7 treatments produce the same increase in UTS for all three alloys relative to the tensile strength of the as-cast base alloy R. Essentially, a similar trend is also observed with respect to the ΔP_{YS} values of the three alloys. In regard to ductility, Figure 5.12(c)

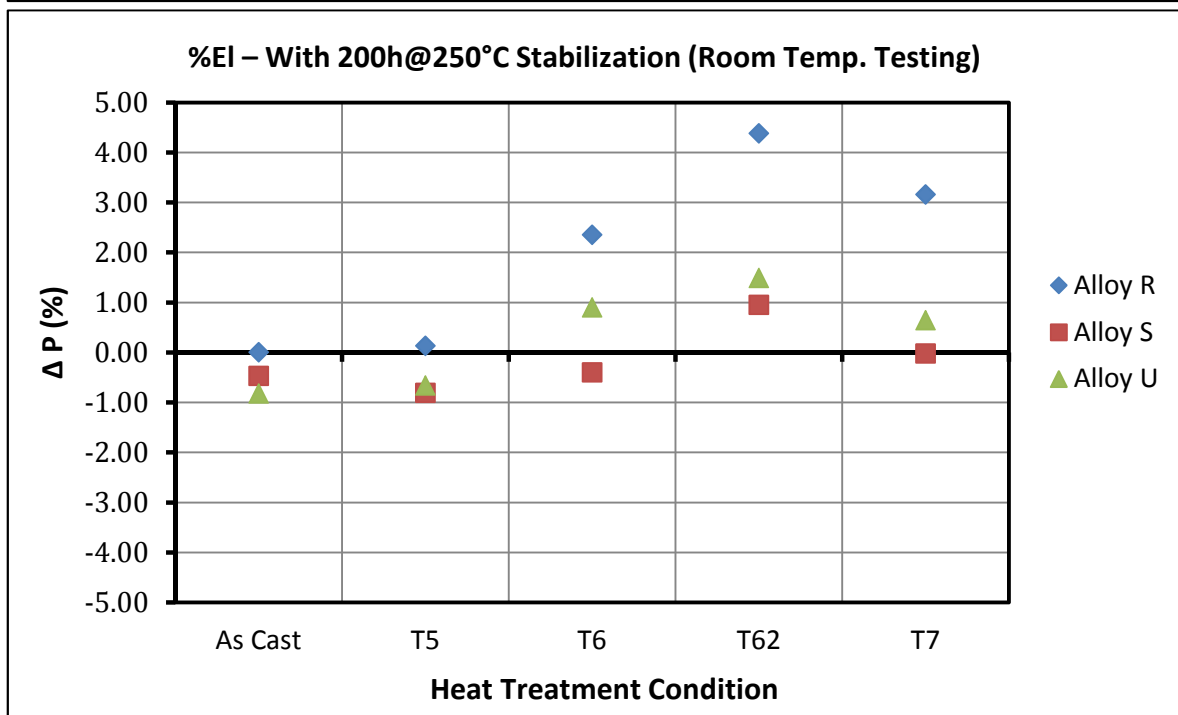
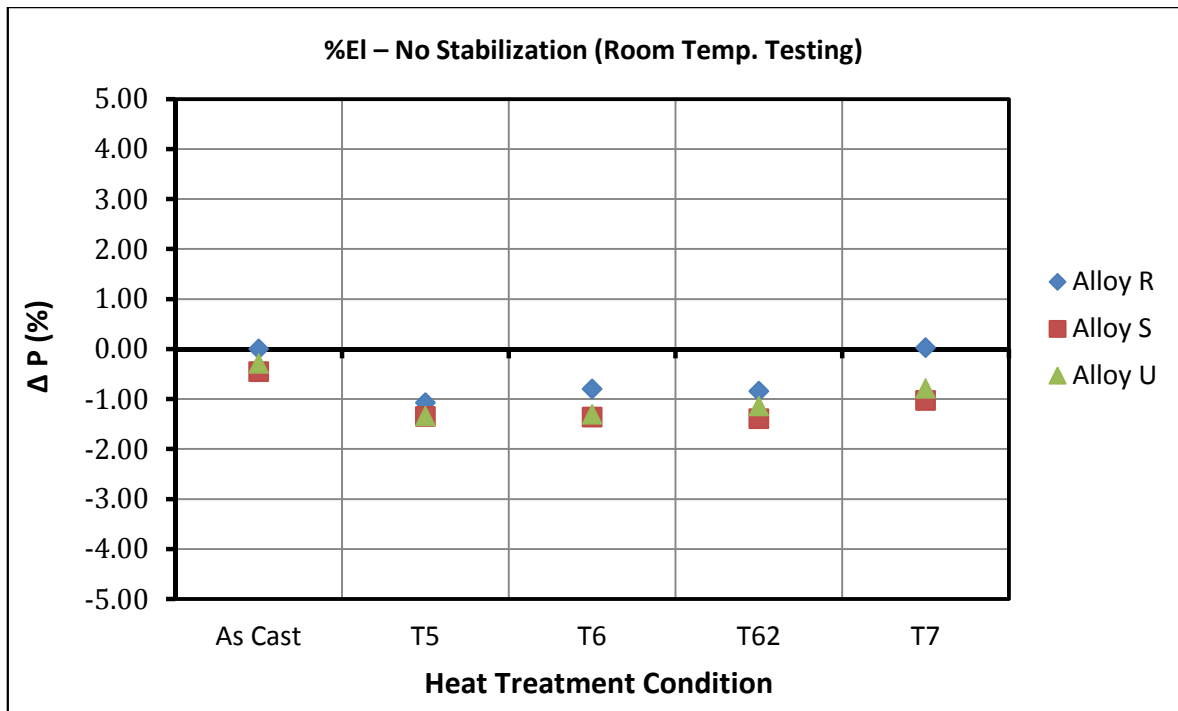
reveals that Alloy R exhibits higher ductilities than Alloys S and U, the highest being obtained with the T62 treatment, followed by the T7 and T6. All three alloys exhibit their highest ductility values after T62 heat treatment.



(a)
Figure 5.12 Cont.



(b)
Figure 5.12 Cont.



(c)

Figure 5.12 Comparison of tensile properties of R, S and U alloys relative to those of as-cast base alloy R: (a) UTS, (b) YS, and (c) %El without, and after 200h stabilization at 250°C.

5.5 TENSILE PROPERTIES OF ALLOYS R, S AND U AT HIGH TEMPERATURE

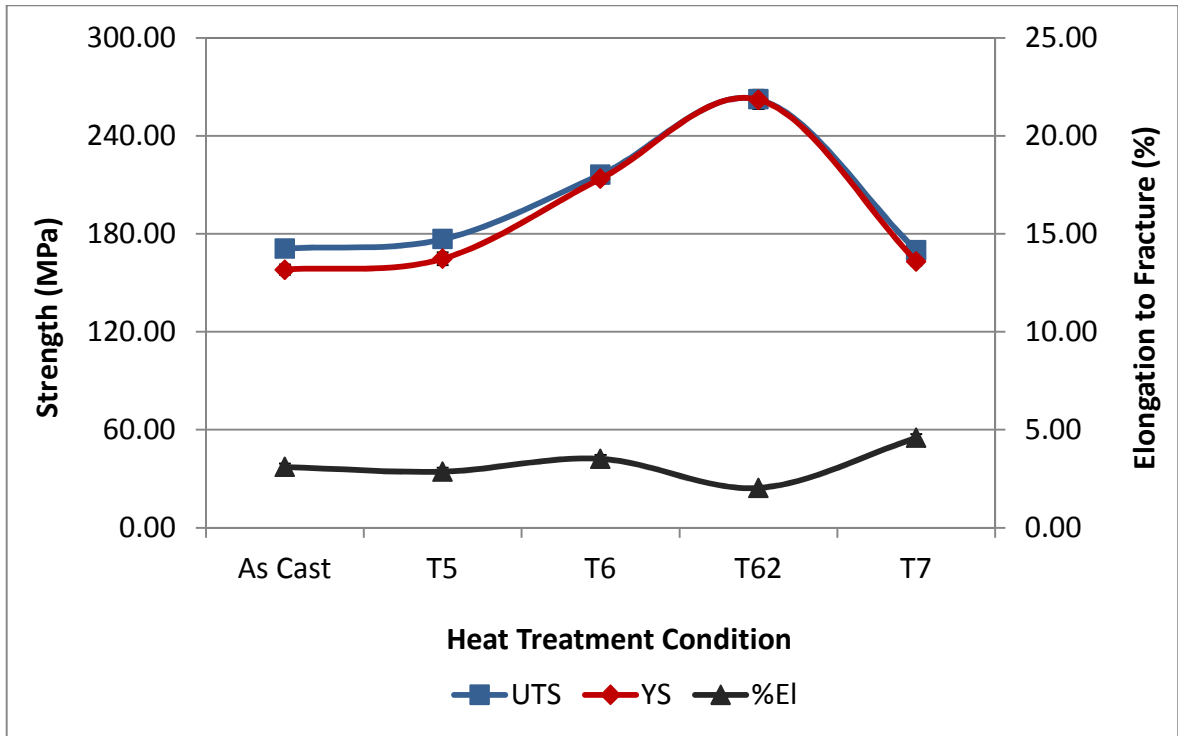
Tensile tests were performed at 250 °C to determine the effect of the alloying additions used and the heat treatment and stabilization conditions employed on the high temperature mechanical performance of the 354 alloys. It was found that the tensile properties showed a different tendency to that observed at room temperature, resulting in improved strength, particularly the yield strength, at temperatures above 200°C. The tensile properties of the selected Alloys R, S and U are discussed in this section together with those of Alloys Z and L for comparison purposes. The alloys were tested at 250 °C using stabilization times of 1 hour and 200 hours at 250 °C prior to conducting the tensile tests.

5.5.1 Alloy R (354 + 0.25wt% Zr)

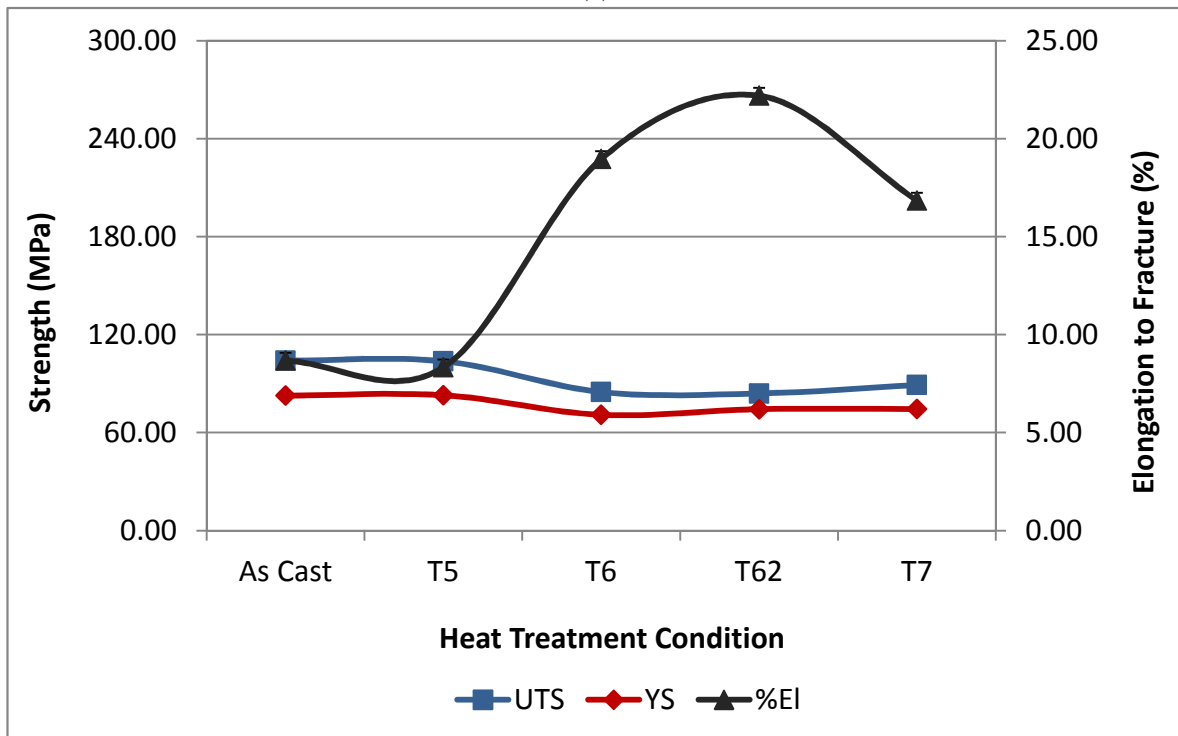
Figure 5.13 shows the high temperature tensile properties obtained from the R alloy under the various heat treatment and stabilization conditions employed. Compared to the as-cast condition, the heat treatments improve the tensile performance of the alloy. As observed from Figure 5.13(a), in case of one hour stabilization, the strength of the alloy increases with the T6 and T62 heat treatments, in which the formation of coherent precipitates is the main source of strengthening in the R alloy, whereas it remains practically the same after T5 heat treatment, and softening occurs when the T7 heat treatment is applied to the alloy. The ductility varies according as the strength increases or decreases, exhibiting almost 5% after the T7 treatment.

With 200 h stabilization at 250°C, also, there is no change in the tensile and yield strengths after T5 heat treatment compared to the as-cast case, while a slight decrease is

noted after T6 treatment, with the T62 and T7 treatments providing no further change in the alloy strength. The alloy ductility increases significantly, from about 8% in the as-cast and T5 conditions, to $\sim 18 \pm 1\%$ after T6 and T7 treatments, with the T62 treatment exhibiting a maximum ductility of $\sim 23\%$.



(a)

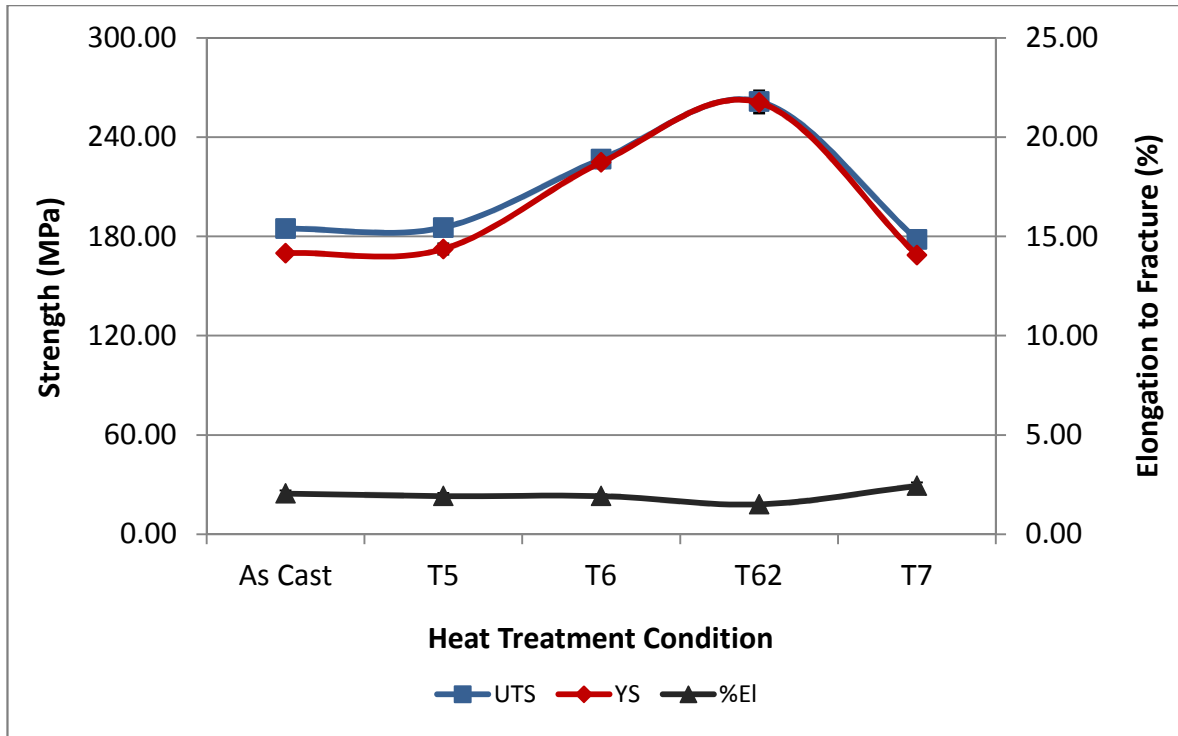


(b)

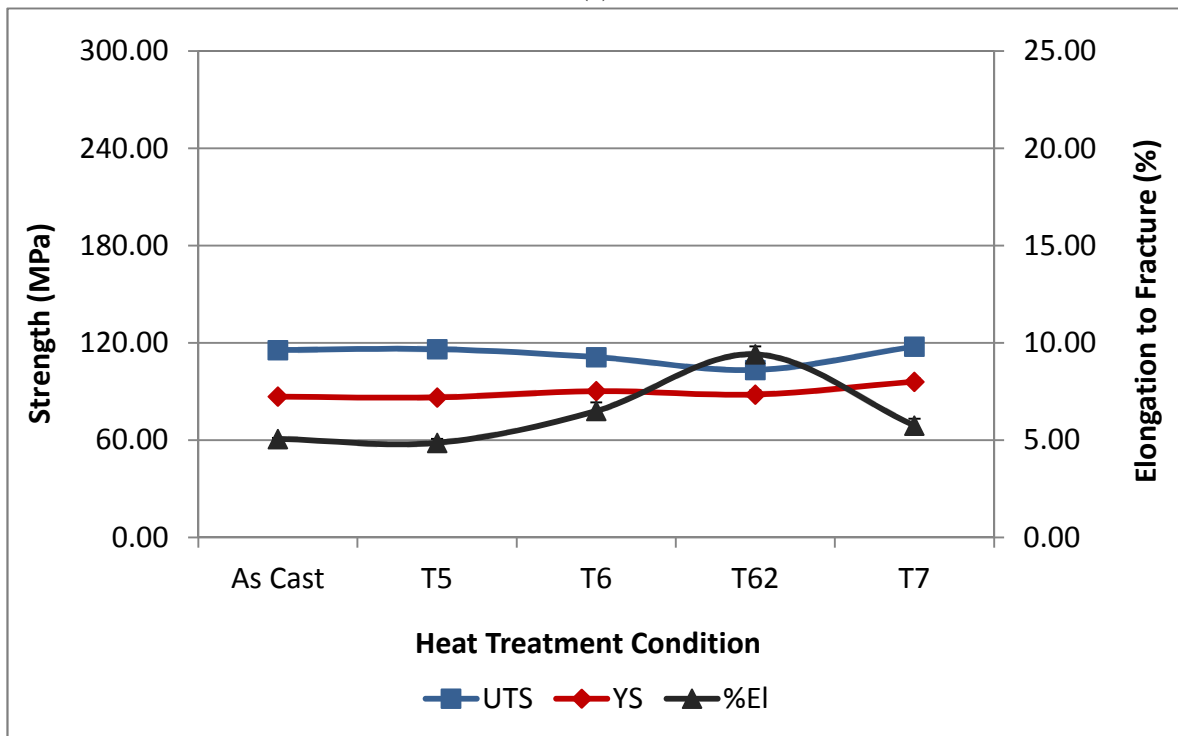
Figure 5.13 Mean values for UTS, YS, % El for alloy R at the given heat treatment conditions for; (a) One and (b) 200 hours stabilization at 250°C.

5.5.3 Alloy S (354 + 0.25wt% Zr + 2wt% Ni)

Figure 5.14 shows the tensile properties obtained from the S alloy, containing 0.25 wt% Zr + 2 wt% Ni, for the various heat treatment conditions and the two stabilizing times used. As discussed in the previous section, after one hour stabilizing time, the heat treatments T6 and T62 improve the alloy strength considerably, whereas no change is noted after T5 and T7 treatments. The ductility remains more or less the same, at about 2%, for the different heat treatments applied as that observed in the as-cast case, except for the slight increase to 2.43% in the case of T7. As seen from Fig. 5.14(b), with 200 h stabilization, the alloy strength is lowered considerably, and remains almost the same as in the as-cast condition (~117 MPa UTS and 90 MPa YS), while the ductility differs from one condition to another, ranging between 5 and 9%, with the T62 treatment producing the maximum ductility.



(a)

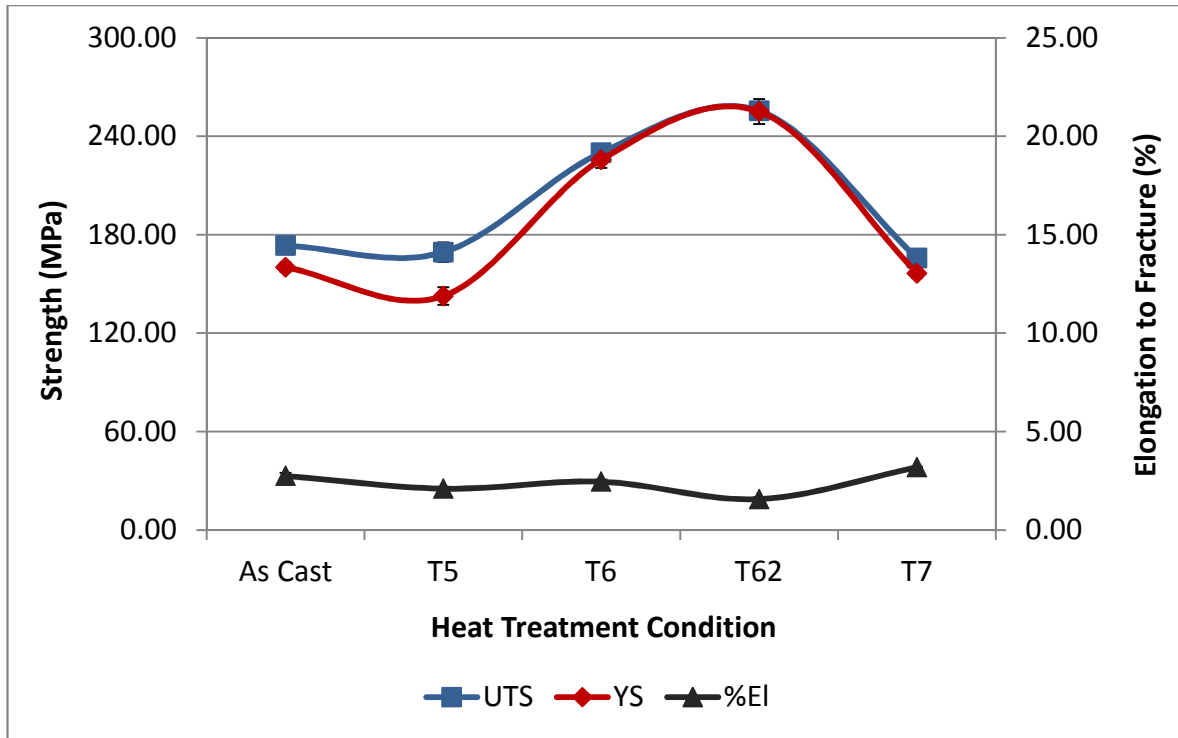


(b)

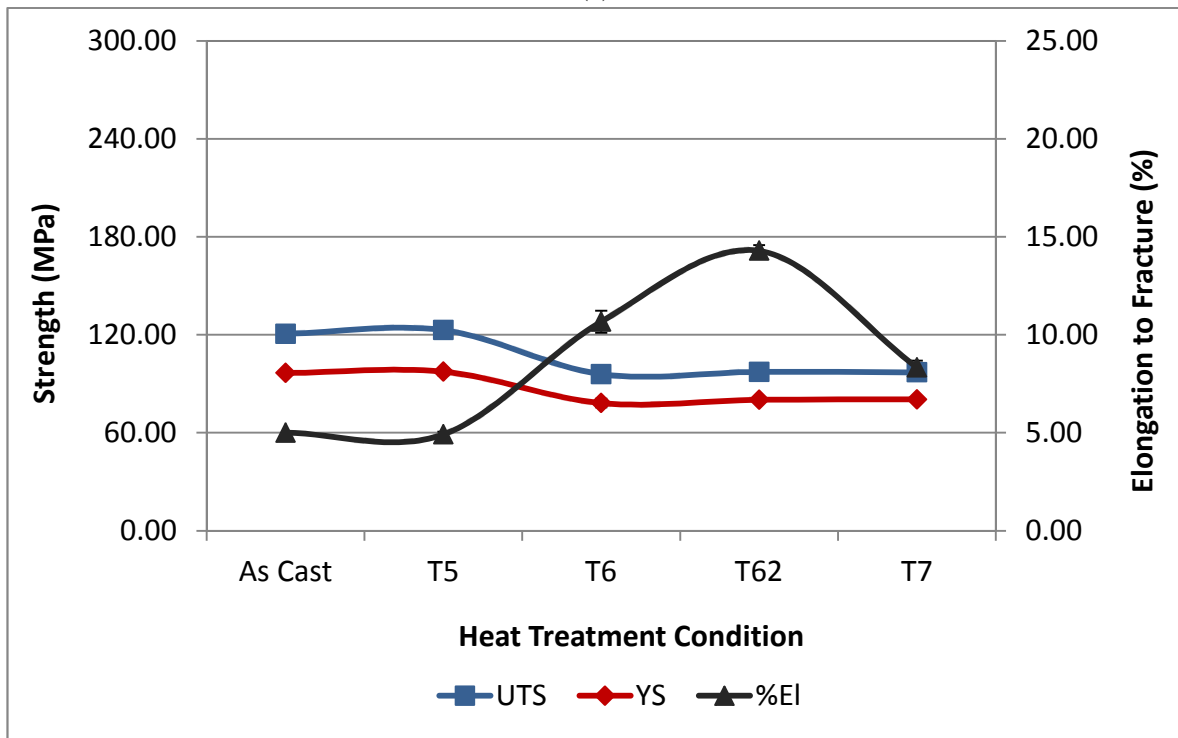
Figure 5.14 Mean values for UTS, YS, % EI for alloy S at the given heat treatment conditions for; (a) One and (b) 200 hours stabilization at 250°C.

5.5.4 Alloy U (354 + 0.25wt% Zr + 0.75wt% Mn)

Figure 5.15 shows the tensile properties obtained from the U alloy, under the different heat treatment conditions and after (a) 1h and (b) 200h stabilization at 250°C. Compared to the as-cast condition, and for the one hour stabilization time, the T62 condition corresponds to the peak aging condition, with strength values of 255.58 MPa UTS and 255.11 MPa YS. Alloy softening is observed following T7 heat treatment, although the ductility increases only slightly above the average 2.5% observed for the other conditions. In contrast, with 200 h stabilization, the T6, T62 and T7 heat-treated alloys display the lowest strength values: ~97 MPa UTS, and ~78-80 MPa YS, respectively, whereas the ductility in the T62 condition increases to almost triple that of the as-cast value (*cf.* 14.3% with 5%).



(a)



(b)

Figure 5.15 Mean values for UTS, YS, % EI for alloy U at the given heat treatment conditions for; (a) One and (b) 200 hours stabilization at 250°C.

From the results observed in Figures 5.13 through 5.15, in the context of the high temperature performance of the three selected 354 alloys, much higher strength values are observed when the stabilization is carried out only for one hour prior to testing. The tensile strength and yield strength show very similar trends with respect to the heat treatment conditions, with the T62 treatment providing the best strength values, 262 MPa UTS/YS in the case of Alloy R, with Alloys S and U showing very similar strength values, ~261 MPa and ~255 MPa, respectively. The ductility values range from ~1.5% to ~3%, with Alloy R showing slightly higher ductility than Alloys S and U (~3.5% in the as-cast condition).

5.5.5 Quality charts of Alloys R, S and U - high temperature tensile data

Quality charts were constructed from the tensile test data obtained for the three alloys subjected to the various heat treatment conditions and the two stabilization times. Equations 1 and 2 were used to calculate the quality index (Q) values and plot the *iso-Q* lines and the *iso-YS* lines, respectively. Figures 5.16 and 5.17 present the quality charts for Alloys R, S and U tested at 250°C for the two stabilization times, respectively, depicting how the properties and quality of each alloy vary with the heat-treatment conditions. The contoured curves indicate how each heat treatment affects the tensile performance of the three alloys. After one hour stabilization at the 250°C testing temperature, all alloys exhibit the highest UTS values after the T62 treatment, but with ductilities lower than the as-cast values. The alloy quality is also improved with the T62 treatment.

After 200 h stabilization at 250°C, and as Figure 5.17 shows, the strength of the alloys deteriorates, the decrease in strength and increase in ductility being related to the softening which occurs as a result of the onset of over-aging during which the equilibrium precipitates form, leading to the loss of coherency strain between the precipitates and the

matrix. In addition, the over-aging results in the continuous growth of the large precipitates at the expense of smaller ones, ultimately leading to coarser precipitates with less density in the metal matrix, and having larger inter-particle spacing [94]. Figure 5.18 displays the relevant part of the quality chart shown in Figure 5.17, rescaled to distinguish the contour curves one from the other. The tendency towards low UTS and YS values and high ductilities indicates the large extent to which softening has occurred after the long stabilization time at the testing temperature, especially for the T62-treated alloy. The alloy quality is also lowered to some extent (*cf.* 250-288 MPa with 287-337 MPa in the case when 1 h stabilization was used).

It should be noted that, due to the changes in the strength and ductility observed with the 200 h stabilization, the X and Y-axis scales are necessarily different from those given in Figure 5.16 for the one hour stabilization time.

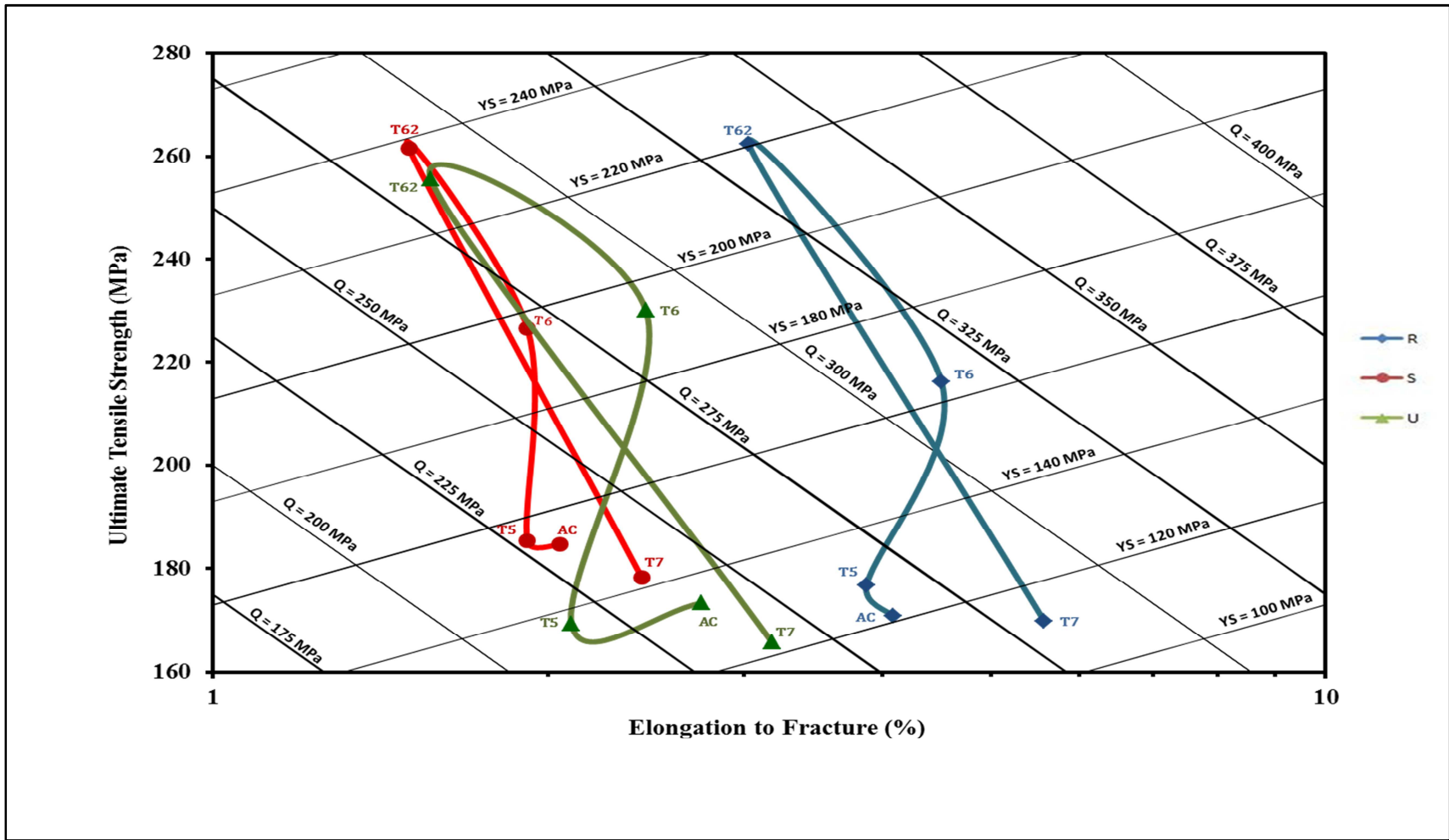


Figure 5.16 Quality charts showing UTS vs % El plots for Alloys R, S and U subjected to various heat treatment conditions (testing at 250°C after 1h stabilization).

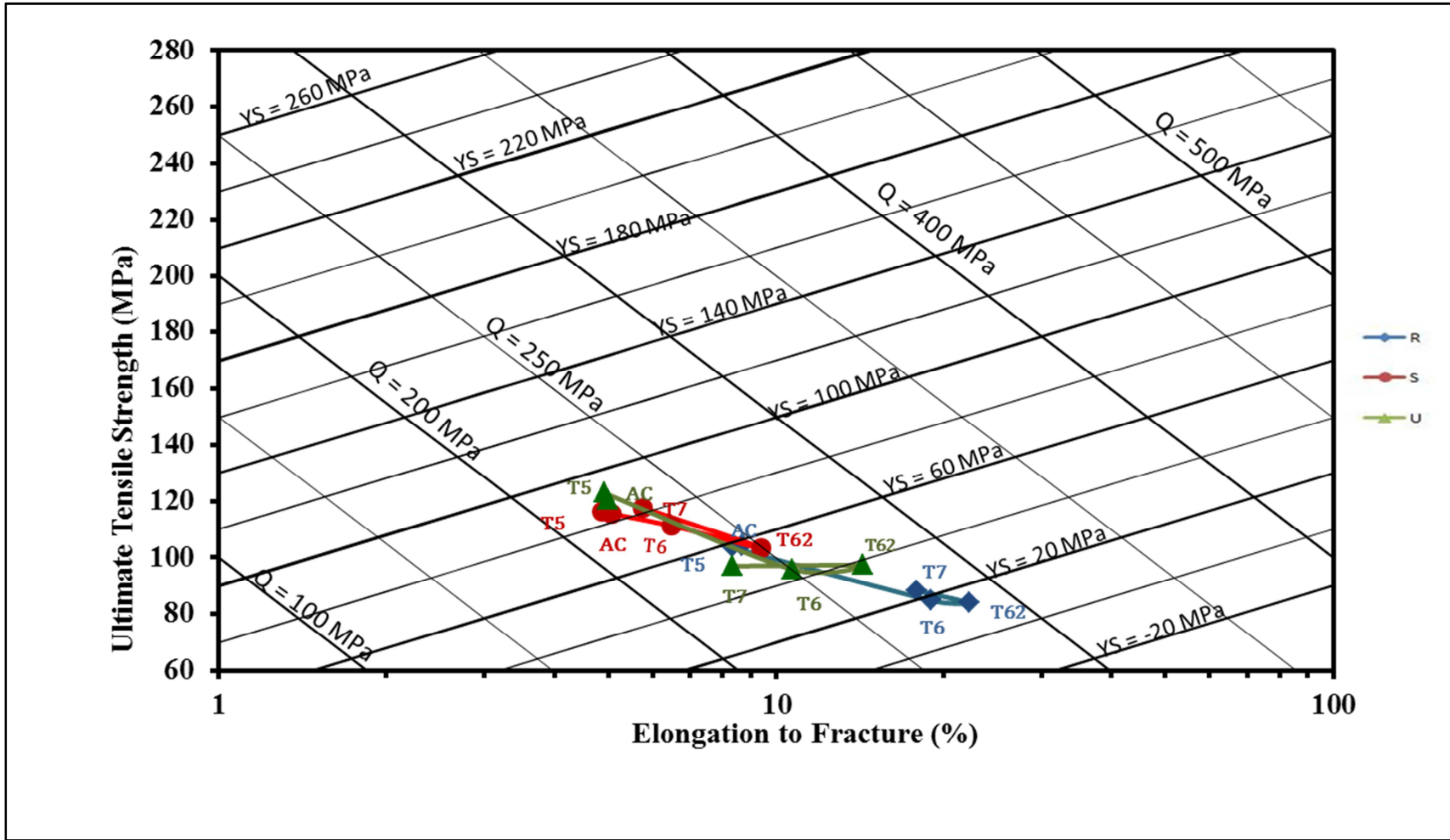


Figure 5.17 Quality charts showing UTS vs % El plots for Alloys R, S and U subjected to various heat treatment conditions (testing at 250°C after 200h stabilization).

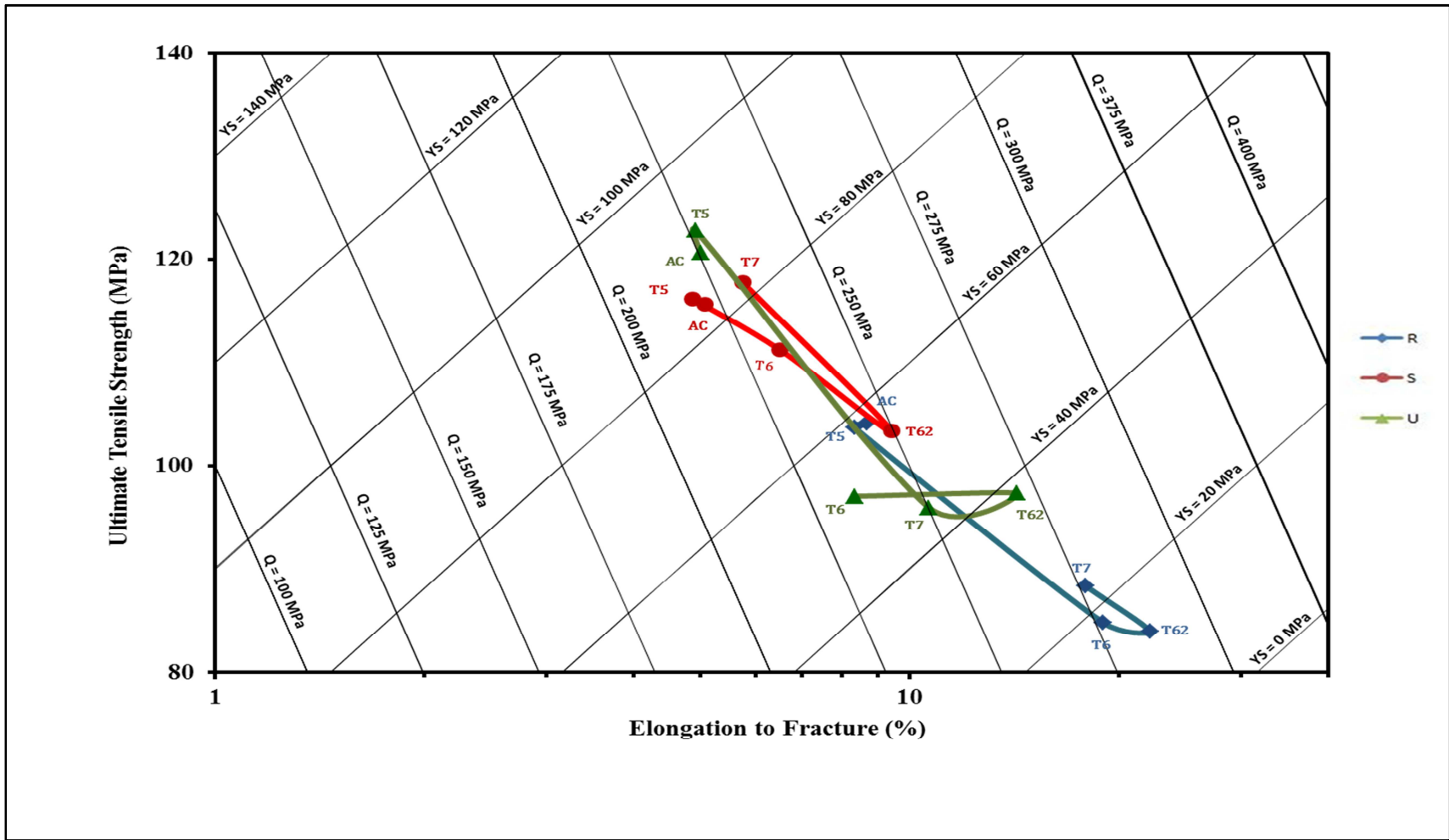


Figure 5.18 Relevant part of Figure 5.17 rescaled to distinguish the contour lines obtained for Alloys R, S and U.

5.5.6 Comparison between the high temperature tensile properties of as-cast and T6-treated 354 alloy with different alloying additions and a new alloy

In this section, the high temperature tensile properties of as-cast and T6-heat treated 354 alloys R, S and U (tested at 250°C and using the two stabilization times at testing temperature) will be compared to determine the effect of the various alloying additions, together with the tensile properties of Alloy Z (354 alloy, containing 0.25 wt% Zr + 0.15 wt% Sc) and Alloy L (398 alloy, containing the same levels of Zr and Sc as alloy Z) to examine (i) the effect of a combined Zr and Sc addition in enhancing the high temperature behavior of 354 alloy, and (ii) the feasibility of using the new alloy 398 with the same Zr and Sc additions as an alternative for similar high temperature applications.

Table 5.5 lists the tensile properties obtained for the five alloys when tested at 250°C after 1 hour of stabilization at testing temperature, while Table 5.6 shows the tensile properties for the same five alloys after 200 h stabilization at the same testing temperature. The results are displayed in Figures 5.19 and 5.20, respectively.

Table 5.5 Comparison of high temperature tensile properties of Alloys R, S, U, Z and L (tested at 250°C after 1 h stabilization at testing temperature).

	1 h / 250°C stabilization									
	Alloy R (354 + 0.25% Zr)		Alloy S (354 + 0.25% Zr + 2%Ni)		Alloy U (354 + 0.25% Zr + 0.75% Mn)		Alloy Z (354 + 0.2 % Zr + 0.15% Sc)		New Alloy L (398 + 0.25%Zr + 0.15% Sc)	
Av.	As Cast	T6	As Cast	T6	As Cast	T6	As Cast	T6	As Cast	T6
UTS	170.93	216.21	184.69	226.64	173.36	230.05	139.80	222.67	124.28	178.05
SD	3.35	2.74	2.55	3.48	0.59	5.03	0.92	0.28	8.28	9.25
YS	158.03	213.77	169.96	224.72	160.17	225.73	125.96	220.89	123.88	174.67
SD	3.08	2.96	2.20	3.41	2.82	8.24	0.56	1.12	8.43	10.53
EI	4.17	4.61	2.05	1.92	2.75	2.45	4.17	1.25	1.37	1.02
SD	0.15	0.45	0.33	0.29	0.25	0.18	0.88	0	0.05	0

Table 5.6 Comparison of high temperature tensile properties of Alloys R, S, U, Z and L (tested at 250°C after 200 h stabilization at testing temperature).

	200 h / 250°C Stabilization									
	Alloy R (354 + 0.25% Zr)		Alloy S (354 + 0.25% Zr + 2%Ni)		Alloy U (354 + 0.25% Zr + 0.75% Mn)		Alloy Z (354 + 0.2 % Zr + 0.15% Sc)		New Alloy L (398 + 0.25%Zr + 0.15% Sc)	
Av.	As Cast	T6	As Cast	T6	As Cast	T6	As Cast	T6	As Cast	T6
UTS	104.14	84.84	115.61	111.26	120.63	95.90	153.59	88.51	106.54	114.05
SD	1.94	0.23	0.22	0.98	0.35	1.50	0.5	2.25	4.26	4.12
YS	82.64	70.89	86.91	90.28	96.55	78.16	125.56	78.29	94.9	103.8
SD	1.86	1.05	0.43	0.71	0.19	2.69	0.19	2.6	3.17	1.78
EI	8.67	18.96	5.07	6.50	5.00	10.67	7.5	15.83	2.2	2.45
SD	0.67	0.53	0.06	0.87	0.00	0.76	0	1.42	0	0.1

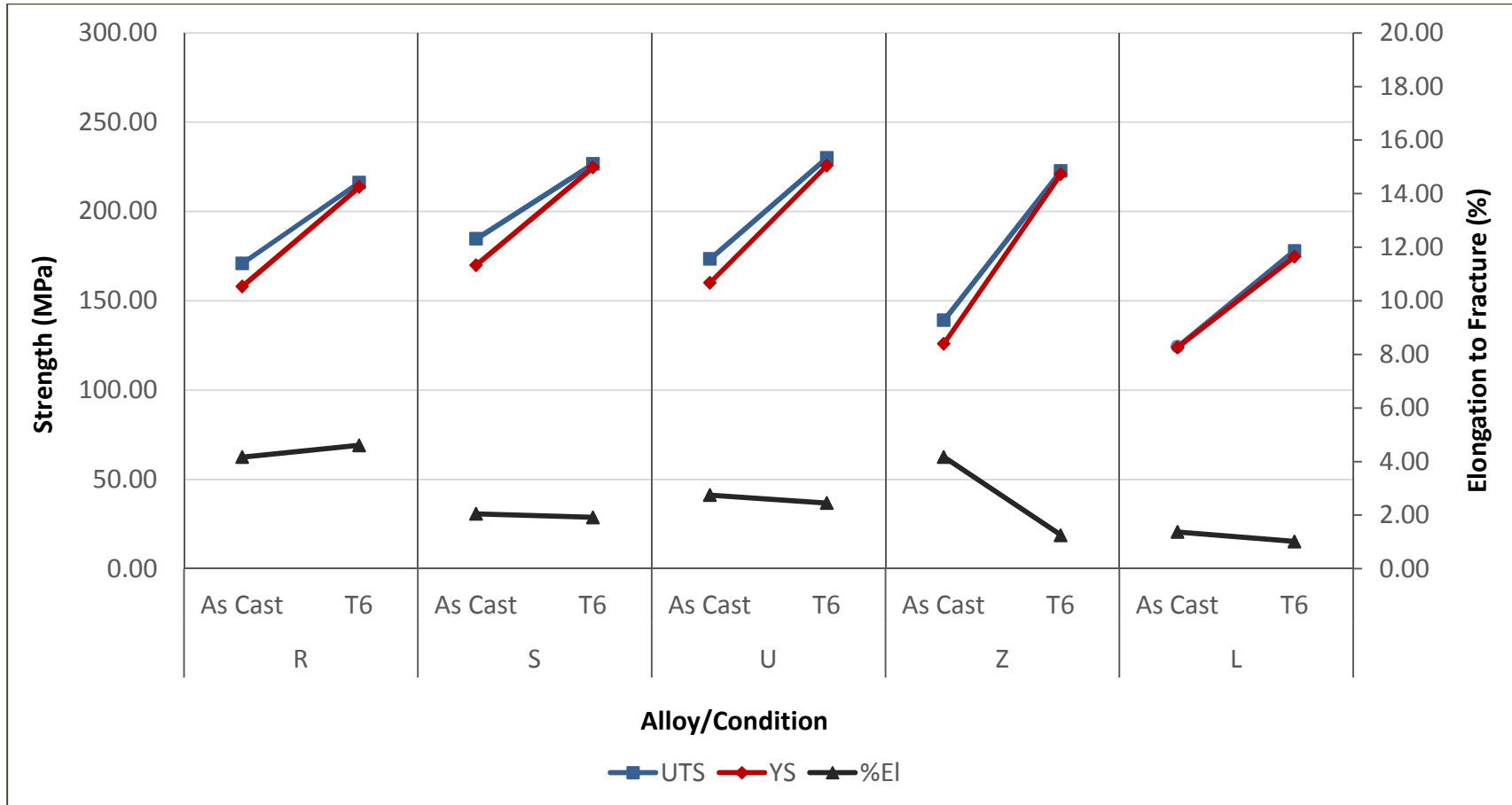


Figure 5.19 Comparison of tensile test data of Alloys R, S, U, Z and Alloy L listed in Table 5.5 (tested at 250°C after 1 h stabilization).

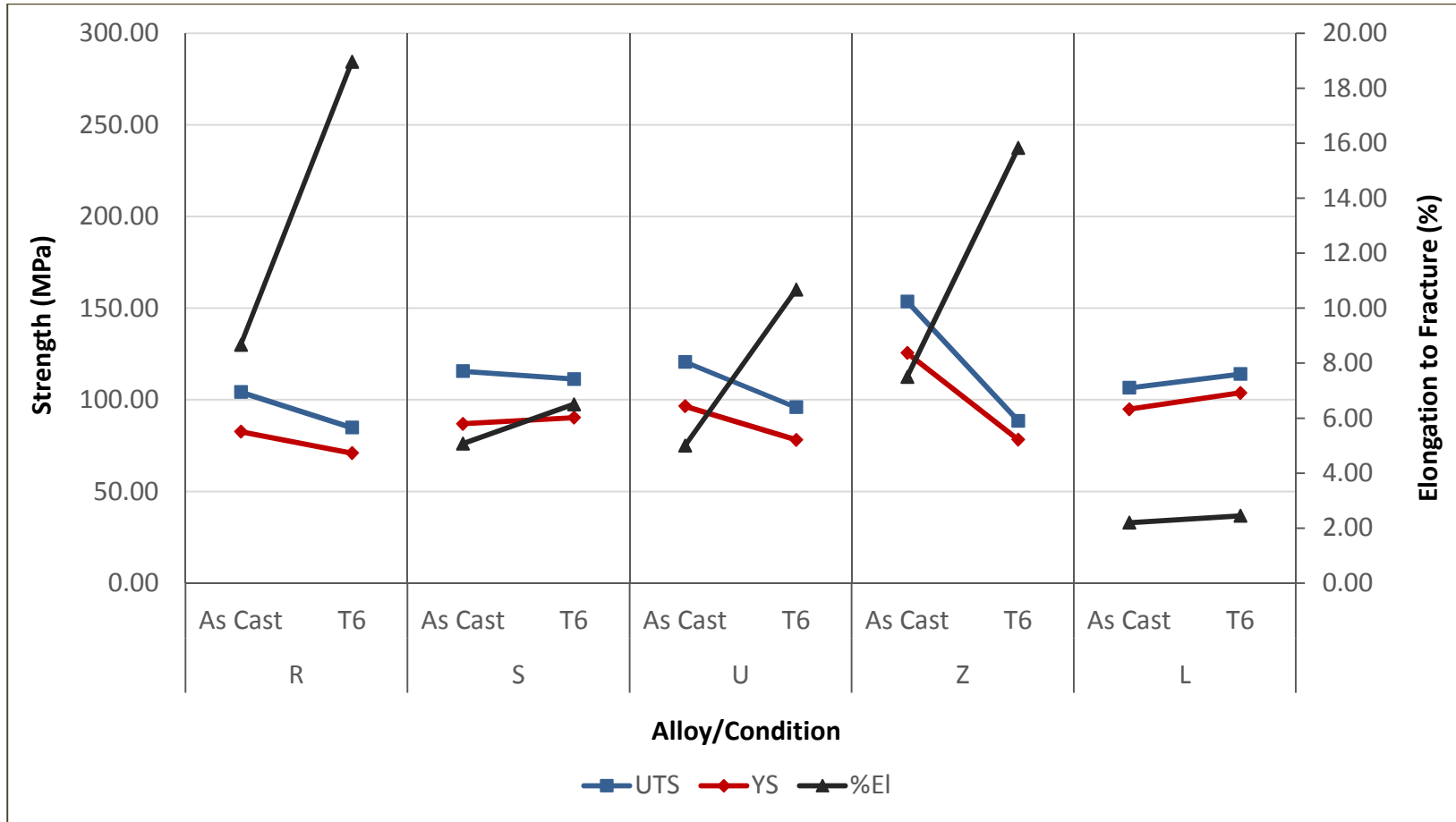


Figure 5.20 Comparison of tensile test data of Alloys R, S, U, Z and Alloy L listed in Table 5.6 (tested at 250°C after 200 h stabilization).

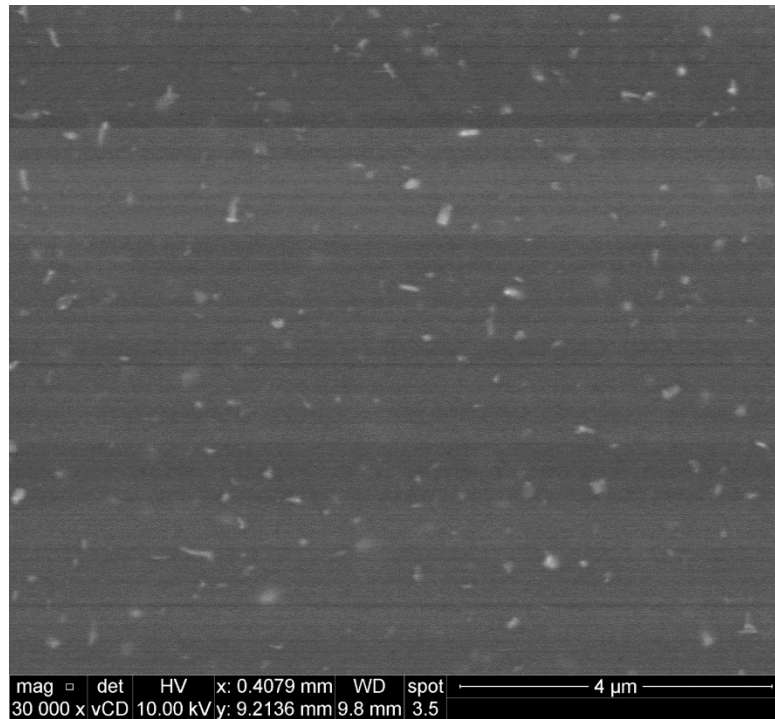
As may be seen from Table 5.5, with one hour stabilization, the alloy strength in the as-cast condition is increased with the addition of Ni in Alloy S and Mn in the case of Alloy U but it decreases in Alloy Z and Alloy L (398 alloy with the same Zr and Sc additions as Alloy Z); after T6 heat treatment incorporating the SHT 1 solution treatment, the strength of all alloys is enhanced, by about 40-80 MPa, with Alloy Z showing the greatest improvement. As may also be observed from Table 5.5, Alloy U (containing 0.75wt% Mn + 0.25wt% Zr) in the T6 (SHT 1) condition seems to be the best alloy with respect to mechanical properties at high temperature, since it displays higher tensile properties taking into consideration both as-cast and T6 conditions.

From Table 5.6, which displays the high temperature tensile properties after 200 hours stabilization at 250°C, it may be seen that Alloy Z (354 + 0.25wt% Zr + 0.15wt% Sc) shows a large increase in strength compared to the base alloy R for the as-cast condition. The addition of Sc to Al alloys is more effective than Zr addition in improving recrystallization resistance [134], due to the formation of a high density of Al₃Sc particles. However, a combined addition of Sc and Zr produces Al₃(Sc,Zr) particles which are more stable than the Al₃Sc dispersoids, and that leads to the improvement of the recrystallization resistance [70]. Additionally, it has been shown that Zr increases the resistance to overaging when it is added to binary Al-Sc alloy [62].

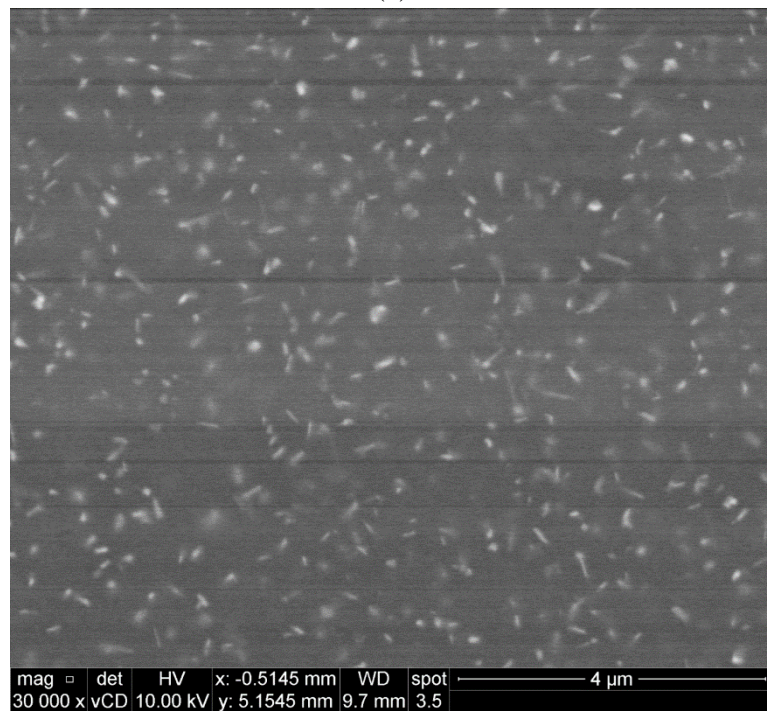
Table 5.6 also shows that, in general, the strength of the 354 alloys (UTS and YS) decreases considerably on going from the as-cast to the T6 heat-treated condition, with the exception of Alloy S, which shows a decrease in the UTS of ~4.5 MPa and an increase in the YS of ~3 MPa. The reduction in strength of the other 354 alloys results from the coarsening of the different strengthening precipitates in the alloys based on the additions

made in each case. In contrast, alloy L (398 + 0.25wt% Zr + 0.15wt% Sc) the strength values increase by ~6.5 MPa and ~ 9 MPa for the UTS and YS.

While a detailed investigation of the precipitation behavior using transmission electron microscopy (TEM) was not within the scope of the present study, as an example, TEM analysis was carried out for the Alloy U samples tested at high temperature following the two stabilization times to demonstrate the change in the precipitates over prolonged periods of heating. Figure 5.21 compares the precipitates observed in the U alloy samples after (a) 1 hr stabilization and (b) 200 hrs stabilization at 250 °C. As may be seen, the finer precipitates in Figure 5.21(a) have coarsened so that a lot more of them are visible after the 200 hrs stabilization period, as seen in Figure 5.21(b).



(a)



(b)

Figure 5.21 Comparison of the precipitates observed in Alloy U tested at 250 °C, after (a) 1 hr, and (b) 200 hrs stabilization at testing temperature.

In order to analyze the mechanical quality by means of quality charts, two heat treatment conditions per alloy were selected from among all the conditions used: the as-cast and T6 conditions, which are important to our study. As observed from Figure 5.22, Alloy U alloy exhibits the best tensile properties after T6 heat treatment following the 1 hr stabilization. The L alloy is comparatively more brittle than expected in the as-cast condition but its properties improve somewhat after T6 treatment. Material-wise, the combined Zr and Sc addition in Alloy Z improves the yield and tensile strength considerably which is to be expected given the beneficial influence of both additions which increases the resistance to overaging, i.e., softening.

In contrast, when stabilization is carried out for 200 hrs, the alloy strength of the 354 alloys is considerably lowered in the T6 condition, whereas the L alloy displays very little change compared to the as-cast condition. In keeping with the lowered strengths, the 354 alloys exhibit much higher ductilities, ranging between 10 and 20%. It is interesting to note how the alloy quality remains the same in the case of Alloy Z in both as-cast and T6-treated conditions in the two charts, and improves with the prolonged stabilization time (towards the 300 MPa *iso-Q* line), compared to ~230 MPa with the 1 h stabilization time.

Such quality charts are thus very useful for estimating how the added elements are influenced by the heat treatment and stabilization conditions applied and what are the consequences on the alloy properties and performance.

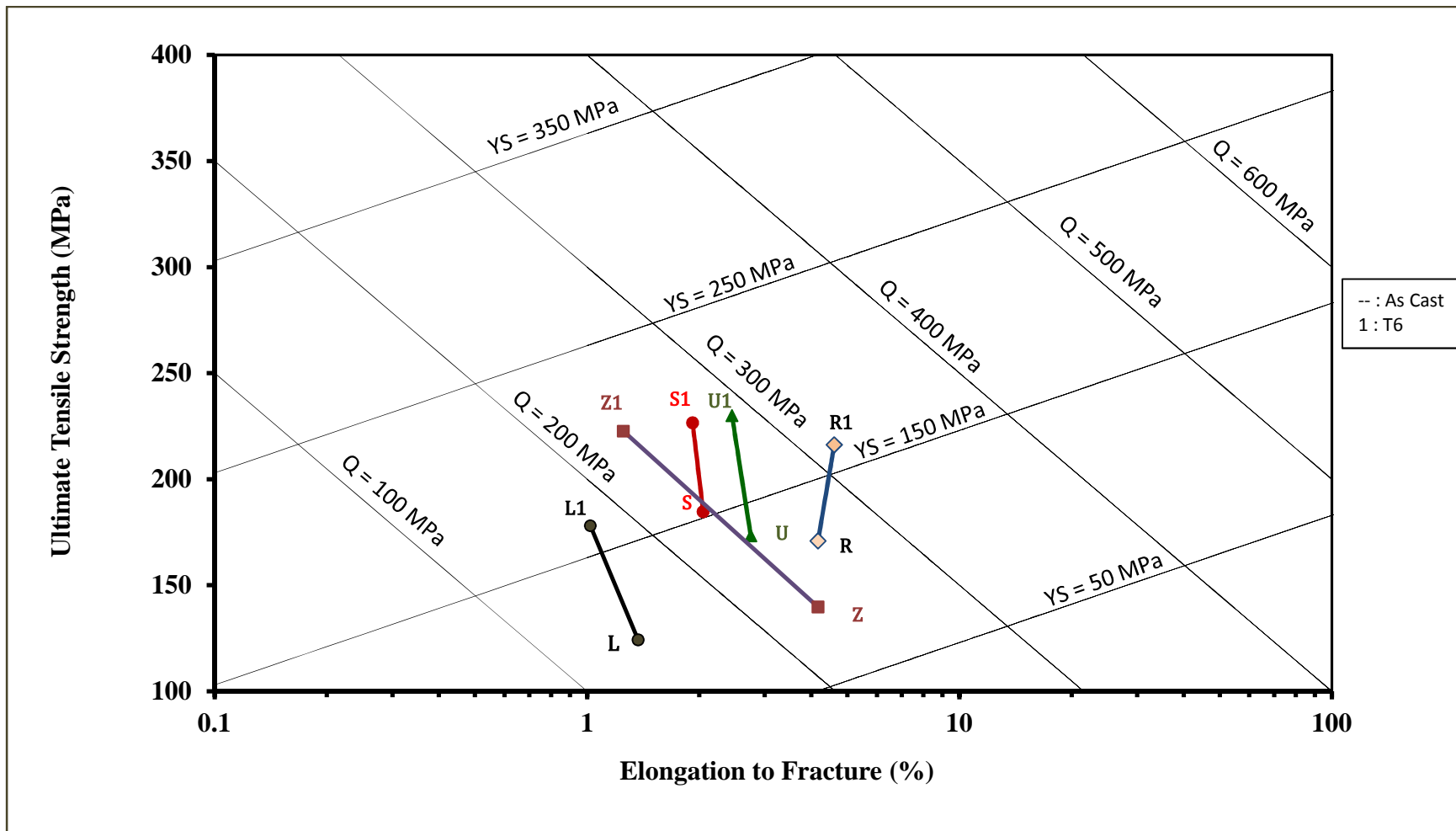


Figure 5.22 Quality charts showing UTS vs %El plots for Alloys R, S, U, Z and L in the as-cast and T6-heat treated conditions (testing at 250°C after 1 h stabilization at testing temperature).

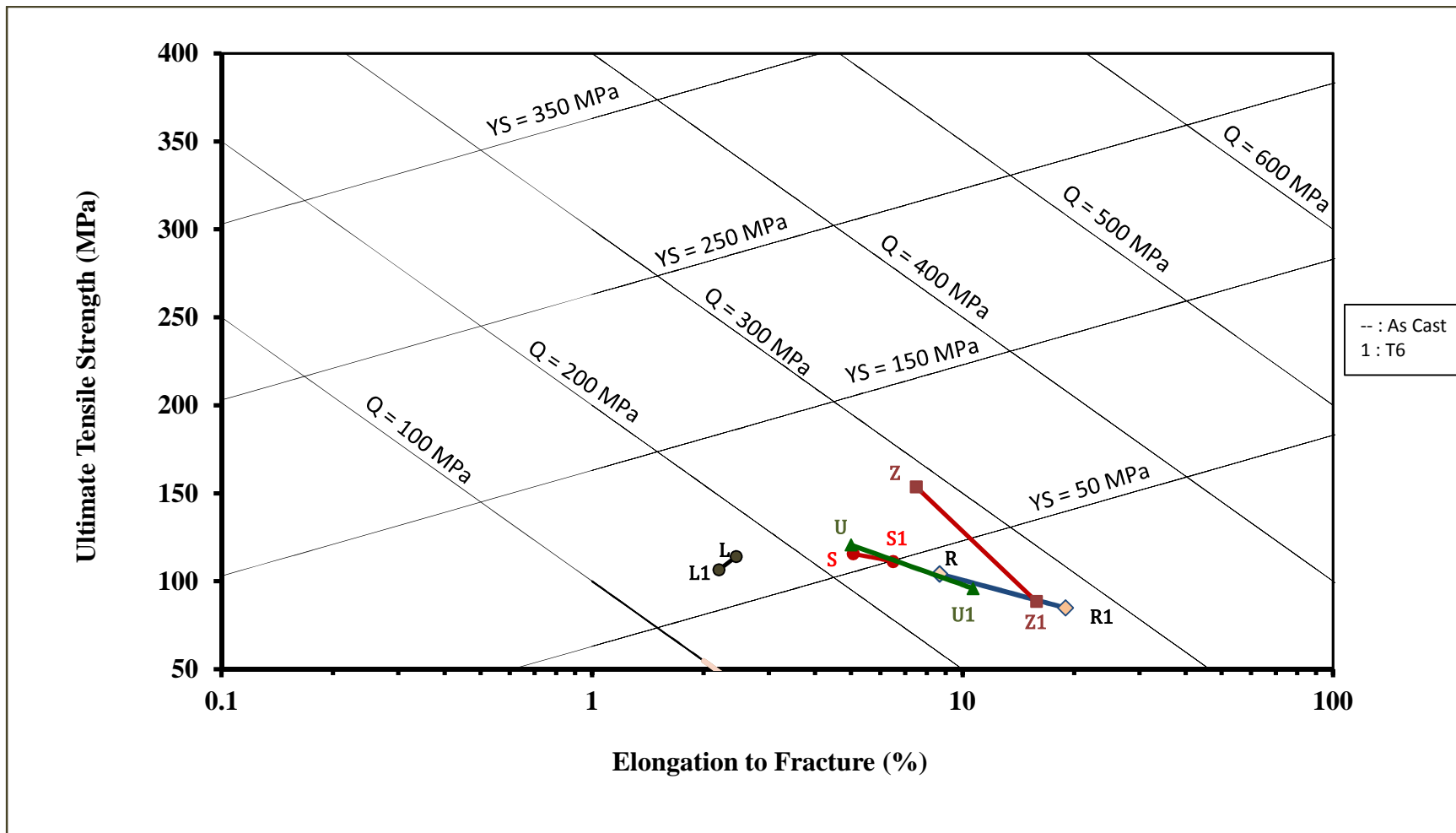


Figure 5.23 Quality charts showing UTS vs %El plots for Alloys R, S, U, Z and L in the as-cast and T6 heat-treated conditions (testing at 250°C after 200 h stabilization at testing temperature).

5.5.7 Statistical analysis

Figure 5.24 shows the high temperature tensile properties obtained for alloys R, S and U at the 250°C testing/stabilization temperature for the two stabilization times used, where the ΔP ($P = \text{Property} + \text{UTS, YS and \%EI}$) values were obtained relative to the values for the as-cast R alloy (taken as the base or reference alloy). Table 5.7 shows the reference alloy properties used to calculate the ΔP values plotted in Figure 5.24.

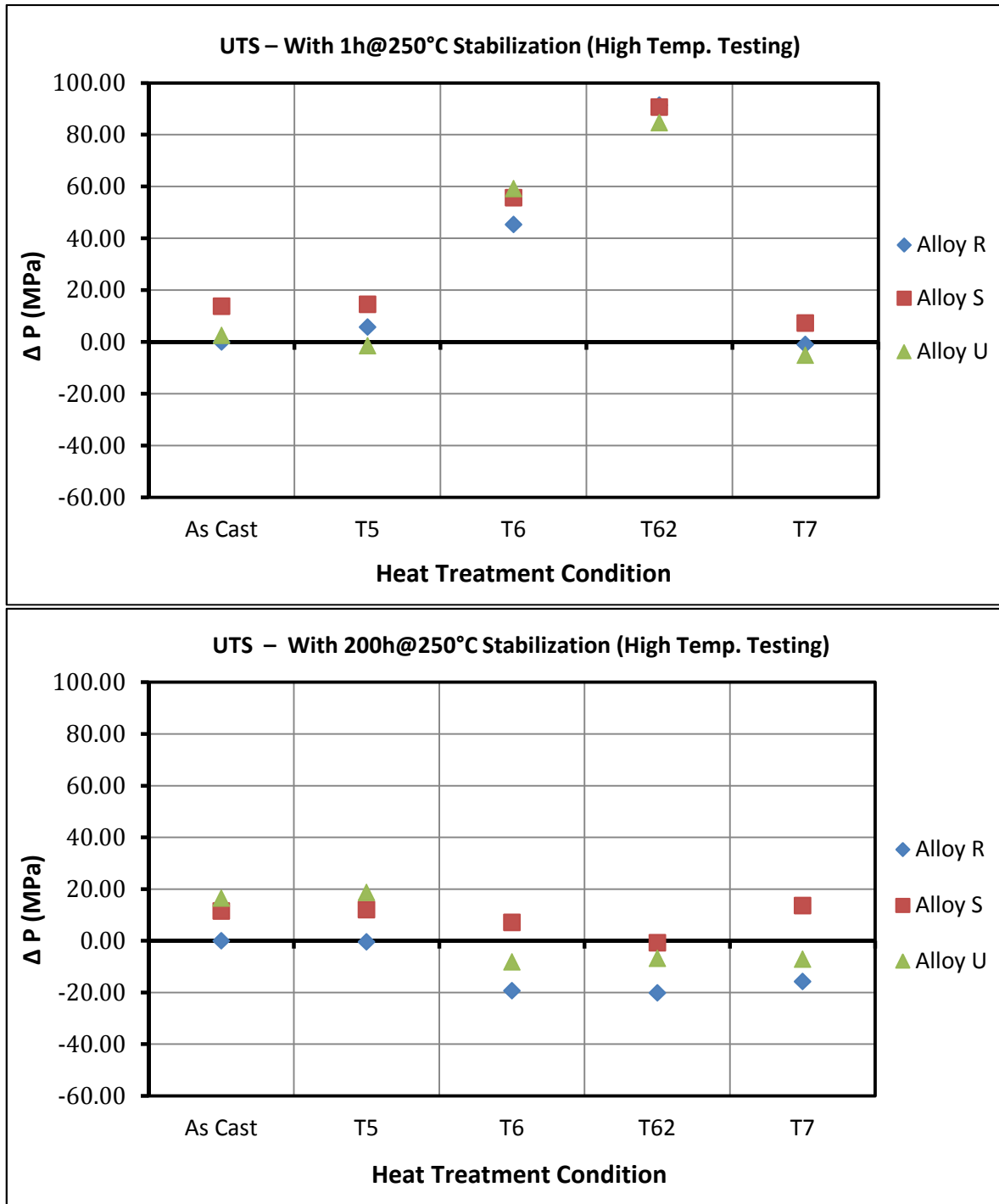
Table 5.7 High temperature tensile properties of reference alloy R, (tested at 250°C after 1 and 200 h stabilization at testing temperature).

Tensile Properties	1 h @ 250 °C	200 h @ 250 °C
UTS (MPa)	170.93	104.14
YS (MPa)	158.03	82.64
%EI	4.17	8.67

As may be seen from the figure, additions of these elements improve the alloy performance at high temperature (250°C). After 1 h stabilization at 250°C, the strength of alloys R, S and U is improved to the same extent, with the T62 heat treatment providing the best properties at high temperature, followed by the T6 treatment. Figure 5.24(b) shows that the yield strength of Alloy S is higher than the YS values of the other alloys for most of the heat treatment conditions. Figure 5.24(c) shows that the $\Delta P_{\%EI}$ values for all alloys are lower than those of the R base alloy, which is to be expected, in light of the results observed in Figure 5.24(a).

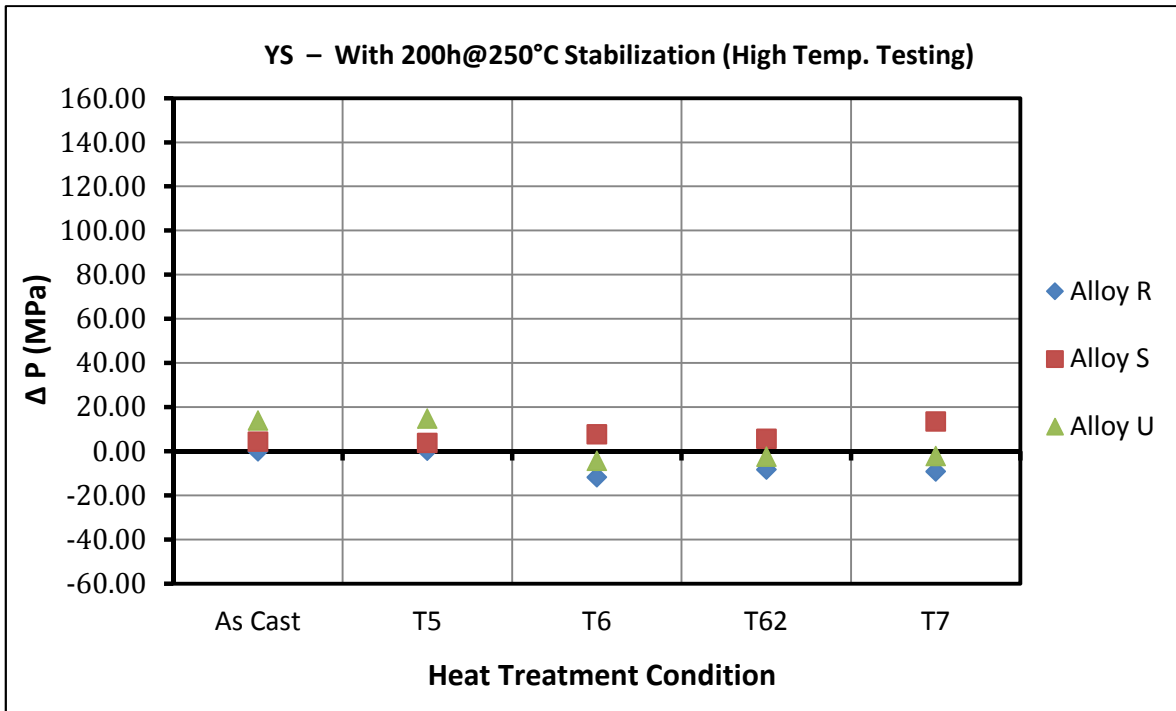
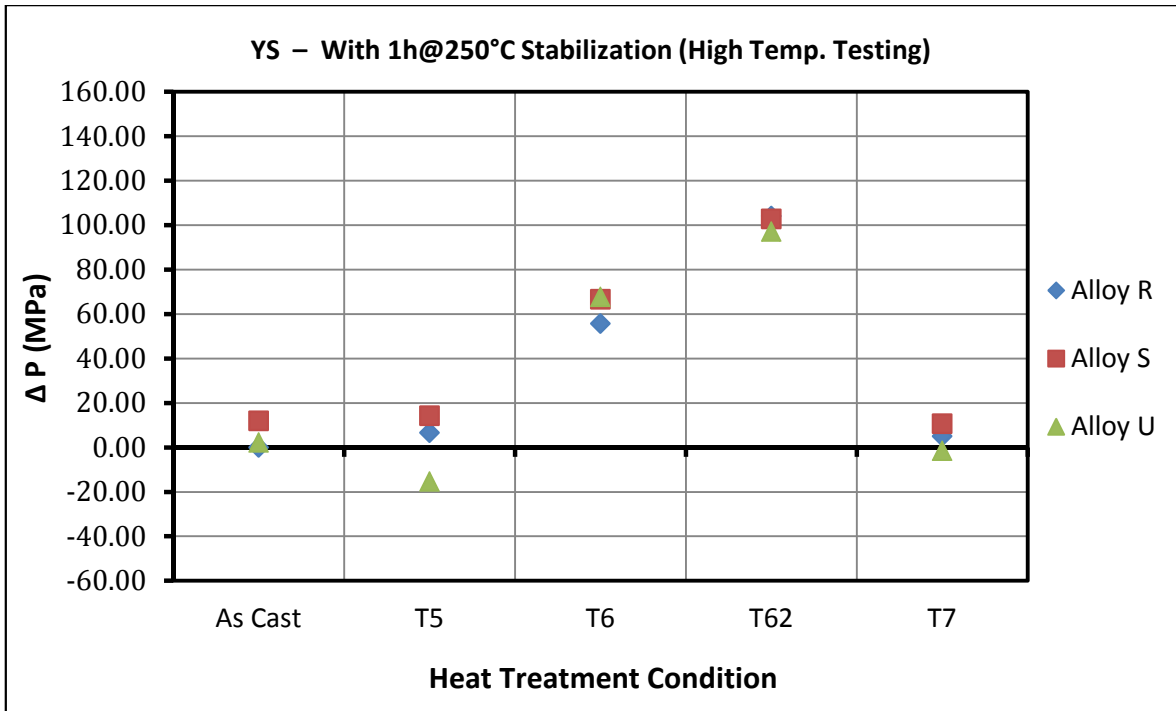
After 200 hours stabilization, however, at 250°C, not much variation in the UTS values are observed, the values lying approximately within a band of ± 20 MPa with respect to the reference alloy R. Likewise, the YS values also range within ± 10 MPa.

Alloy R shows the highest ductility values for the T62, T6 and T7 conditions among the three alloys, corresponding to its UTS and YS values observed in Figure 5.24(a) and (b) for these three conditions (lowest among the three alloys).

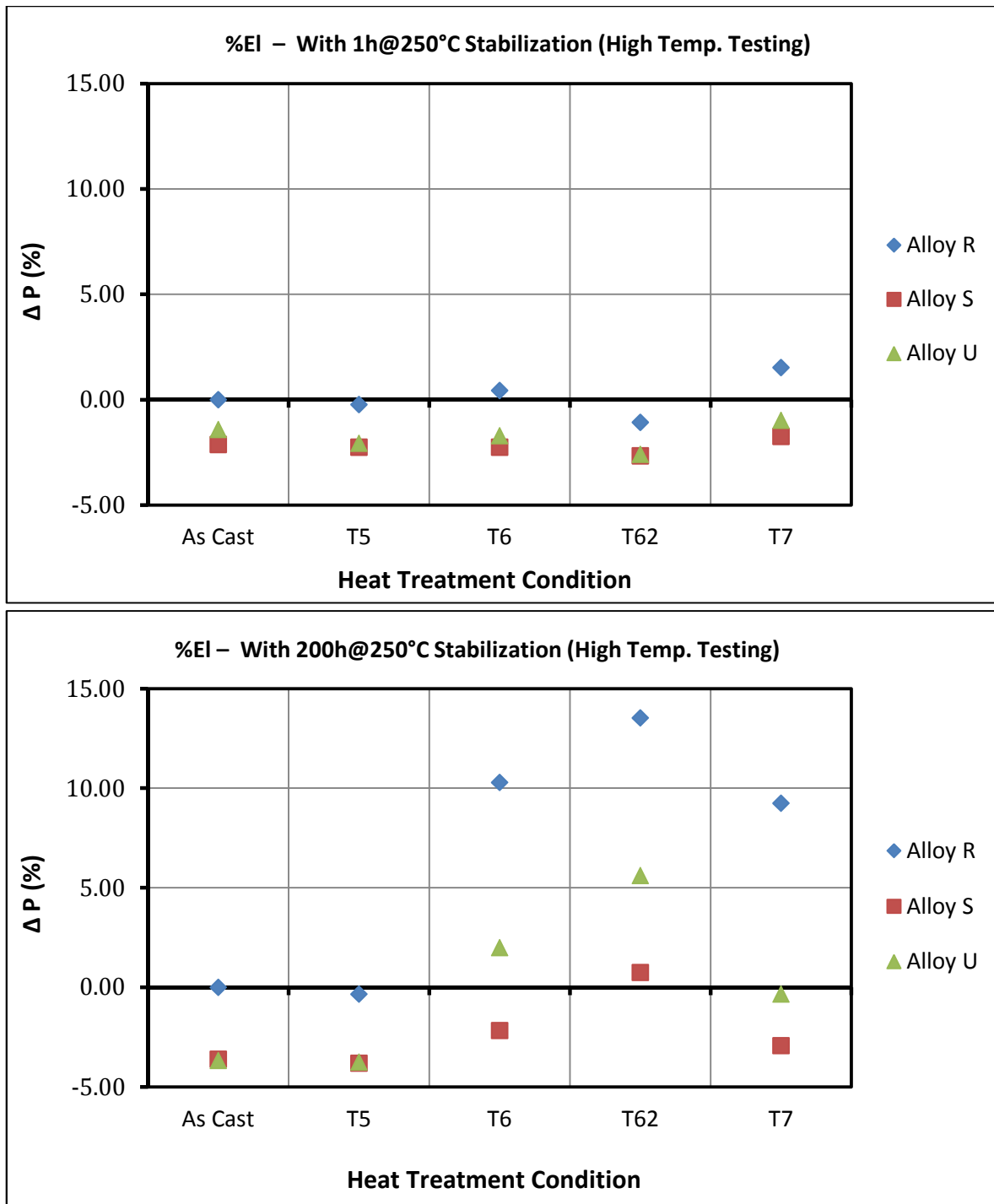


(a)

Figure 5.24 Cont.



(b)
Figure 5.24 Cont.



(c)

Figure 5.24 Comparison of high temperature tensile properties of R, S and U alloys relative to those of the as-cast base alloy: (a) UTS, (b) YS, and (c) %El after 1 h and 200 h stabilization at 250°C.

CHAPTER 6
CONCLUSIONS

CHAPTER 6

CONCLUSIONS

This chapter presents the conclusions drawn from the experimental data obtained which were presented in Chapters 4 and 5. These are presented in two separate parts, A and B, as shown below.

Part A

Based on the microstructural results, thermal analysis data and porosity formation measurements presented in Chapter 4, corresponding to the different 354 alloys containing Zr, Ni, Mn and Sc additions (viz., alloys R, S, T, U, V and Z), the following conclusions may be drawn:

1. Six main reactions are detected during the solidification of the 354 base alloy:
(i) formation of the α -Al dendritic network at 598°C, followed by (ii) precipitation of the Al-Si eutectic and the post-eutectic β -Al₅FeSi phase at 560°C; (iii) Mg₂Si phase formation at 540°C; (iv) transformation of the β -iron Al₅FeSi phase into π -Al₈Mg₃FeSi₆ phase at 525°C; and lastly, precipitation of the copper-containing phases Al₂Cu and Q -Al₅Mg₈Cu₂Si₆ that precipitate almost simultaneously at 498°C and 488°C.
2. While minimum iron content is always recommended in the production of the 354 casting alloys, when such alloy castings contain high iron levels, appropriate

solution heat treatment procedures may partially neutralize the deleterious effect of the iron-bearing phases.

3. As a result of the low solidification rate of the thermal analysis castings, and a Zr content of 0.25 wt%, all Zr-containing alloys are located in the L + Al₃Zr region of the Al-Zr phase diagram during the melting stage.
4. Three main reactions are detected with the addition of Ni, *i.e.*, the formation of AlFeNi, AlCuNi and AlSiNiZr phases.
5. Larger sizes of AlFeNi and AlCuNi phase particles are observed in the T alloy with a Ni content of 4 wt%, when compared to those seen in the S alloy sample with its lower Ni content of 2 wt%.
6. Mn addition in Alloy U helps in reducing the detrimental effect of the platelet morphology of the β -iron Al₅FeSi phase by replacing it with the more compact and hence less detrimental Chinese script α -Al₁₅(Fe,Mn)₃Si₂ phase and sludge particles.
7. Sc-containing intermetallic phases observed in this study appear in two different forms: (Al,Ti)(Sc,Zr) and (Al,Si)(Sc,Zr,Ti).
8. When the as-cast alloys are subjected to the multi-step solution treatment – involving higher solution temperatures and longer durations, an increased amount of incipient melting is expected to occur.
9. After multi-step solution heat treatment coarsening of the Si particles is observed, with larger particles growing bigger at the expense of smaller ones.
10. Primary Si particles are observed in the microstructure of the 398 hypereutectic Al-Si alloy L with its high Si content of 16 wt%.

Part B

Based on the results presented in Chapter 5 on the room temperature and high temperature tensile properties of the 354 alloys investigated, the following conclusions may be drawn:

Room Temperature Tensile Testing

11. The multi-step solution heat treatment (or SHT 2) results in higher tensile properties than those achieved with the SHT 1 treatment or in the as-cast condition, due to the increase in the amount of dissolution of the Cu-phases and a reduced risk of the occurrence of incipient melting.
12. The ultimate tensile strength and ductility of the given alloys in the multi-step solution heat-treated condition increase by as much as 70 MPa and 3% respectively, in comparison with the as-cast and SHT 1 conditions, while the yield strength remains almost the same.
13. Without stabilization, T6 and T62 treatments provide the best improvements in both UTS and YS values of all alloys.
14. The best tensile properties of alloys tested at room temperature after stabilization at 250°C for 200h are obtained with the T6 heat treatment.
15. Alloy R shows the best quality index values after T62 treatment, i.e., 411 MPa and 418.64 MPa without, and with 200 hours stabilization, respectively, followed by Alloy U which displays a Q value of 397.84 MPa after T62 treatment (with no stabilization) and 404.62 MPa following T6 treatment and 200 h stabilization at 250°C before testing.

16. The presence of 2 wt% Ni in Alloy S leads to the formation of Al-Cu-Ni phase particles in addition to the Al₂Cu phase. The persistence of this phase after T6, T62 and T7 heat treatments would explain the increased strength observed in these cases, and would also account for the high YS values, as the Al-Cu-Ni particles would act as barriers to the movement of dislocations in the matrix.
17. After T62 treatment, Alloy U (containing 0.75wt% Mn + 0.25wt% Zr) shows the maximum increase in tensile properties, with the UTS and YS values increasing by ~100 MPa and ~160 MPa, respectively.

High Temperature Tensile Testing

18. The addition of Zr, Ni, Mn and Sc to 354-type alloys improves the high temperature tensile properties compared to the base alloy.
19. Alloy S (Al 354 + 0.25wt% Zr + 2wt% Ni) and alloy U (Al 354 + 0.25wt% Zr + 2wt% Ni) perform better in case of high temperature conditions, with one hour stabilization at 250°C, displaying strength values of 226.64/230.05 MPa UTS and 224.72/225.73 MPa YS, respectively. For a prolonged stabilization time (200 h at 250°C), however, the strength values are reduced to 111.26/95.9 MPa UTS, and 90.28/78.16 MPa YS, respectively.
20. The decrease in strength and increase in ductility observed for the 354 alloys after prolonged stabilization of 200 h at 250°C is related to the softening which occurs as a result of the over-aging conditions during which the equilibrium precipitates form, leading to the loss of the coherency strain between the precipitates and the matrix.
21. The L alloy (398 + 0.25wt% Zr + 0.15wt% Sc) is more brittle than expected in the as-cast condition but it improves slightly after T6 treatment. After 200 hours

stabilization at 250°C, the T6-treated L alloy shows much better strength values of 114.05 MPa UTS and 103 MPa YS, in comparison with the 354 alloys.

22. Analysis of the tensile data using quality charts, color contour maps and ΔP plots provide different tools to interpret the data and facilitate the selection of the appropriate alloying additions and heat treatment conditions needed to achieve properties specified for a required application, as well as determine how these parameters would affect the properties and quality of the base alloy.
23. The addition of Zr with Mn to 354-alloy after T62 heat treatment gives best tensile properties at room and high temperature as Mn addition in Alloy U helps in reducing the detrimental effect of the β -iron phase by replacing it with the less-detrimental Chinese script α - $\text{Al}_{15}(\text{Fe},\text{Mn})_3\text{Si}_2$ phase and sludge particles. In addition, the use of the T62 heat treatment, incorporating the multi-step solution treatment, allows for maximum dissolution of the copper phases in the multiple stages of solution treatment, such dissolution produces the greatest improvement in both UTS and YS values.

RECOMMENDATIONS FOR FUTURE WORK

ClicCours.com

RECOMMENDATIONS FOR FUTURE WORK

According to the results obtained in this study, the following aspects may be further explored to provide a complete and well-established background for the Al-Si-Cu-Mg 354-type alloys investigated in this study.

- Studying the effect of sample geometry such as flat samples with different thicknesses, round samples with notches or holes one side to physically simulate the different parts located in real castings e.g. engine blocks.
- Using an electron microprobe analyzer in order to identify the actual stoichiometric composition of the different phases reported in the present work.
- Detailed fractographic investigation of samples tested at ambient and high temperatures using scanning electron microscopy to establish the possible failure mechanisms.

REFERENCES

REFERENCES

- 1- Franetovic, V., Lints, R.C. and Carter, J.T., 2003. Aluminum 2003. Proceedings of the TMS 2003, 133-144.
- 2- Vatsayan, U., Pandey, K.M. and Biswas, A., 2014. Effects of Heat Treatment on Materials Used In Automobiles: A Case Study. *J. Mech. Civ. Eng.*, 11(5), pp.90-95.
- 3- Wang, E.R., Hui, X.D. and Chen, G.L., 2011. Eutectic Al–Si–Cu–Fe–Mn alloys with enhanced mechanical properties at room and elevated temperature. *Materials & Design*, 32(8), pp.4333-4340.
- 4- Ammar, H.R., Samuel, A.M. and Samuel, F.H., 2008. Effect of casting imperfections on the fatigue life of 319-F and A356-T6 Al–Si casting alloys. *Materials Science and Engineering: A*, 473(1), pp.65-75.
- 5- Jia, Z., Hu, G., Forbord, B. and Solberg, J.K., 2007. Effect of homogenization and alloying elements on recrystallization resistance of Al–Zr–Mn alloys. *Materials Science and Engineering: A*, 444(1), pp.284-290.
- 6- Garza-Elizondo, G.H., Alkahtani, S.A., Samuel, A.M. and Samuel, F.H., 2014. Role of Ni and Zr in Preserving the Strength of 354 Aluminum Alloy at High Temperature. In *Light Metals 2014* (pp. 305-314). Springer International Publishing.
- 7- Dobrzański, L.A., Maniara, R. and Sokolowski, J.H., 2006. The effect of cast Al-Si-Cu alloy solidification rate on alloy thermal characteristics. *Journal of Achievements in Materials and Manufacturing Engineering*, 17(1-2), pp.217-220.
- 8- Mohamed, A.M.A. and Samuel, F.H., 2013. Microstructure, tensile properties and fracture behavior of high temperature Al–Si–Mg–Cu cast alloys. *Materials Science and Engineering: A*, 577, pp.64-72.

- 9- Jonathan, L., 2001. NASA 398 Material Properties Data Sheet. NASA-Marshall Space Flight Center, Huntsville, AL.
- 10- Cole, G.S. and Sherman, A.M., 1995. Lightweight materials for automotive applications. *Materials Characterization*, 35(1), pp.3-9.
- 11- Miller, W.S., Zhuang, L., Bottema, J., Wittebrood, A., De Smet, P., Haszler, A. and Vieregge, A., 2000. Recent development in aluminium alloys for the automotive industry. *Materials Science and Engineering: A*, 280(1), pp.37-49.
- 12- Palazzo, F., 1977. The Future of Aluminum in the Automotive Industry. *Aluminio*, Vol. 46 (9), pp. 323-334.
- 13- Pardo, A., Merino, M.C., Coy, A.E., Arrabal, R., Viejo, F. and Matykina, E., 2008. Corrosion behaviour of magnesium/aluminium alloys in 3.5 wt.% NaCl. *Corrosion Science*, 50(3), pp.823-834.
- 14- Hatch, J.E., (1984) *Aluminum: properties and physical metallurgy*. ASM International, pp. 134-424.
- 15- Garza-Elizondo, G.H., 2014. Ambient and High Temperature performance of Al-Si-Cu-Mg Based Alloys. Seminar Report. University of Quebec at Chicoutimi, Nov. 2014.
- 16- Spada, A.T., 2002. In Search of Light-Weight Components: Automotive's Cast Aluminum Conversion. *Engineered Casting Solutions (USA)*, 4(2), pp.28-31.
- 17- Immarigeon, J.P., Holt, R.T., Koul, A.K., Zhao, L., Wallace, W. and Beddoes, J.C., 1995. Lightweight materials for aircraft applications. *Materials Characterization*, 35(1), pp.41-67.
- 18- Fridlyander, I.N., 2001. Aluminum alloys in aircraft in the periods of 1970–2000 and 2001–2015. *Metal Science and Heat Treatment*, 43(1), pp.6-10.

- 19- Kaufman, J.G. and Rooy, E.L., 2004. Aluminum alloy castings: properties, processes, and applications. ASM International, Materials Park, OH.
- 20- Wang, T., Fu, H., Chen, Z., Xu, J., Zhu, J., Cao, F. and Li, T., 2012. A novel fading-resistant Al–3Ti–3B grain refiner for Al–Si alloys. *Journal of Alloys and Compounds*, 511(1), pp.45-49.
- 21- Lashgari, H.R., Zangeneh, S., Shahmir, H., Saghafi, M. and Emamy, M., 2010. Heat treatment effect on the microstructure, tensile properties and dry sliding wear behavior of A356–10% B₄C cast composites. *Materials & Design*, 31(9), pp.4414-4422.
- 22- Rana, R.S., Purohit, R. and Das, S., 2012. Reviews on the influences of alloying elements on the microstructure and mechanical properties of aluminum alloys and aluminum alloy composites. *International Journal of Scientific and Research Publications*, 2(6), pp.1-7.
- 23- Lumley, R.N., O'Donnell, R.G., Gunasegaram, D.R., Kittel-Sherri, T., Gershenzon, M., Yob, A.C. and Polmear, I.J., 2013. The role of alloy composition in the heat treatment of aluminium high pressure die castings. *Metallurgical Science and Technology*, 26(2).
- 24- Lee, J.A., 2003. Cast aluminum alloy for high temperature applications. 132nd TMS, 2-6 March 2003, San Diego, California.
- 25- Zeren, M., 2005. Effect of copper and silicon content on mechanical properties in Al–Cu–Si–Mg alloys. *Journal of Materials Processing Technology*, 169(2), pp.292-298.
- 26- Sjölander, E. and Seifeddine, S., 2010. The heat treatment of Al–Si–Cu–Mg casting alloys. *Journal of Materials Processing Technology*, 210(10), pp.1249-1259.

- 27- Caceres, C.H., Svensson, I.L. and Taylor, J.A., 2003. Strength-ductility behaviour of Al-Si-Cu-Mg casting alloys in T6 temper. *International Journal of Cast Metals Research*, 15(5), pp.531-543.
- 28- Abhishek, S., 2008. Strength and fracture studies of as-cast Al-Si-Cu alloys, Thapar University, India: Master of Technology in Materials Science and Engineering thesis.
- 29- Xiao, D.H., Wang, J.N., Ding, D.Y. and Chen, S.P., 2002. Effect of Cu content on the mechanical properties of an Al-Cu-Mg-Ag alloy. *Journal of alloys and compounds*, 343(1), pp.77-81.
- 30- Samuel, A.M., Gauthier, J. and Samuel, F.H., 1996. Microstructural aspects of the dissolution and melting of Al₂Cu phase in Al-Si alloys during solution heat treatment. *Metallurgical and Materials Transactions A*, 27(7), pp.1785-1798.
- 31- Wang, P.S., Lee, S.L., Lin, J.C. and Jahn, M.T., 2000. Effects of solution temperature on mechanical properties of 319.0 aluminum casting alloys containing trace beryllium. *Journal of Materials Research*, 15(09), pp.2027-2035.
- 32- Reiso, O., Øverlie, H.G. and Ryum, N., 1990. Dissolution and melting of secondary Al₂Cu phase particles in an AlCu alloy. *Metallurgical Transactions A*, 21(6), pp.1689-1695.
- 33- Askeland, D.R., 1996. *The Science and Engineering of Materials: 3rd SI Edi.*, Chapman and Hall, London.
- 34- Smith, W.F., 1986. *Principles of materials science and engineering*, McGraw-Hill Inc., York, PA.
- 35- Ringer, S.P. and Hono, K., 2000. Microstructural evolution and age hardening in aluminium alloys: atom probe field-ion microscopy and transmission electron microscopy studies. *Materials Characterization*, 44(1), pp.101-131.

- 36- Polmear, I.J., 1995. Metallurgy of the Light Metals. 3rd edition, Arnold Hodder Headline PLC, London.
- 37- Dieter, Ellwood, G. and Bacon, D.J., 1986. Mechanical Metallurgy. Vol. 3, New York, McGraw-Hill.
- 38- Molina, R., Amalberto, P. and Rosso, M., 2011. Mechanical characterization of aluminium alloys for high temperature applications Part1: Al-Si-Cu alloys. Metallurgical Science and Tecnology, 29(1), p.5.
- 39- Ammar, H.R., Moreau, C., Samuel, A.M., Samuel, F.H. and Doty, H.W., 2008. Influences of alloying elements, solution treatment time and quenching media on quality indices of 413-type Al–Si casting alloys. Materials Science and Engineering: A, 489(1), pp.426-438.
- 40- Caceres, C.H., Davidson, C.J., Griffiths, J.R. and Wang, Q.G., 1999. The effect of Mg on the microstructure and mechanical behavior of Al-Si-Mg casting alloys. Metallurgical and Materials Transactions A, 30(10), pp.2611-2618.
- 41- Davis, J., 1999. Corrosion of Aluminum and Aluminum alloys. ASM International, Ohio.
- 42- Tavitias-Medrano, F.J., Gruzleski, J.E., Samuel, F.H., Valtierra, S. and Doty, H.W., 2008. Effect of Mg and Sr-modification on the mechanical properties of 319-type aluminum cast alloys subjected to artificial aging. Materials Science and Engineering: A, 480(1), pp.356-364.
- 43- Zhu, M., Jian, Z., Yang, G. and Zhou, Y., 2012. Effects of T6 heat treatment on the microstructure, tensile properties, and fracture behavior of the modified A356 alloys. Materials & Design (1980-2015), 36, pp.243-249.

- 44- Mallapur, D.G., Udupa, K.R. and Kori, S.A., 2011. Studies on the influence of grain refining and modification on microstructure and mechanical properties of forged A356 alloy. *Materials Science and Engineering: A*, 528(13), pp.4747-4752.
- 45- Ceschini, L., Morri, A., Toschi, S. and Seifeddine, S., 2016. Room and high temperature fatigue behaviour of the A354 and C355 (Al–Si–Cu–Mg) alloys: Role of microstructure and heat treatment. *Materials Science and Engineering: A*, 653, pp.129-138.
- 46- Baradarani, B. and Raiszadeh, R., 2011. Precipitation hardening of cast Zr-containing A356 aluminium alloy. *Materials & Design*, 32(2), pp.935-940.
- 47- Lasa, L. and Rodriguez-Ibabe, J.M., 2004. Evolution of the main intermetallic phases in Al-Si-Cu-Mg casting alloys during solution treatment. *Journal of Materials Science*, 39(4), pp.1343-1355.
- 48- Han, Y., Samuel, A.M., Doty, H.W., Valtierra, S. and Samuel, F.H., 2014. Optimizing the tensile properties of Al–Si–Cu–Mg 319-type alloys: role of solution heat treatment. *Materials & Design*, 58, pp.426-438.
- 49- Kasprzak, W., Amirkhiz, B.S. and Niewczas, M., 2014. Structure and properties of cast Al–Si based alloy with Zr–V–Ti additions and its evaluation of high temperature performance. *Journal of Alloys and Compounds*, 595, pp.67-79.
- 50- Man, J., Jing, L. and Jie, S.G., 2007. The effects of Cu addition on the microstructure and thermal stability of an Al–Mg–Si alloy. *Journal of Alloys and Compounds*, 437(1), pp.146-150.
- 51- Murayama, M., Hono, K., Saga, M. and Kikuchi, M., 1998. Atom probe studies on the early stages of precipitation in Al–Mg–Si alloys. *Materials Science and Engineering: A*, 250(1), pp.127-132.

- 52- Zhen, L., Fei, W.D., Kang, S.B. and Kim, H.W., 1997. Precipitation behaviour of Al-Mg-Si alloys with high silicon content. *Journal of Materials Science*, 32(7), pp.1895-1902.
- 53- Miao, W.F. and Laughlin, D.E., 1999. Precipitation hardening in aluminum alloy 6022. *Scripta Materialia*, 40(7), pp.873-878.
- 54- Eskin, D.G., Decomposition of supersaturated solid solutions in Al-Cu-Mg-Si alloys, *Journal of Materials Science*, 38 (2003) 279–290.
- 55- Son, S.K., Takeda, M., Mitome, M., Bando, Y. and Endo, T., 2005. Precipitation behavior of an Al-Cu alloy during isothermal aging at low temperatures. *Materials Letters*, 59(6), pp.629-632.
- 56- Wang, S.C., Starink, M.J. and Gao, N., 2006. Precipitation hardening in Al-Cu-Mg alloys revisited. *Scripta Materialia*, 54(2), pp.287-291.
- 57- Ratchev, P., Verlinden, B., De Smet, P. and Van Houtte, P., 1998. Effect of cooling rate and pre deformation on the precipitation hardening of an Al-4.2 wt.% Mg-0.6 wt.% Cu alloy. *Scripta Materialia*, 38(8), pp.1195-1201.
- 58- Chakrabarti, D.J. and Laughlin, D.E., 2004. Phase relations and precipitation in Al-Mg-Si alloys with Cu additions. *Progress in Materials Science*, 49(3), pp.389-410.
- 59- Cayron, C. and Buffat, P.A., 2000. Transmission electron microscopy study of the β' phase (Al-Mg-Si alloys) and QC phase (Al-Cu-Mg-Si alloys): ordering mechanism and crystallographic structure. *Acta Materialia*, 48(10), pp.2639-2653.
- 60- Hernandez-Sandoval, J., Garza-Elizondo, G.H., Samuel, A.M., Valtierra, S. and Samuel, F.H., 2014. The ambient and high temperature deformation behavior of Al-Si-Cu-Mg alloy with minor Ti, Zr, Ni additions. *Materials & Design*, 58, pp.89-101.

- 61- Elagin, V.I., 2007. Ways of developing high-strength and high-temperature structural aluminum alloys in the 21st century. *Metal Science and Heat Treatment*, 49(9), pp.427-434.
- 62- Tolley, A.J., Radmilovic, V. and Dahmen, U., 2004. On the effect of Zr on precipitate evolution in Al-Sc-Zr alloys," in Congress CONAMET/SAM 2004 Proceedings, La Serena, Chile.
- 63- Wang, G., Bian, X., Wang, W. and Zhang, J., 2003. Influence of Cu and minor elements on solution treatment of Al-Si-Cu-Mg cast alloys. *Materials Letters*, 57(24), pp.4083-4087.
- 64- Belov, N.A., Eskin, D.G. and Avxentieva, N.N., 2005. Constituent phase diagrams of the Al-Cu-Fe-Mg-Ni-Si system and their application to the analysis of aluminium piston alloys. *Acta Materialia*, 53(17), pp.4709-4722.
- 65- Stadler, F., Antrekowitsch, H., Fragner, W., Kaufmann, H. and Uggowitzer, P.J., 2011. The effect of Ni on the high-temperature strength of Al-Si cast alloys. In *Materials Science Forum* (Vol. 690, pp. 274-277). Trans Tech Publications.
- 66- Cho, Y.H., Joo, D.H., Kim, C.H. and Lee, H.C., 2006. The effect of alloy addition on the high temperature properties of over-aged Al-Si (CuNiMg) cast alloys. In *Materials Science Forum* (Vol. 519, pp. 461-466). Trans Tech Publications, Switzerland.
- 67- Seifeddine, S., Johansson, S. and Svensson, I.L., 2008. The influence of cooling rate and manganese content on the β -Al₅FeSi phase formation and mechanical properties of Al-Si-based alloys. *Materials Science and Engineering: A*, 490(1), pp.385-390.

- 68- Mohamed, A.M.A., Samuel, F.H., Samuel, A.M. and Doty, H.W., 2009. Influence of additives on the impact toughness of Al–10.8% Si near-eutectic cast alloys. *Materials & Design*, 30(10), pp.4218-4229.
- 69- Hwang, J.Y., Doty, H.W. and Kaufman, M.J., 2008. The effects of Mn additions on the microstructure and mechanical properties of Al–Si–Cu casting alloys. *Materials Science and Engineering: A*, 488(1), pp.496-504.
- 70- Davydov, V.G., Rostova, T.D., Zakharov, V.V., Filatov, Y.A. and Yelagin, V.I., 2000. Scientific principles of making an alloying addition of scandium to aluminium alloys. *Materials Science and Engineering: A*, 280(1), pp.30-36.
- 71- Marquis, E.A. and Seidman, D.N., 2001. Nanoscale structural evolution of Al₃Sc precipitates in Al (Sc) alloys. *Acta Materialia*, 49(11), pp.1909-1919.
- 72- Krug, M.E., 2011. *Microstructural Evolution and Mechanical Properties in Al-Sc Alloys with Li and Rare Earth Additions* (Doctoral dissertation, Northwestern University).
- 73- Van Dalen, M.E., Seidman, D.N. and Dunand, D.C., 2008. Creep-and coarsening properties of Al–0.06 at.% Sc–0.06 at.% Ti at 300–450° C. *Acta Materialia*, 56(16), pp.4369-4377.
- 74- Fuller, C.B., Seidman, D.N. and Dunand, D.C., 1999. Creep properties of coarse-grained Al (Sc) alloys at 300° C. *Scripta Materialia*, 40(6), pp.691-696.
- 75- Seidman, D.N., Marquis, E.A. and Dunand, D.C., 2002. Precipitation strengthening at ambient and elevated temperatures of heat-treatable Al (Sc) alloys. *Acta Materialia*, 50(16), pp.4021-4035.

- 76- Prukkanon, W., Srisukhumbowornchai, N. and Limmaneevichitr, C., 2009. Modification of hypoeutectic Al–Si alloys with scandium. *Journal of Alloys and Compounds*, 477(1), pp.454-460.
- 77- Kendig, K.L. and Miracle, D.B., 2002. Strengthening mechanisms of an Al–Mg–Sc–Zr alloy. *Acta Materialia*, 50(16), pp.4165-4175.
- 78- Marquis, E.A., Seidman, D.N. and Dunand, D.C., 2003. Effect of Mg addition on the creep and yield behavior of an Al–Sc alloy. *Acta Materialia*, 51(16), pp.4751-4760.
- 79- Knipling, K.E., Seidman, D.N. and Dunand, D.C., 2011. Ambient-and high-temperature mechanical properties of isochronally aged Al–0.06 Sc, Al–0.06 Zr and Al–0.06 Sc–0.06 Zr (at.%) alloys. *Acta Materialia*, 59(3), pp.943-954.
- 80- Harada, Y. and Dunand, D.C., 2002. Microstructure of Al₃Sc with ternary transition-metal additions. *Materials Science and Engineering: A*, 329, pp.686-695.
- 81- Fuller, C.B., Seidman, D.N. and Dunand, D.C., 2003. Mechanical properties of Al (Sc, Zr) alloys at ambient and elevated temperatures. *Acta Materialia*, 51(16), pp.4803-4814.
- 82- Van Dalen, M.E., Dunand, D.C. and Seidman, D.N., 2005. Effects of Ti additions on the nanostructure and creep properties of precipitation-strengthened Al–Sc alloys. *Acta Materialia*, 53(15), pp.4225-4235.
- 83- Kaiser, M.S. and Kurny, A.S.W., 2011. Effect of scandium on the grain refining and ageing behaviour of cast Al–Si–Mg alloy. *Iranian Journal of Materials Science & Engineering*, 8(4), pp.1-8.
- 84- Prukkanon, W., Srisukhumbowornchai, N. and Limmaneevichitr, C., 2009. Influence of Sc modification on the fluidity of an A356 aluminum alloy. *Journal of Alloys and Compounds*, 487(1), pp.453-457.

- 85- Riddle, Y.W. and Sanders, T.H., 2004. A study of coarsening, recrystallization, and morphology of microstructure in Al-Sc-(Zr)-(Mg) alloys. *Metallurgical and Materials Transactions A*, 35(1), pp.341-350.
- 86- Ocenasek, V. and Slamova, M., 2001. Resistance to recrystallization due to Sc and Zr addition to Al-Mg alloys. *Materials Characterization*, 47(2), pp.157-162.
- 87- Røyset, J. and Ryum, N., 2005. Scandium in aluminium alloys. *International Materials Reviews*, 50(1), pp.19-44.
- 88- Norman, A.F., Prangnell, P.B. and McEwen, R.S., 1998. The solidification behaviour of dilute aluminium-scandium alloys. *Acta Materialia*, 46(16), pp.5715-5732.
- 89- Hegde, S. and Prabhu, K.N., 2008. Modification of eutectic silicon in Al-Si alloys. *Journal of Materials Science*, 43(9), pp.3009-3027.
- 90- Closset, B. and Gruzleski, J.E., 1982. Structure and properties of hypoeutectic Al-Si-Mg alloys modified with pure strontium. *Metallurgical Transactions A*, 13(6), pp.945-951.
- 91- Merlin, M. and Garagnani, G.L., 2013. Mechanical and microstructural characterisation of A356 castings realised with full and empty cores. *Metallurgical Science and Technology*, 27(1), pp.21-30.
- 92- Zeren, M. and Karakulak, E., 2008. Influence of Ti addition on the microstructure and hardness properties of near-eutectic Al-Si alloys. *Journal of Alloys and Compounds*, 450(1), pp.255-259.
- 93- Sigworth, G.K. and Kuhn, T.A., 2007. Grain refinement of aluminum casting alloys. *International Journal of Metal Casting*, American Foundry Society, Schaumburg, IL USA, 1(1), pp.31-40.

- 94- Ammar, H.R., 2010. Influence of Metallurgical Parameters on the Mechanical Properties and Quality Indices of Al-Si-Cu-Mg and Al-Si-Mg Casting Alloys. Thesis. University of Quebec at Chicoutimi.
- 95- El Sebaie, O., Samuel, A.M., Samuel, F.H. and Doty, H.W., 2008. The effects of mischmetal, cooling rate and heat treatment on the eutectic Si particle characteristics of A319. 1, A356. 2 and A413. 1 Al-Si casting alloys. *Materials Science and Engineering: A*, 480(1), pp.342-355.
- 96- Lasa, L. and Rodriguez-Ibabe, J.M., 2002. Characterization of the dissolution of the Al₂Cu phase in two Al-Si-Cu-Mg casting alloys using calorimetry. *Materials Characterization*, 48(5), pp.371-378.
- 97- Mohamed, A.M.A. and Samuel, F.H., 2012. A review on the heat treatment of Al-Si-Cu/Mg casting alloys. *Heat Treatment, Rijeka, Croatia, InTech Science*, pp.229-246.
- 98- Shuey, R. and Tiryakioglu, M., 2010. Quenching of aluminium alloys. *Quenching Theory and Technology*, pp.43-83.
- 99- Chen, S.Y., Chen, K.H., Peng, G.S., Liang, X. and Chen, X.H., 2012. Effect of quenching rate on microstructure and stress corrosion cracking of 7085 aluminum alloy. *Transactions of Nonferrous Metals Society of China*, 22(1), pp.47-52.
- 100- Cuniberti, A., Tolley, A., Riglos, M.C. and Giovachini, R., 2010. Influence of natural aging on the precipitation hardening of an AlMgSi alloy. *Materials Science and Engineering: A*, 527(20), pp.5307-5311.
- 101- Wang, Q. and Jones, P.E., GM Global Technology Operations LLC, 2012. Artificial aging process for aluminum alloys. U.S. Patent 8,323,425

- 102- Wang, R.Y., Lu, W.H. and Hogan, L.M., 1999. Growth morphology of primary silicon in cast Al–Si alloys and the mechanism of concentric growth. *Journal of Crystal Growth*, 207(1), pp.43-54.
- 103- Dahle, A.K., Nogita, K., McDonald, S.D., Dinnis, C. and Lu, L., 2005. Eutectic modification and microstructure development in Al–Si Alloys. *Materials Science and Engineering: A*, 413, pp.243-248.
- 104- Mohamed, A.M.A. and Samuel, F.H., 2012. Influence of Mg and solution heat treatment on the occurrence of incipient melting in Al–Si–Cu–Mg cast alloys. *Materials Science and Engineering: A*, 543, pp.22-34.
- 105- Asghar, Z., Requena, G., Degischer, H.P. and Cloetens, P., 2009. Three-dimensional study of Ni aluminides in an AlSi₁₂ alloy by means of light optical and synchrotron microtomography. *Acta Materialia*, 57(14), pp.4125-4132.
- 106- Asghar, Z., Requena, G. and Kubel, F., 2010. The role of Ni and Fe aluminides on the elevated temperature strength of an AlSi₁₂ alloy. *Materials Science and Engineering: A*, 527(21), pp.5691-5698.
- 107- Stadler, F., Antrekowitsch, H., Fragner, W., Kaufmann, H. and Uggowitzer, P.J., 2012. Effect of main alloying elements on strength of Al–Si foundry alloys at elevated temperatures. *International Journal of Cast Metals Research*, 25(4), pp.215-224.
- 108- Hamasha, M.M., Mayyas, A.T., Hassan, A.M. and Hayajneh, M.T., 2012. The effect of time, percent of copper and nickel on naturally aged Al-Cu-Ni cast alloys. *Journal of Minerals and Materials Characterization and Engineering*, 11(02), p.117.

- 109- Ouellet, P. and Samuel, F.H., 1999. Effect of Mg on the ageing behaviour of Al-Si-Cu 319 type aluminium casting alloys. *Journal of Materials Science*, 34(19), pp.4671-4697.
- 110- Mahmudi, R., Sepehrband, P. and Ghasemi, H.M., 2006. Improved properties of A319 aluminum casting alloy modified with Zr. *Materials Letters*, 60(21), pp.2606-2610.
- 111- https://commons.wikimedia.org/wiki/File:Brittle_v_ductile_stress_strain_behaviour.png
- 112- Hurtalová, L., Tillová, E. and Chalupová, M., 2013. Influence of intermetallic phases on the fracture surfaces in secondary aluminum cast alloy," In *Acta Metallurgica Slovaca-Conference*, Vol. 3, pp. 65-74.
- 113- Wang, Q.G., 2003. Microstructural effects on the tensile and fracture behavior of aluminum casting alloys A356/357. *Metallurgical and Materials Transactions A*, 34(12), pp.2887-2899.
- 114- Van der Voort, G.F., 1987. *Visual Examination and Light Microscopy*. *Metals Handbook*, 9th Edition, Vol. 12: Fractography, American Society for Metals, Metals Park, OH, pp. 91-165.
- 115- Drouzy, M., Jacob, S. and Richard, M., 1980. Interpretation of tensile results by means of quality index and probable yield strength-application to Al-Si₇ Mg foundry alloys-France. *International Cast Metals Journal* 5.2, pp 43-50.
- 116- Caceres, C.H. and Taylor, J.A., 2005. Enhanced ductility in Al-Si-Cu-Mg foundry alloys with high Si content. *TMS Annual Meeting*, pp. 245-254.

- 117- Westengen, H. and Holta, O., 1988. Low Pressure Permanent Mold Casting of Magnesium-Recent Developments (No. 880509). SAE Technical Paper.
- 118- Samuel, A.M. and Samuel, F.H., 1995. Relevance of the use of the quality index concept in cast SiCP-reinforced Al-Si-Mg composites. *Journal of Materials Science*, 30(3), pp.568-572.
- 119- Caceres, C.H., Din, T., Rashid, A.K. and Campbell, J., 1999. Effect of aging on quality index of an Al-Cu casting alloy. *Materials Science and Technology*, 15(6), pp.711-716.
- 120- Mohamed, A.M.A., April 2008. Effect of Additives on the Microstructure and Mechanical properties of Aluminum-Silicon Alloys. PhD Thesis, Université du Québec à Chicoutimi, Quebec, Canada, pp. 31-34.
- 121- Backerud, L., Chai, G. and Tamminen, J., 1990. Solidification characteristics of aluminum alloys. Vol. 2. Foundry alloys. American Foundrymen's Society, Inc., 1990, pp. 266.
- 122- Garza-Elizondo, G.H., 2016. Effect of Ni, Mn, Zr and Sc additions on the performance of Al-Si-Cu-Mg alloys. PhD, Thesis, Université du Québec à Chicoutimi, Chicoutimi, Quebec, Canada.
- 123- F.H. Samuel, A.M. Samuel and H.W. Doty, 1996. Factors controlling the type and morphology of Cu-containing phases in 319 Al alloys. *AFS Transactions*, Vol.104, pp. 893-901.
- 124- Nabawy, A.M., 2010. Influence of Zirconium and Scandium on the Microstructure, Tensile Properties, and Hot-Tearing Susceptibility of Al-2wt%Cu-Based Alloys. PhD, Thesis, Université du Québec à Chicoutimi, Chicoutimi, Quebec, Canada.

- 125- Srinivasan, D. and Chattopadhyay, K., 2005. Non-equilibrium Transformations Involving, $L1_2$ - Al_3Zr in Ternary Al-X-Zr Alloys. Metallurgical and Materials Transactions A, Vol. 36A, 2005, pp. 311-320.
- 126- Yu, K., Li, W., Li, S. and Zhao, J., 2004. Mechanical properties and microstructure of aluminum alloy 2618 with Al_3 (Sc, Zr) phases. Materials Science and Engineering: A, 368(1), pp.88-93.
- 127- Zeng, F., Xia, C. and Gu, Y., 2004. The 430°C Isothermal Section of the Al-4Mg-Sc-Zr Quaternary System in the Al-rich Range. Journal of Alloys and Compounds, Vol. 363, pp.175-181.
- 128- De la Sablonnière, H. and Samuel, F.H., 1996. Solution heat treatment of 319 aluminum alloy containing ~0.5wt%Mg. Part2—microstructure and fractography. International Journal of Cast Metals Research, 9(4), pp.213-225.
- 129- El Sebaie, O., Samuel, A.M., Samuel, F.H. and Doty, H.W., 2014. Impact toughness of Al–Si–Cu–Mg–Fe cast alloys: effects of minor additives and aging conditions. Materials & Design, 60, pp.496-509.
- 130- Northwood, D., Sun, X., Byczynski, G., Sokolowski, J.H., 1995. The development of a two-stage solution heat treatment for cast Al-Si-Cu alloys. IMMA ADCA conference proceedings, Vol. 4, 1995, pp. 15-19.
- 131- Sokolowski, J.H., Sun, X.C. and Esseltine, A., 1995. The removal of copper-phase segregation and the subsequent improvement in mechanical properties of cast 319 aluminium alloys by a two-stage solution heat treatment. Journal of Materials Processing Technology, Vol. 53, no. 1, pp. 385-392.

- 132- Alexopoulos, N. and Pantelakis, S., 2004. A New Quality Index for Characterizing Aluminum Cast Alloys with Regard to Aircraft Structure Design Requirements. Metallurgical and Materials Transactions A, Vol. 35A, pp. 301-308.
- 133- Lee, Jonathan A., and Po Shou Chen, 2003. High strength and wear resistant aluminum alloy for high temperature applications. 5th Conference on Aerospace Materials, Processes, and Environmental Technology, Huntsville, AL.
- 134- Dong-Woo Suh, Sang-Yong Lee, Kyong-Hwan Lee, Su-Keun Lim and Kyu Hwan Oh, 2004. Microstructural evolution of Al-Zn-Mg-Cu-(Sc) alloy during hot extrusion and heat treatments. Journal of Materials Processing Technology, Vols. 155-156, pp. 1330-1336.